

General Disclaimer

One or more of the Following Statements may affect this Document

- This document has been reproduced from the best copy furnished by the organizational source. It is being released in the interest of making available as much information as possible.
- This document may contain data, which exceeds the sheet parameters. It was furnished in this condition by the organizational source and is the best copy available.
- This document may contain tone-on-tone or color graphs, charts and/or pictures, which have been reproduced in black and white.
- This document is paginated as submitted by the original source.
- Portions of this document are not fully legible due to the historical nature of some of the material. However, it is the best reproduction available from the original submission.

1-A-A
UCLA-ENG-8349

VAPOR-LIQUID PHASE SEPARATOR STUDIES

by

S. W. K. Yuan
J. M. Lee
Y. I. Kim
W. A. Hepler
T. H. K. Frederking



Principal Investigator: T. H. K. Frederking

School of Engineering and Applied Science
University of California, Los Angeles

(NAS A-CK-166545) VAPOR-LIQUID PHASE
SEPARATOR STUDIES (California Univ.) 87 p
HC A05/MF A01 CSCL 20D

N84-17527

Unclassified
G3/34 15218

Grant NCC 2-64, Suppl. No. 1

Prepared for
National Aeronautics and Space Administration
AMES RESEARCH CENTER

October 1983

UCLA-ENG-8349

VAPOR-LIQUID PHASE SEPARATOR
STUDIES

by

S. W. K. Yuan, J. M. Lee, Y. I. Kim, W. A. Hepler and T. H. K. Frederking

Principal Investigator: T. H. K. Frederking

School of Engineering and Applied Science
University of California, Los Angeles

Grant NCC 2-64, Suppl. No. 1

Prepared for
National Aeronautics and Space Administration
AMES RESEARCH CENTER

October 1983

TABLE OF CONTENTS

	PAGE
Progress Summary	1
Introduction	2
Characteristic Lengths	3
Transport Equations	8
Plug Results and Conclusions	12
References	13
<hr/>	
Appendix A	15
Appendix B	25
Appendix C	38

PRECEDING PAGE BLANK NOT FILMED

Progress Summary

The present summary of activities under NASA Grant NCC 2-64 (Suppl. No. 1) outlines porous plug work in the preceding period of time, i.e. until September 30, 1983. The plugs serve as both entropy rejection devices and phase separation components separating the vapor phase on the downstream side from liquid Helium II upstream. The liquid upstream is the cryo-reservoir fluid needed for equipment cooling by means of Helium II, i.e. Helium-4 below its lambda temperature in near-saturated states. Aside from comments on preceding work, the topics outlined are characteristic lengths, transport equations and plug results.

INTRODUCTION

The controlled storage of liquid Helium-4 below its lambda temperature in liquid He II states, i.e. superfluid conditions, has become significant in recent time with the flight performance demonstration of cryogenic support technology for IR telescopes. The appearance on the sky of IRAS¹⁾ (Infra-Red Astronomical Satellite) in the beginning of 1983 has triggered renewed interest in quantification of many subsystem components. Among them is the porous plug serving as phase separator at the vent tube-liquid storage vessel connection. Though existing systems have passive modes of operation with fixed geometries of the plug, means of activation appear to be available. This implies that separator-flow control systems are not restricted only to pin-type devices employed in the commonly known needle valve systems with its various modifications for achievement of a particular control characteristic. The class of control devices may include as well porous media components which appear to have sufficient flexibility as they may be shaped conveniently for various requirements. In this area our initial work has opened up quite a few questions to which answers have been attempted using a step-by-step procedure aiming at a better quantification of most important plug parameters.

Aside from brief reference to preceding work, the present summary contains various topics related to characteristic lengths of the plugs, theoretical equations, and throughputs. Concerning data we refer to recent conference presentations included as Appendix sections of the present report and Ref. 2. Essential points of the preceding work with a variable area phase separation device using a porous plug are given in Appendix A.

CHARACTERISTIC LENGTHS

The motivation for a search of meaningful characteristic lengths is first of all plug identification by means of a plug size (e.g. diameter, radius) and second, plug throughput characterization by means of a throughput-related length (e.g. hydraulic radius). Originally the successful proof-of-principle testing of a plug flow modulation device (Appendix A) had offered the option of introducing controlled system operation. For instance, the bath temperature may be kept constant by variation of the shutter position using negative feedback. The multitude of parameters involved however for various types of plugs provided the challenge of coming up with a better quantification of plug characterization. Therefore, various lengths and related equations have been of primary interest. Examples considered are the bubble test size, the particle retention size of filtration, the equivalent packed bed diameter, the characteristic throughput lengths and others.

The bubble radius has been considered in some papers as a measure of plug size. However, it is noted that it takes care of surface conditions of the plug. The bubble radius is twice the surface tension (liquid-vapor) divided by the pressure difference producing appearance of a vapor bubble in a liquid submerged plug.

The particle retention size also is most likely a measure of surface domain conditions which may differ from bulk plug geometries. The nominal size (radius or diameter) of particles filtered out has been useful for solid-fluid filtration. This separation operation however is not of direct interest in the present vapor-liquid separation using only fluid phases (if

contamination of the liquid He II is avoided). Because of the surface conditions involved, the two lengths considered so far are not necessarily related directly to mass throughput of fluid flow.

The third length may be deduced from equations which employ the permeability of the porous medium. An example is the bed of near-spherical particles whose details have been treated on the basis of the Carman-Kozeny approach (References are given in Appendix B). An example of this approach is the Ergun equation. The Carman-Kozeny-Ergun permeability $K_{p,CKE}$ is known as a function of the porosity (ε) and the diameter of the particles (D_p). Once $K_{p,CKE}$ is known along with the porosity, the packed bed particle diameter may be deduced from the Ergun equation in the limit of small flow rates, i.e. in the laminar flow regime of Darcy transport:

$$D_p = (K_{p,CKE})^{1/2} (150)^{1/2} \varepsilon / (1 - \varepsilon)^{3/2} \quad (1)$$

In the range of plug conditions encountered, there is an order of magnitude difference between D_p and the characteristic lengths $L_{K,CKE} = (K_{p,CKE})^{1/2}$. For instance, for a value of L_K of the order 2 μm a diameter D_p of the order of 30 μm results. More important is the observation that sintered porous plugs and fibrous materials do not resemble near-spherical particle assemblies of packed beds. Thus, a length related directly to throughput is desirable.

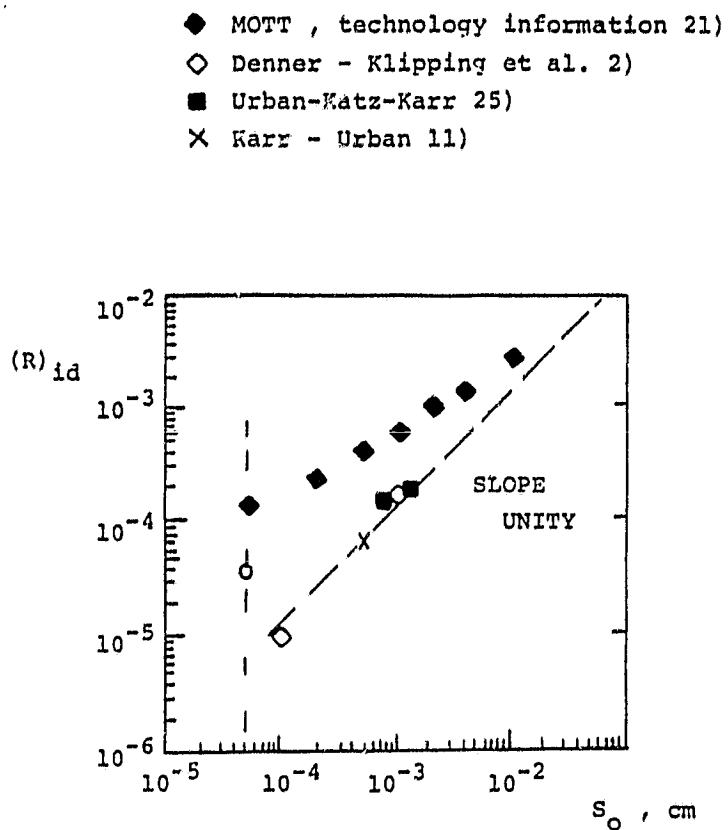
In the course of the work the square root of the permeability turned out to be a most useful quantity for size characterization. This characteristic length is written as

$$L_K = (K_p)^{1/2} \quad (2)$$

The permeability K_p is measured for each plug considered. Then L_K represents the plug's throughput conditions under consideration.

In the historical search for a meaningful length other attempts have been made. For instance a slightly different length has been based on the observation that for capillary flow and for slit flow one may write the mean speed \bar{v} as a simple function of the pressure gradient (∇P) in the laminar regime where the shear viscosity (η) impedes the flow effectively: $\bar{v} = \frac{\nabla P}{\eta(d/2)^2}$. The factor ζ is between (1/12) and (1/8), i.e. of the order of magnitude 0.1. Based on this observation, the early work on plug size definitions has considered the length $(K_p/0.1)^{1/2}$. For a perspective on sintered stainless steel plugs and other metal plugs, the summarizing graph from a previous report³⁾ is reproduced below as Figure 1. It is noted that the stainless steel data above 2 μm represent the state of the art around 1978. The 1/2 μm plug added more recently to the stainless steel production line has been studied by Hendricks et al.⁴⁾. Its permeability has been assessed on the basis of the low temperature measurements⁴⁾, at low speed (Figure 2) with $L_K = 34 \mu\text{m}$. Inclusion of the value in Figure 1 indicates that the manufacturing of this limit-size plug may still be difficult. Aside from the classification difficulties a rather uniform application of pressure during the presintering stage may be required.

ORIGINAL PAGE IS
OF POOR QUALITY



"Ideal hydraulic radius" based on cylindrical parallel duct system versus pore size (s_o).

$$(R)_{id} = (K_p / \zeta_o)^{1/2}; \zeta_o = 0.1$$

Figure 1. Initial evaluation of a characteristic plug size for throughput (from RN 576 (7-80) and Ref. 3 respectively; s_o represents the retention (nominal) of spherical particles during filtration;

○ (open circle) = Value deduced from the $0.5 \mu\text{m}$ plug data of Hendricks et al. 4) (dashed line, Fig. 2).

ORIGINAL PAGE IS
OF POOR QUALITY

STAINLESS STEEL POROUS PLUG

3×10^{-9} (5×10^{-5} cm)

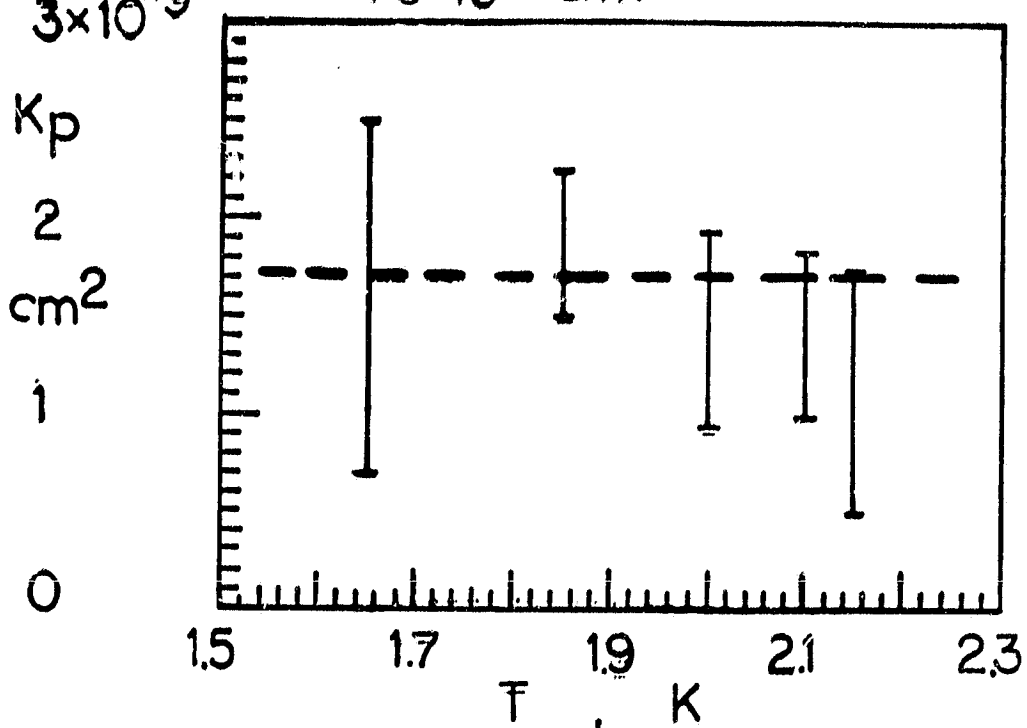


Figure 2. Permeability of normal fluid flow at low temperatures of a $1/2\text{-}\mu\text{m}$ plug (nominal size) of Reference 4 ;
The dashed line indicates $K_p = 1.7 \times 10^{-9} \text{ cm}^2$ for the roton depletion limit .

TRANSPORT EQUATIONS

In this discussion the two-fluid model of Helium II is used with occasional reference to microscopic approaches.

Because of the occurrence of the flow transition from laminar to turbulent convection, very much attention has been given to critical velocities. They have been treated exhaustively in the Huntsville Liquid Helium II Conference⁵⁾. It is mentioned here that one of the more recent criteria employed is Dimotakis' critical condition.⁶⁾ In the limit of low temperatures with high superfluid ratio ($\rho_s/\rho \rightarrow 1$), i.e. roton depletion conditions, Dimotakis' criterion may be compared to the classical Reynolds number of normal fluid flow. It turns out that both, the classical number, and the Dimotakis' number, in this limit have the same order of magnitude of 10^3 . Consequently, use has been made of this condition (by relating the normal fluid shear viscosity (η_n) to the Gorter-Mellink transport function ($A_{GM} = A_{GM}(T,P)$)). Thus, in general, A_{GM} is a function of pressure plus temperature T. A_{GM} is referred to in Dimotakis' criterion,⁶⁾ and it is noted that the original work by Gorter-Mellink has been solely restricted to zero net mass flow. However, early flow investigations of He II mass flow have incorporated attempts to extend the use of the Gorter-Mellink function to turbulent He II convection in general including forced convection modes. In the subsequent discussion, some of the most frequently mentioned mean field flow equations for ducts are listed, and it is noted that the zero net mass flow mode provides an upper bound to entropy/heat flow of a phase separator for a specified temperature difference. For this reason the zero mass flow mode ($j = 0$) has been the first step in gaining a better understanding of phase separator transport.

While $j = 0$ is emphasized, also a few other equations are given below.

For microscopic details of zero net mass flow we refer to the recent summary by Tough⁷⁾ and Donnelly-Vinen et al.⁸⁾. As in classical fluid mechanics, the turbulent regime is the most challenging area of inquiry. For instance, the pressure drop through a long duct with fully developed turbulent flow often is quoted using the Blasius rule⁹⁾. According to the duct flow experiments, the product of the friction factor and the fourth root of the Reynolds number is constant ($= 0.3164$). The rule is written for the purposes of the He II flow assessment as⁷⁾

$$|\nabla P| = 0.158 \eta_n^2 [qD/(\eta_n ST)]^{1.75}/(\rho D^3) \quad (3)$$

(ρ density, D diameter, S entropy per unit mass, q heat flux density, T temperature). Equation (3) indicates that the shear viscosity of the normal fluid exerts only a small influence because of the dominance of vortex shedding processes. A serious disadvantage of equation (3) for porous media use is the requirement of smooth walls which certainly is not satisfied with the porous plugs employed as phase separators so far. Thus, one may only get order of magnitude estimates from the Blasius rule.

The zero net mass flow equations for a duct are usually written in terms of heat flux density (q)-temperature gradient ($|\nabla T|$) equations. The original Gorter-Mellink result contains the unknown transport function A_{GM} :

$$|\nabla T| = A_{GM} (\rho_n/S) [q/(\rho_s ST)]^3 \quad (4)$$

(ρ_n = normal fluid density, $(\rho_n/\rho) = 1 - \rho_s/\rho$). Use of Dimotakis' criterion⁶⁾ at the low end of the turbulent regime of Gorter-Mellink convection, and addi-

ORIGINAL PAGE IS
OF POOR QUALITY

tional use of a scaling power law near the lambda point vicinity has permitted elimination of considerable uncertainties. Thus, the function A_{GM} , which is empirical from the macroscopic point of view, has been replaced by

$$A_{GM} = K_{GM}^{-3} (\rho/\rho_s) / \eta_n \quad (5)$$

Thus, only one single constant ($K_{GM} = 11.3$) has remained as parameter to be determined from experiments. All other quantities are thermophysical properties of He II. The temperature gradient, recast in this manner in terms of the known thermophysical properties, is

$$|\nabla T| = K_{GM}^{-3} (\rho/\rho_s) (\rho_n/\eta_n) S^{-1} [q/(\rho_s ST)]^3 \quad (6)$$

Thus the temperature gradient rises strongly with an increase in q . The explicit form for the heat flux is

$$Q = A_c q = A_c K_{GM} \rho_s ST (\rho_s/\rho)^{1/3} [(\eta_n/\rho_n)^{2/3} |\nabla T|]^{1/3} \quad (7)$$

Thus, Q is proportional to the cross section and a weak function of an externally imposed temperature gradient. For porous media, modifications are necessary, as discussed in Appendix A.

Remarks on the history of the determination of the Gorter-Mellink function A_{GM} appear to be appropriate. The microscopic approach of Vinen⁸⁾ has considered interaction of a quantized vortex system with normal fluid in order to permit prediction of A_{GM} . This has led to use of microprobes, such as ions, for experimental verification of the microscopics.

Macroscopically, B. W. Clement in his M.Sc. thesis at UCLA (1966)¹¹⁾ has adopted a non-dimensional measure of A_{GM} by evaluation of the ratio of the

dimensionless normal fluid flow rate to the third root of the dimensionless driving force. It turned out that this quantity, designated as $C(T)$ at that time, is to first order only a function of the order parameter of He II. It is interesting to note that Sink-Peck-Liggett¹²⁾ have used this early form which is incorporated in the 1968 survey by John Clark in Reference 13.

The introduction of Dimotakis' criterion⁶⁾ in 1974 allowed an immediate contact with the Gorter-Mellink approach at its low temperature and low speed end. A check of the ratio $C(T)$ at the LT-15¹⁴⁾ in 1975 turned out to be quite encouraging. Therefore S. C. Soloski studied in his Ph.D. research¹⁰⁾ extensively the validity of the combined Dimotakis-Clement approach for the evaluation of A_{GM} . This work led to the numerical value of $K_{GM} = 11.3$ for relatively wide ducts with diameters above the order 10^{-3} cm. Thus a very successful reduction of an unknown function to a constant in conjunction with thermophysical properties of He II was the result of that work. The recent detailed measurements of Kamioka with pressurized HeII¹⁵⁾ provide quite a satisfactory confirmation of the usefulness of the present form of the Gorter-Mellink equations. In particular the check of the pressure effect on $K_{GM}^{16})$ has been quite rewarding. We note that prior to that work there had been no straightforward means available to predict q on the basis of an unknown function $A_{GM}(P)$.

PLUG RESULTS AND CONCLUSIONS

Concerning plug results we refer primarily to Appendices A and B, and it is noted that Appendix C carries supplementary information. Additional points arising from oral discussion are listed at the end of Appendix A.

It is concluded that the frame of reference established by the plug transport studies at zero net mass flow is quite encouraging. This frame establishes an upper bound to the transport rate at a given driving force. Above the size of $5 \mu\text{m}$ (nominal manufacturer quotation) of sintered metal plugs, the manufacturing process appears to be well defined within the range of uncertainty known for similar packed particle beds with a specified nominal size. Thus, improvements appear to be on the horizon also for the particle size range from nominally $0.5 \mu\text{m}$ to $10 \mu\text{m}$ studied and visualized in the middle of the seventies for initial "Fairbank plug" design and application. The other point concerns the applicability of permeability values at room temperatures to the low temperature conditions of the plugs. There are two types of questions to be answered from both the manufacturer's point of view and the application point of view. The first question concerns the general validity of a one-to-one relationship between the room temperature permeability K_p and the normal fluid permeability K_{pn} at low temperatures. The second point concerns the scaling from K_{pn} and its Darcy-Stokes law respectively for $j = 0$, the finite mass flow case including turbulent flow conditions.

REFERENCES

1. A. R. Urbach and P. V. Mason, IRAS Cryogenics System Flight Performance Report, Cryog. Eng. Conf. Colorado Springs, Aug. 1983, paper CB-1.
2. Jeffrey M. Lee, M.Sc. thesis, Univ. of Calif. Los Angeles, 1983.
3. Sidney W. Yuan, M.Sc. thesis, Univ. of Calif. Los Angeles, 1981; RN 576, Cryogenics Lab., Univ. of Calif. Los Angeles, 1979.
4. J. B. Hendricks and G. R. Karr, Proc. ICEC-9 (Kobe, Japan), Butterworth, 1982, p. 190.
5. D. R. Ladner, A Review of Superfluid Critical Velocities, Space Helium Dewar Conf. and Workshop, Huntsville, Alabama, Aug. 1983.
6. P. E. Dimotakis, Phys. Rev. A10, 1721, 1974.
7. J. T. Tough, , in Progr. Low Temp. Phys. (Ed. D. F. Brewer), North Holland, Amsterdam, 1982, Vol. VIII, Ch. 3.
8. C. F. Barenghi, R. J. Donnelly and W. F. Vinen, J. Low Temp. Phys. 52, 189, 1983.
9. H. Schlichting, Boundary Layer Theory, McGraw-Hill, New York, 4th Ed., 1960, p. 502
10. S. C. Soloski, Ph.D. dissertation, Univ. Calif. Los Angeles, 1977; S. C. Soloski and T. H. K. Frederking, Int. J. Heat Mass Transfer 23, 437, 1980.

11. B. W. Clement, M.Sc. thesis, Univ. Calif. Los Angeles, 1966; B. W. Clement and T. H. K. Frederking, Boulder Meeting, IIR 1966, p. 49.
12. C. A. Sink, S. D. Peck and M. W. Liggett, Cryog. Engr. Conf., Colorado Springs, 1983, paper IC-21.
13. J. A. Clark, Adv. Heat Transfer 5, 325, 1968.
14. T. H. K. Frederking et al., Proc. LT-14, North-Holland, Vol. 1, 291, 1975.
15. Y. Kamioka, Cryogenics 23, 367, 1983.
16. Y. Kamioka, J. M. Lee and T. H. K. Frederking, Proc. ICEC-9, Kobe, Butterworth, 1982, p. 283.

APPENDIX A **

SINTERED PLUG FLOW MODULATION OF A VAPOR-LIQUID PHASE SEPARATOR FOR A HELIUM II VESSEL*

T. H. K. Frederking, C. Chuang, Y. Kamioka, J. M. Lee
and S. W. K. Yuan

University of California
Los Angeles, California 90024

ABSTRACT

A sintered stainless steel plug system is described which has the purpose of acting as a vapor-liquid phase separator between a liquid Helium II bath and the vapor vent line. A variable cross sectional area component is incorporated in order to modulate the mass flow rate through the separator. System details and data are presented.

INTRODUCTION

Future planned space missions will require extended cryogen storage. Thermodynamic state control of the cryogenic liquid He II requires well-defined separation of the vapor from the liquid at the vessel vent line exit. For such systems designed to operate in the range from 1 K to 2 K, passive vapor-liquid phase separation of superfluid He II has been extensively studied under conditions of constant heat load²⁻⁶.

In practical systems however, variable heat loading of the cold He II reservoir is often encountered. To prolong cryogen life span, optimum performance of such systems by the use of active flow modulation devices are needed. System developments

*Work supported in part by the National Aeronautics and Space Administration, Ames Research Center, Moffett Field.

**) Presented at Cryogenic Engineering Conference, Colorado Springs 1983
(paper CB-3)

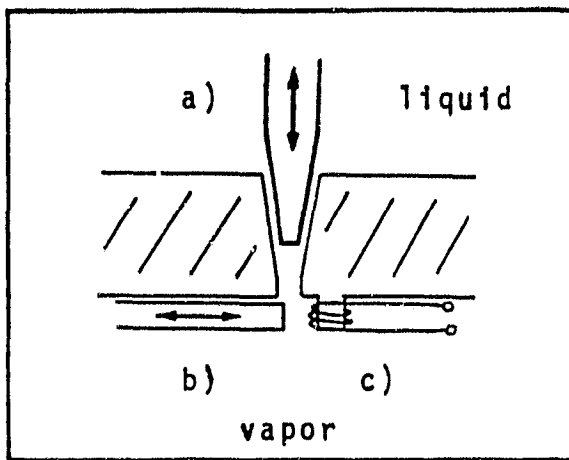


Figure 1. Schematic diagram of mechanical and thermal means of varying the throughput of a phase separator.

and designs under consideration include mass flow modulation using components movable in either the flow direction (Fig. 1a)^{7,8} or perpendicular to the flow (Fig. 1b) through the separator. Variation of the thermomechanical driving potential by use of a downstream heating element has also been investigated (Fig. 1c)⁶.

The present paper has the purpose of describing a system incorporating a variable area component of the type (1b), i.e., downstream of the plug. After a discussion of porous plug flow characterization, the system is outlined, and experimental results are presented. Finally, conclusions are drawn.

POROUS MEDIA CHARACTERIZATION

The transport at zero net mass flow has been found to be a useful reference case for the vapor-liquid phase separation mode⁹. Counterflow of normal fluid, carrying heat and entropy, and superfluid¹⁰ is described in the frame of reference of the two-fluid model¹⁰. Two convective flow regimes of heat transport exist: first, laminar, linear transport, and second, turbulent non-linear mean field transport. The laminar flow equation may be written as a modified Darcy flow equation for the normal fluid component, driven by thermo-osmotic (thermomechanical) forces^{11,12}. The mean, superficial flow velocity is

$$v_n = K_{pn} |\nabla P_T| / \eta_n \quad (1)$$

The speed v_n is the ratio of the volumetric flow rate of normal fluid to the total cross section of the porous medium. The gra-

ORIGINAL PAGE IS
OF POOR QUALITY

dient $|\nabla P_T|$ is equal to $\rho S |\nabla T|$. The related superficial rate of convective heat transport is expressed also as a mean quantity.

$$q = \rho S T v_n = \rho S T K_{pn} |\nabla P_T| / \eta_n \quad (2)$$

The comparison with the solid state thermal conductivity of the porous medium is conveniently based on the apparent thermal conductivity evaluated from Equation (2):

$$k_{app} = (\rho S)^2 T K_{pn} / \eta_n \quad (3)$$

Again, k_{app} constitutes a superficial quantity representing mean field conditions. The geometry parameter $(K_{pn})^{1/2}$ is a characteristic size of the space filled with He II during the counter-flow conditions imposed.

In the non-linear high heat flux regime for fully developed turbulent convection, the normal fluid velocity is described by¹³

$$v_n = K_{GM} (\rho_s / \rho) ((\rho_s / \rho) (\eta_n / \rho_n) |\nabla P_T| / \rho)^{1/3} \quad (4)$$

The dimensionless parameter K_{GM} is known for wide insulated ducts operated in the high heat flux regime of Gorter-Mellink turbulence ($K_{GM} = 11.3$ for duct diameters above 10^{-3} cm)¹⁴. Thus, the related superficial heat flux density becomes

$$q = K_{GM} \rho_s S T ((\rho_s / \rho) (\eta_n / \rho_n) \rho S |\nabla T| / \rho)^{1/3} \quad (5)$$

In general K_{GM} varies as a function of porous media parameters. A comparison of Equations (2) and (5) shows that k_{app} is no longer a well-defined quantity in the turbulent regime.

Figure 2 displays k_{app} of Equation (3) associated with normal fluid Darcy flow through the porous medium. Because of $S \sim T^{3.6}$ k_{app} is a strong function of the temperature. Figure 2 is based on results of Refs. 15 to 17 and 13. The K_p -values include the order of magnitude range of phase separator plugs. For instance, at 1.8 K, for $(K_{pn})^{1/2}$ of the order of 10^{-5} cm, the apparent thermal conductivity reaches the order $1 \text{ W}/(\text{cm} \text{ K})$. Thus, for this type of transport, the k_{app} -value of the normal fluid exceeds the thermal conductivity of plug materials, such as stainless steel.

EXPERIMENTAL EQUIPMENT AND RESULTS

The phase separator plug is the main component of the system. A sintered stainless steel plug of Mott Metallurgical Corporation (Farmington, CT) of alloy 316L is used (with nominal size of 2 μm for spherical particle retention; thickness 1/8 in = 0.318

ORIGINAL PAGE IS
OF POOR QUALITY

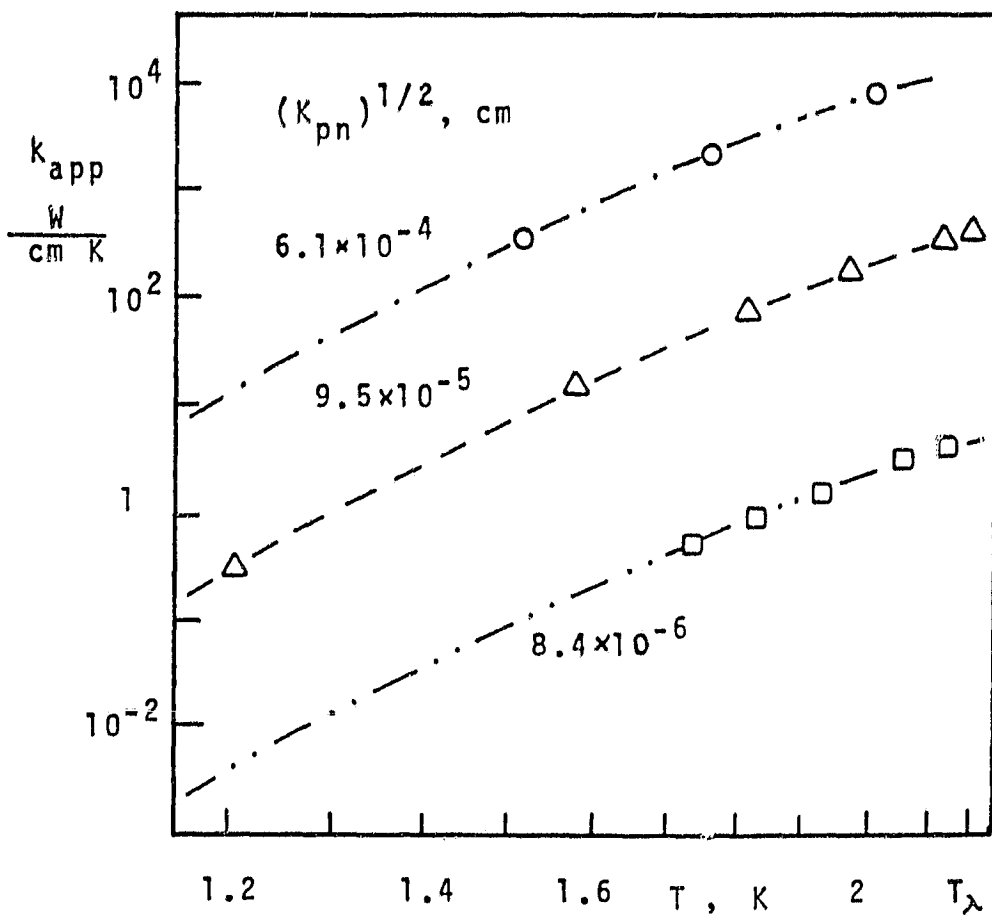


Figure 2. Apparent thermal conductivity associated with Darcy flow of normal fluid through porous media.

cm, diameter 2.54 cm). The plug is located in the system shown schematically in Figure 3. Static pressure taps and carbon resistance thermometers measure differential pressure and temperature across the plug. A flow control plate and a shutter assembly driven by an electric motor allow modulation of the flow through the separator system. The latter is located at the lower end of the vent tube which in turn is insulated from the outer bath confining wall. A heater in the outer bath simulates variable heat loads.

Figure 4 shows the flow control plate and shutter assembly. Both have semi-circular regions which permit maximum mass throughput when the semi-circles coincide. When the shutter is rotated 180 degrees away from the "full open" position, minimum throughput is attained. The plate contains 40 holes with a diameter of 0.159 cm (= 1/16 in). The porous plug terminates in a

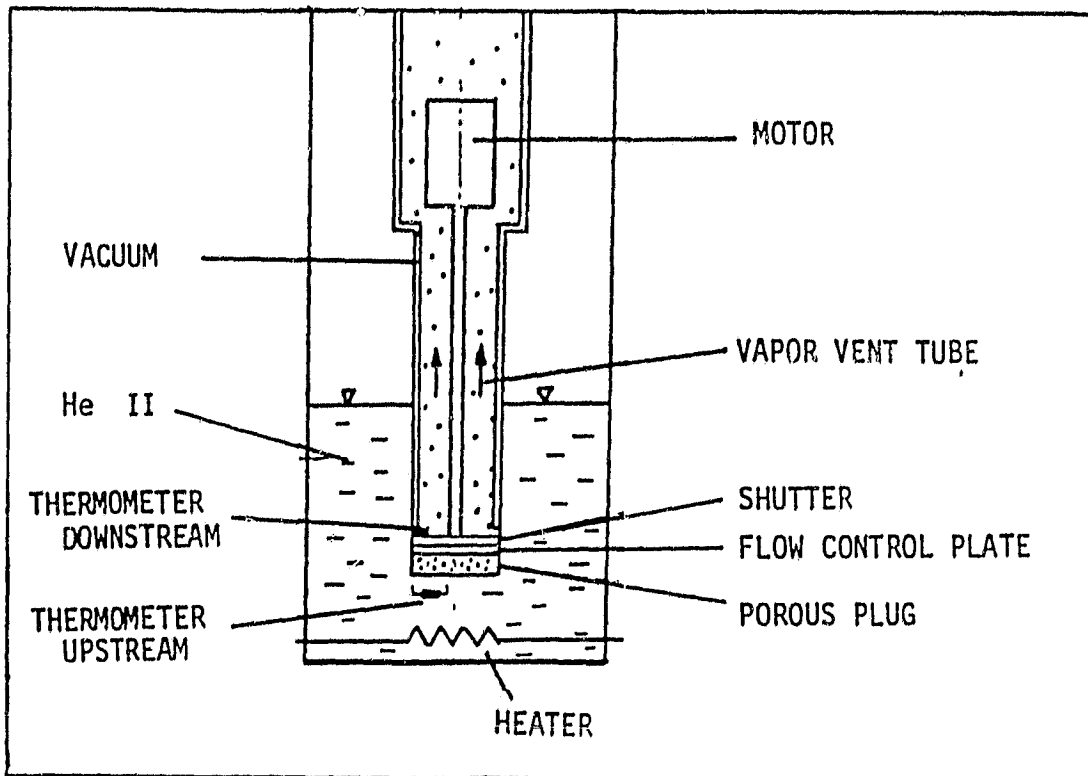


Figure 3. Vapor-liquid phase separator system(schematically)

"rough surface". In order to match geometries, a filter material (0.02 cm thick, glass microfiber paper) is located between the plug and the control plate.

During the initial runs the throughput of the stationary system has been determined. An external bypass valve connecting

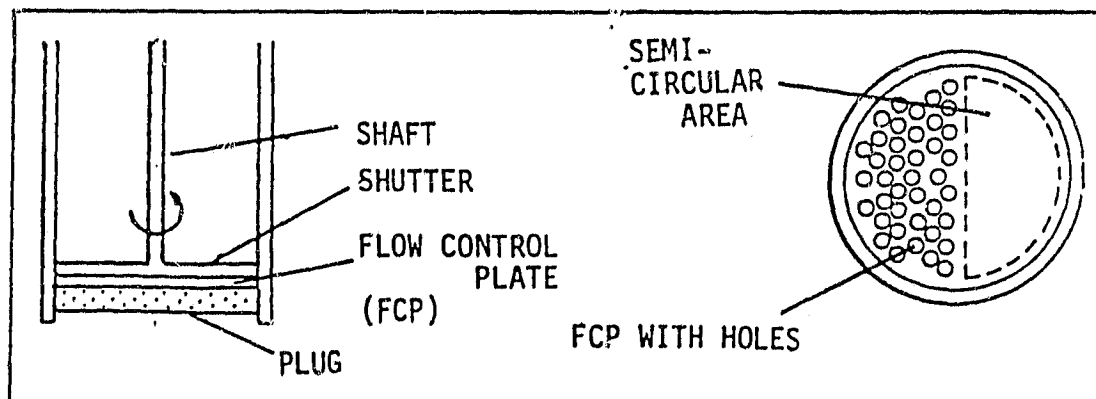


Figure 4. Flow modulation system (schematically);
a . Assembly; b. Flow control plate.

ORIGINAL PAGE IS
OF POOR QUALITY

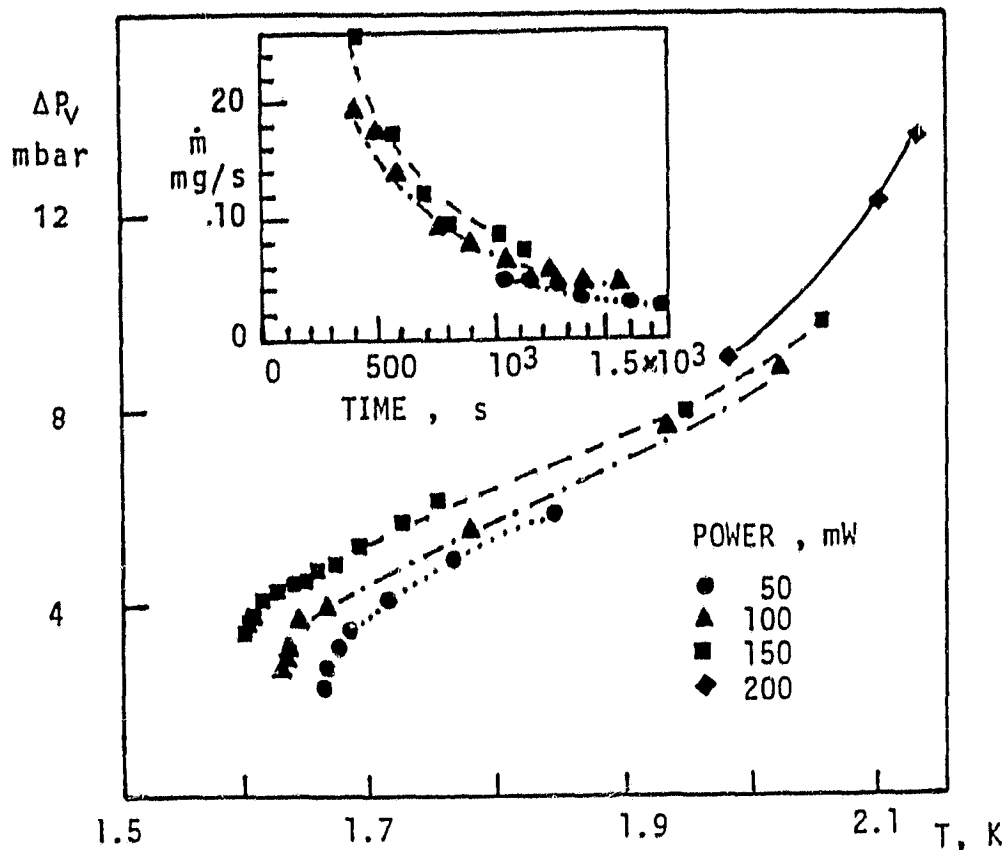


Figure 5. Pressure difference across plug assembly during stationary system experiments; insert: mass flow rate as a function of time at various external power inputs.

the upstream and downstream sides of the plug provides pressure equilization during the helium transfer and cooldown process. Below the lambda temperature, runs have been conducted making use of slow downstream pumping rates with the external bypass valve closed and an upstream pump system shut off from the liquid bath. The heater permits simulation of various heat loads on the liquid bath. The mass flow through the plug was determined from the rate of change of the He II level with time.

The vapor pressure differences across the plug registered during the runs are presented in Figure 5 for various externally applied power inputs to the heater. The inset of Figure 5 shows mass flow rates as a function of time.

Using the same procedure as described above, flow modulation has been verified during slow rotation of the motor (0.1 rpm at 27 V nominal voltage). The modulation results are shown as mass flow rate versus time in Figure 6. It is seen that \dot{m} varies from 10 mg/s to 22 mg/s.

ORIGINAL PAGE IS
OF POOR QUALITY

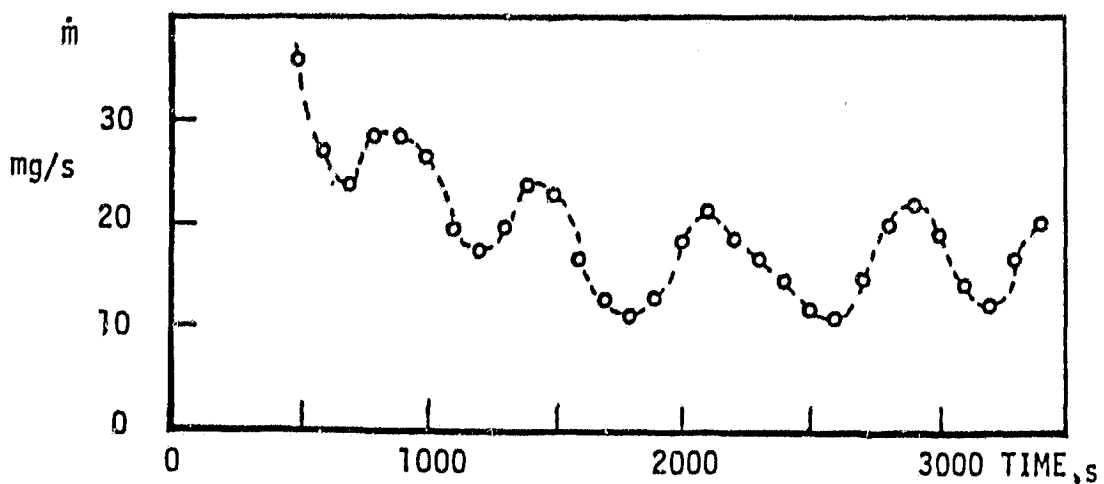


Figure 6. Mass flow rate during slow rotation of the shutter at zero externally applied heater power.

CONCLUSIONS

Phase separation flow modulation by means of a downstream variation of the mass throughput has been demonstrated using transverse motion of a movable shutter-like component.

Acknowledgment. We are indebted to Dr. Y. I. Kim, G. S. Brown and M. Johansson for their contributions in the course of this work. The plug characterization efforts have been supported in part by NSF.

NOMENCLATURE

k_{app}	Apparent thermal conductivity
X_{GM}	Dimensionless Gorter-Mellink parameter (Eq. 4)
K^{pn}	Normal fluid permeability
\dot{m}^{pn}	Mass flow rate
P	Pressure
q	Heat flux density (mean value)
S	Entropy
T	Temperature
v	Mean flow speed
η_n	Normal fluid shear viscosity
ρ	Density

Subscripts

n	normal fluid
o	superficial value (rate per total cross section)
s	superfluid
T	thermo-osmotic (thermomechanical)
v	vapor pressure

ORIGINAL PAGE IS
OF POOR QUALITY

REFERENCES

1. P. V. Mason, Space cryogenics in the 1980's, Proc. 8th Int. Cryog. Eng. Conf., IPC Press, Guildford, 1980, p. 6.
2. K. Lüders and G. Klipping, Phase separation under zero g conditions, Proc. 8th Int. Cryog. Eng. Conf., IPC, 1980, p. 14.
3. J. B. Hendricks and G. R. Karr, Characterization of superfluid porous plug performance, Proc. 9th Int. Cryog. Eng. Conf., Butterworth, Guildford, 1982, p. 190.
4. U. Schotte and H. D. Denner, The mechanism governing phase separation of Helium II by means of narrow channels, Proc. 8th Int. Cryog. Eng. Conf., IPC Press, Guildford, 1980, p. 27.
5. J. R. Becker, P. Blaser, M. Perdu and R. Prost, Passive phase separator for superfluid helium for the European space cryostat "Chresus", Proc. 8th Int. Cryog. Eng. Conf., IPC Press, Guildford, 1980, p. 22.
6. M. Murakami, N. Nakaniwa and K. Uyama, Porous plug phase separator for superfluid He II, Proc. 9th Int. Cryog. Eng. Conf., Butterworth, Guildford, 1982, p. 194.
7. H. D. Denner, G. Klipping, I. Klipping, K. Lüders, J. Menzel, U. Ruppert and H. Walter, Performance of an active phase separator for helium, Proc. 8th Int. Cryog. Eng. Conf., IPC Press, Guildford, 1980, p. 32.
8. H. D. Denner, G. Klipping, I. Klipping, K. Lüders, T. Oesterlich, U. Ruppert, Z. Szűcs and H. Walter, Improved active phase separator for Helium II space cooling systems, Adv. Cryog. Eng., Vol. 27, Plenum Press, New York, 1982, p. 1079.
9. C. Chuang, Y. I. Kim and T. H. K. Frederking, Vapor-liquid phase separation of cryogenic liquid storage systems below the lambda point (He^4), Cryog. Processes and Equipment in Energy Systems, ASME Pub. No. H00164, 1980, p. 135.
10. L. D. Landau, The theory of superfluidity of Helium II, J. Phys. (USSR), Vol. 5, 1941, p. 71.
11. S. W. K. Yuan, M.Sc. thesis, University of California, Los Angeles, 1981.
12. S. W. K. Yuan and T. H. K. Frederking, Darcy law of thermo-osmosis for zero net mass flow at low temperatures, Proc. ASME-JSME Thermal Eng. Joint Conf., Honolulu, ASME, NY, 1983, p. 191.
13. J. M. Lee, M.Sc. thesis, University of California, Los Angeles, 1983.
14. S. C. Soloski and T. H. K. Frederking, Dimensional analysis and equation for axial heat flow of Gorter-Mellink convection (He II), Int. J. Heat Mass Transfer, Vol. 23, 1980, p. 437.
15. T. H. K. Frederking, H. van Kempen, M. A. Weenen and P. Wyder, Critical counterflow in narrow He II-filled channels, Physica, Vol. 108B, 1981, p. 1129.
16. H. Forstat, Length effect in the heat transport in Helium II, Phys. Rev., Vol. 111, 1958, p. 1450.
17. W. H. Keesom and G. Duyckaerts, Measurements of the thermal conductivity and the thermomechanical effect of liquid He II, Physica, Vol. 13, 1947, p. 153.

Additional Questions, Comments and Discussion

There have been several points raised in the paper discussion pertaining to the mass flow rate, to quasi-steady conditions and to the minimum in the flow rate associated with the device.

Question # 1 is concerned with the mass flow conditions. In the present theoretical discussion the zero net mass flow case is used as reference solution. This leads to the apparent thermal conductivity of Darcy convection based on the normal fluid permeability (K_{pn}). The latter in turn is related to the "classical" flow permeability of room temperature Newtonian fluid. The finite mass flow case is located within an envelope given by the dimensionless laminar Darcy-Stokes data and the related turbulent transport characteristics. Some indirect hints concerning this point are provided by the early studies of the Leiden group (W.M. Van Alphen et al. , LT-9, Plenum 1965). When the driving force for mass flow is in the same direction as the driving force for entropy flow, a larger flow resistance results. In other words, the zero net mass flow solution constitutes an upper bound to finite mass flow data. At low temperatures, both solutions approach each other closely.

Question # 2 pertains to steady state results with the shutter kept stationary in different positions in different runs. This approach requires a large number of data points. The present technique instead probes slowly the transport rates during rotation at quasi-steady conditions. Thus, a rather complete survey of the angular range is obtained. The data show dominance of the fundamental frequency provided by the shutter-motor drive system., i.e. a nearly sinusoidal signal is obtained. Thus, position and flow rate are related to each other by a simple function. Prior to quasi - steady conditions, the initial pumpdown near the lambda temperature involves a relaxation time needed to get from the negative pressure difference (liquid breakthrough condition) to the phase separation mode. This process of flow reversal is a feature

of the present experimental technique , and for the initial period of time heat capacity terms may be used to obtain data over an even more extended range in the temperature of the upper bath.

Question # 3 is concerned with the minimum mass throughput of the flow modulation device. . It is noted that the design adopted does not incorporate a shut-off device built into the system . The present construction of the plug-shutter assembly with the micro-fiber - control plate subsystem extends the flow rate range obtainable with a fixed geometry plug system. Thus, the minima in throughput of mass of He⁴ (Figure 6) constitute the finite mass flow rates established by the shutter in the "fully closed" position.

A P P E N D I X B ⁺

PLUG FLOW COMPARISON

S. W. K. Yuan, J. M. Lee, Y. Kamioka and T.H.K. Frederking

University of California
Los Angeles, CA 90024

ABSTRACT

Flow through porous media including sintered phase separator plugs at low temperatures has been investigated for plugs in the pore size range from 1 to 10 μm . Experiments have been conducted in the liquid Helium II range with 2 μm stainless steel plugs (nominal particle retention size of filtration). It is proposed to provide a common frame of reference for this type of plugs by means of the modified Darcy flow permeability of normal fluid transport.

INTRODUCTION

In Helium II vessels, sintered porous plugs may serve as venting devices which provide well-defined separation of the vapor phase from liquid, and stable vapor removal and entropy passage respectively. Various plug investigations have been reported in the literature, e.g., Reference 1, within different frames of reference. One drawback of this situation is the absence of a common plug characterization frame which allows an easy comparison of data taken under different conditions. It is the purpose of the present contribution to propose a common frame of reference such that some of the difficulties encountered in the assessment of plug suitability for a specific venting task are eliminated.

The frame of reference is based on experiments conducted at both "high" and He II temperatures. First, a conceptual basis is provided relying on the two-fluid model of He II in conjunction with Darcy flow of Newtonian fluid. Subsequently, the experiments are outlined, and after a discussion of the data conclusions are presented.

⁺) Presented at Space Helium Dewar Conference and Workshop, Huntsville AL 35899, Aug. 1983.

TRANSPORT REGIMES: PHENOMENOLOGICAL FLOW REGIME DESCRIPTION BASED ON THE TWO FLUID MODEL

It appears to be useful to describe the transport through porous media, in general, in terms of the two-fluid model for liquid He². (It is noted that in applied physical chemistry, analog conditions referring to mass osmosis have been utilized in the early discussion of two-fluid ideas, e.g. by Tisza³ and Wilks⁴.) For the sintered plugs often used in the evaluation of phase separator capability, a convenient frame of reference is based on the zero net mass flow mode: entropy and heat are carried by the normal fluid which moves in counterflow to superfluid such that there is no net transport of mass. There appear to be two major transport regimes: first, the laminar Stokes regime with entirely negligible inertia effects; second, an asymptotic regime, of highly disordered turbulence achieved after a transition has taken place toward very chaotic flow conditions. The superfluid is an ideal Euler fluid, and the normal fluid has entropy and viscosity. A basic assumption noted in the present context is the adoption of Newtonian fluid properties of the normal fluid subject to the specific constraints of superfluid He II. On the basis of this assumption, a tie-in with "classical" fluid flow in the Stokes regime appears to be readily available. Thus a characterization of the flow may be based on well-known correlations for packed beds and similar porous media.

For classical Newtonian fluids, Reynolds⁵, proposed a linear superposition of a linear flow rate contribution ($\sim v$) in the Stokes regime and a non-linear term ($\sim v^2$) for the pressure gradient prediction in general; (v mean velocity). The linear term for Stokes flow at low speed has been inspected for packed bed flow phenomena in detail by Kozeny⁶, Carman⁷ and others. A more recent equation paralleling Reynolds' approach has been proposed by Ergun⁸. Several modifications of the Ergun equation have been discussed by Macdonald et al.⁹. In the Stokes regime the equations under consideration have an asymptote characterized by

$$\lim_{v \rightarrow 0} (\eta \bar{v}_o) / |\text{grad } P| = K_p \quad (1)$$

K_p is the permeability, η shear viscosity, \bar{v}_o superficial flow speed = volumetric flow rate divided by the total packed bed cross section (empty cross section). The externally applied gradient, grad P , may comprise an applied pressure contribution and a gravitational term. Equation (1) is a simplified form of Darcy's equation for an isotropic medium¹⁰. The Darcy permeability for a system of near-spherical particles is predicted by the Carman-Kozeny-Ergun approach as

$$K_p = \zeta_{CK} \frac{\frac{D_p^2 \epsilon^3}{P}}{(1-\epsilon)^2} \quad (2)$$

(D_p particle diameter, ϵ porosity). The constant ζ_{CK} varies with the type of particles. It has the value (1/150) in the Ergun equation⁸.

ORIGINAL PAGE IS
OF POOR QUALITY

For near-spherical particles, the constants of the Carman-Kozeny approach differ but little. However for fibrous and sintered materials considerable variations in permeability-related parameters may be encountered. Therefore, a very detailed approach may, at best at the present time permit predictions of the order of magnitude of phase separator plugs with very fine pores. For instance, for a porosity of $\epsilon \approx 1/3$, D_p of the order 10 μm , the characteristic size $(K_p)^{1/2}$ of the fluid-filled space turns out to be of the order $10^{-4} \text{ cm} = 1 \mu\text{m}$. This is illustrated in Figure 1 for a stainless steel plug (2 μm nominal particle retention size of filtration).

The Ergun equation is used as the basis of comparison in Fig. 1. The flow resistance in the Stokes regime may be expressed as $R_N = |\nabla P| / v_o = \eta / K_p = 150\eta(1-\epsilon)^2 D_p^{-2} / \epsilon^3$. The resistance ratio R / R_N in general is a function of the appropriate flow rate measure, e.g. modified Reynolds number R_{KE} . In this dimensionless form the Ergun equation is written as

$$R/R_N = 1 + 1.75 R_{KE}/150 \quad (3)$$

With ρ as fluid density the modified Reynolds number is expressed as $R_{KE} = D_p v_o \rho / \eta (1-\epsilon)$.

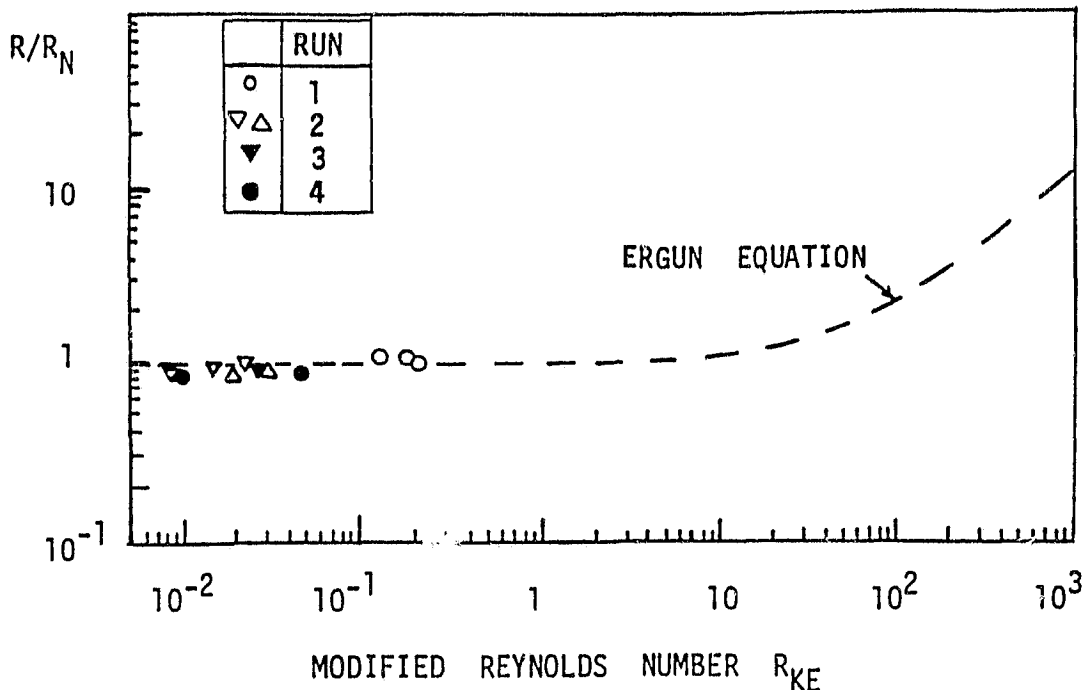


Figure 1 . Flow resistance ratio versus modified Reynolds number R_{KE} for room temperature data of 2 μm plug;
 $D_p = 3.3 \times 10^{-3} \text{ cm}$.

According to Figure 1, the permeability appears to be unchanged, within data accuracy, over an extended flow rate range up to the Reynolds number of unity ($R_{KE} \sim 1$). Thus, the Darcy flow equation (1) may be written as

$$\bar{v}_o = K_p |\nabla p| / \eta \quad (4)$$

Turning to the Stokes regime of zero net mass flow in He II, we note recent research results¹¹⁻¹³: the data support a modified Darcy law for normal fluid transport at low speed:

$$\bar{v}_{no} = K_{pn} |\nabla p_T| / \eta_n \quad (5)$$

(The subscript n characterizes normal fluid properties, e.g. shear viscosity η_n .) The peculiar driving force in He II is the fountain pressure $\nabla p_T = \nabla T(\rho S)$; (ρ density, S entropy of He II per unit mass). The permeability K_p is replaced by the permeability K_{pn} which is of the same order of magnitude as the He I value of K_p above the lambda point. Multiplying both sides of Equation (5) by $[\rho K_{pn}]^{1/2} / \eta_n$, one arrives at a dimensionless form for the normal fluid. Further, heat is transported by normal fluid convection giving rise to a superficial (mean) heat flux density $\bar{q}_o = \rho S T \bar{v}_{no}$. Thus, Equation (5) may be rewritten as

$$N_q = N_{\nabla T} \quad (6)$$

with the dimensionless transport rate

$$N_q = \bar{q}_o K_{pn}^{1/2} (\eta_n S T)^{-1} \quad (7)$$

and a dimensionless driving force, caused by external application of a temperature gradient,

$$N_{\nabla T} = \rho^2 S |\nabla T| K_{pn}^{3/2} / \eta_n^2 \quad (8)$$

In the non-linear regime at high transport rates, the function describing dimensionless flow rate versus dimensionless driving force is at variance with the functional form of Equation (3). In the asymptotic limit of size-independent normal fluid flow through the sintered medium one may write the superficial (mean) heat flux density as¹⁴

$$\bar{q}_o = K_{GM} (\rho_s / \rho) [(\nabla p_T / \rho) (\eta_n / \rho_n) (\rho_s / \rho)]^{1/3} (\rho S T) \quad (9)$$

The parameter K_{GM} is a function of the particular porous medium. It has an upper bound of 11.3 for wide channels¹⁵; (ρ_s / ρ) superfluid density ratio, $\rho_n / \rho = 1 - \rho_s / \rho$. One may write Equation (9) in dimensionless form as

$$N_q (\rho / \rho_s) = K_{GM} (N_{\nabla T} \rho_s / \rho_n)^{1/3} = K_{GM} N_x^{1/3} \quad (10)$$

In some cases it is convenient to express Equation (9) as dimensionless heat flux density q/q_{ref} with a reference heat flux density

$$q_{ref} = (\rho_n / \rho) (T / |\nabla T|) (\eta_n^3 / \rho^2) / K_{pn}^2 \quad (11)$$

This type of transport equation is obtained by multiplication of both sides of Equation (10) by N_x :

$$\bar{q}_o / q_{ref} = K_{GM} (N_{VT} \rho_s / \rho_n)^{4/3} = K_{GM} N_x^{4/3} \quad (12)$$

EXPERIMENTS

Prior to the low temperature runs plug identification at room temperature appears to be convenient avoiding liquid contact with the sintered material. For this purpose the plug surface has been inspected using a surface profilometer with a stylus tip radius of 0.05 cm. Its resolution limit for surface variations is of the order of magnitude 0.3 μm . Records for three stainless steel plugs with size of 2 μm , 5 μm and 10 μm are shown in Figure 2. During the

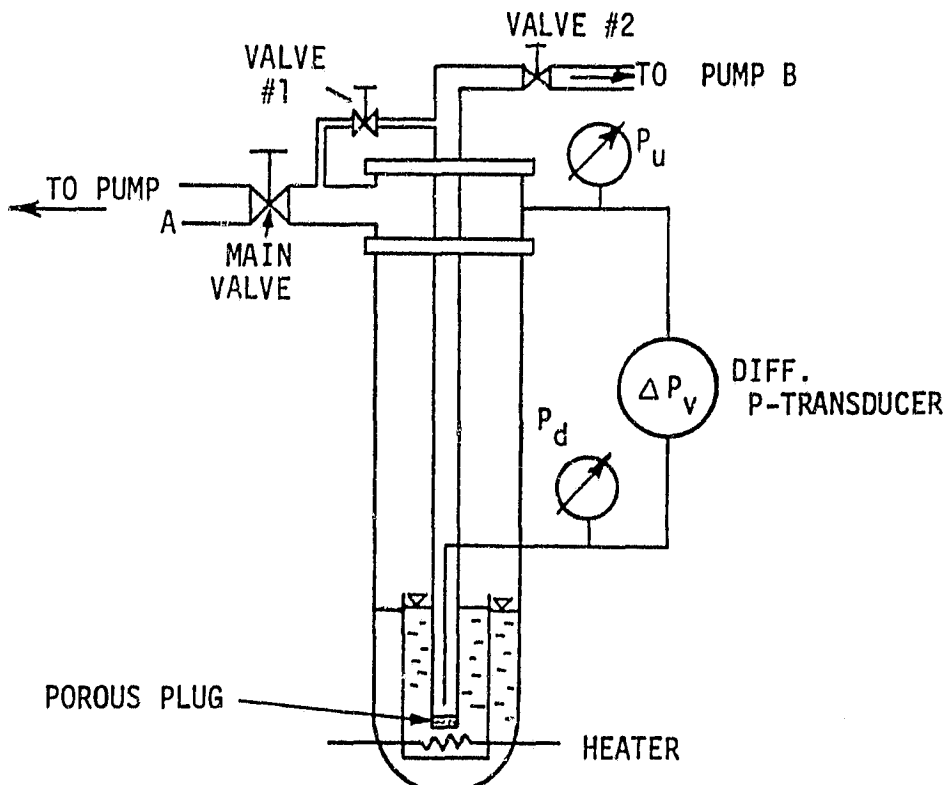
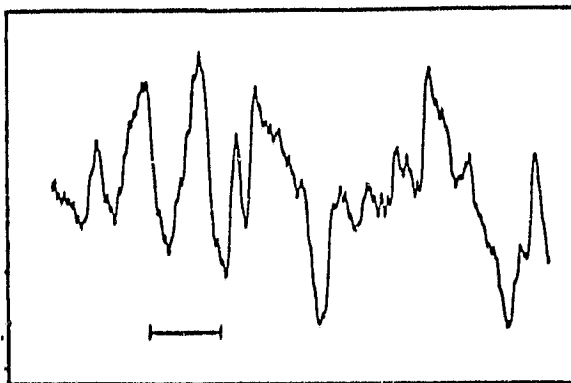
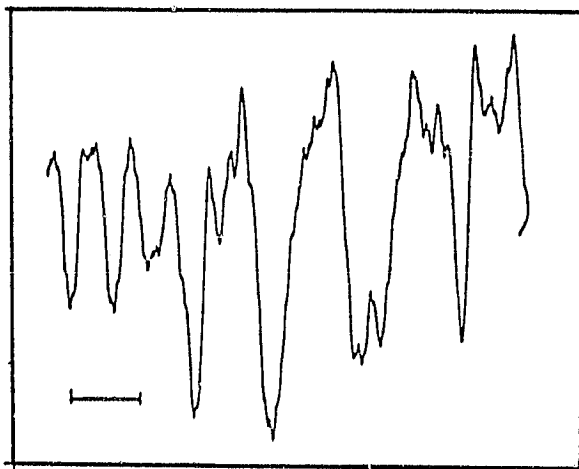


Figure 3 . Experimental system for vapor-liquid phase separation (schematically) .

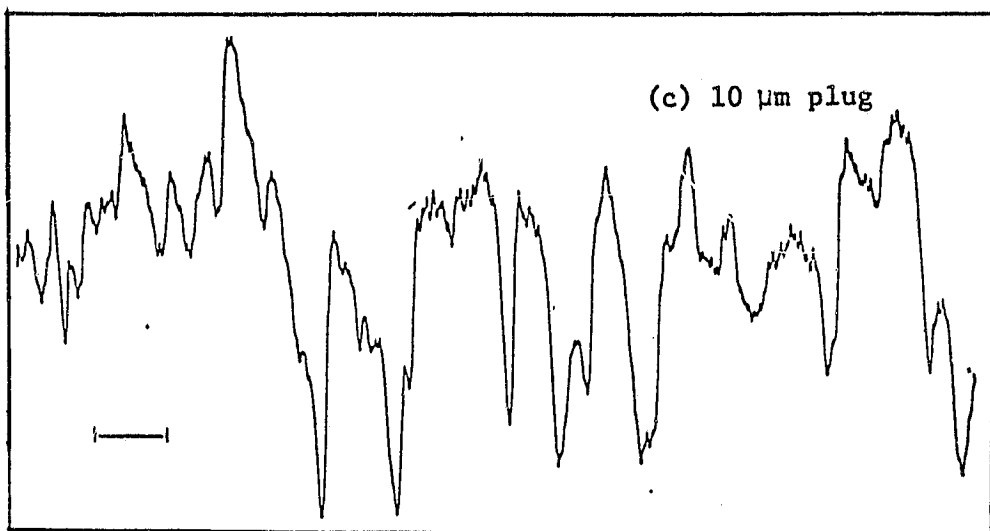
ORIGINAL PAGE IS
OF POOR QUALITY



(a) $2 \mu\text{m}$ plug ; sintered stainless steel;
(sizes given denote size of contaminant particle retained while using the plug as filter device).



(b) $5 \mu\text{m}$ plug



(c) $10 \mu\text{m}$ plug

Figure 2. Profilometer records of stainless steel plugs :
X-Y-plotter signal representing position variations of
plug surface ; [same arbitrary units (A.U.) for (a), (b),
(c)]; $\text{---} = 1 \text{ sec}$ on horizontal axis .

runs, the stylus is moved slowly across the plug's surface. The signal is shown as "plug signature" on an X-Y-plotter (Fig. 2).

The experimental setup for vapor-liquid phase separation experiments is displayed in Figure 3. The liquid He II - filled space surrounds a central vent tube insulated from the outer bath. The plug is located at the bottom of the vent tube. A heater in the vessel is energized to different values during the runs. Carbon thermometers, upstream and downstream of the plug, measure the temperatures T_u and T_d respectively; (subscripts u and d denote upstream and downstream location respectively). In addition, pressure taps permit measurements of the pressures P_u and P_d . The pressure difference $\Delta P_v = P_u - P_d$ is recorded by means of a differential pressure transducer.

In the vapor - liquid phase separation runs , initially the system is kept at approximately equal pressures upstream and downstream by opening bypass valve # 1 (Fig.3) . After pumpdown close to the lambda temperature, valve # 1 is closed along with the main valve . With valve # 2 in "open" position, the liquid He II bath is pumped down slowly . Data are taken during a particular run for a constant heater power .

Various quantities of runs at different heater powers are displayed in Figure 4a through 4d . The abscissa is the liquid level characterized by the position coordinate z . Figure 4a shows the mass flow rate \dot{m} , deduced from liquid level measurements, for externally applied heater powers from 0 to 150 mW . Figure 4 b is a plot of the upstream temperature $T_u = T_u(z)$. Figure 4 c displays the temperature difference $\Delta T = T_u - T_d$ as a function of z , and Figure 4 d exhibits the pressure difference ΔP_v versus z . All of these functions are relatively steep. However when the final pumping power limit of the system is reached , the curves tend to level off at a low z -value . It is noted that the experiments incorporating flow modulation have been described elsewhere ¹⁴ . In Reference 14 a movable component has been employed.

Additional runs have been conducted at zero net mass flow with a system shown schematically in Figure 5. A heater located below

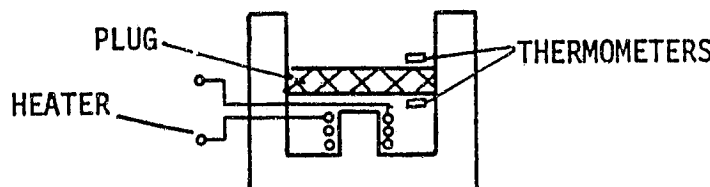


Figure 5 . Zero net mass flow system (schematically).

ORIGINAL PAGE IS
OF POOR QUALITY

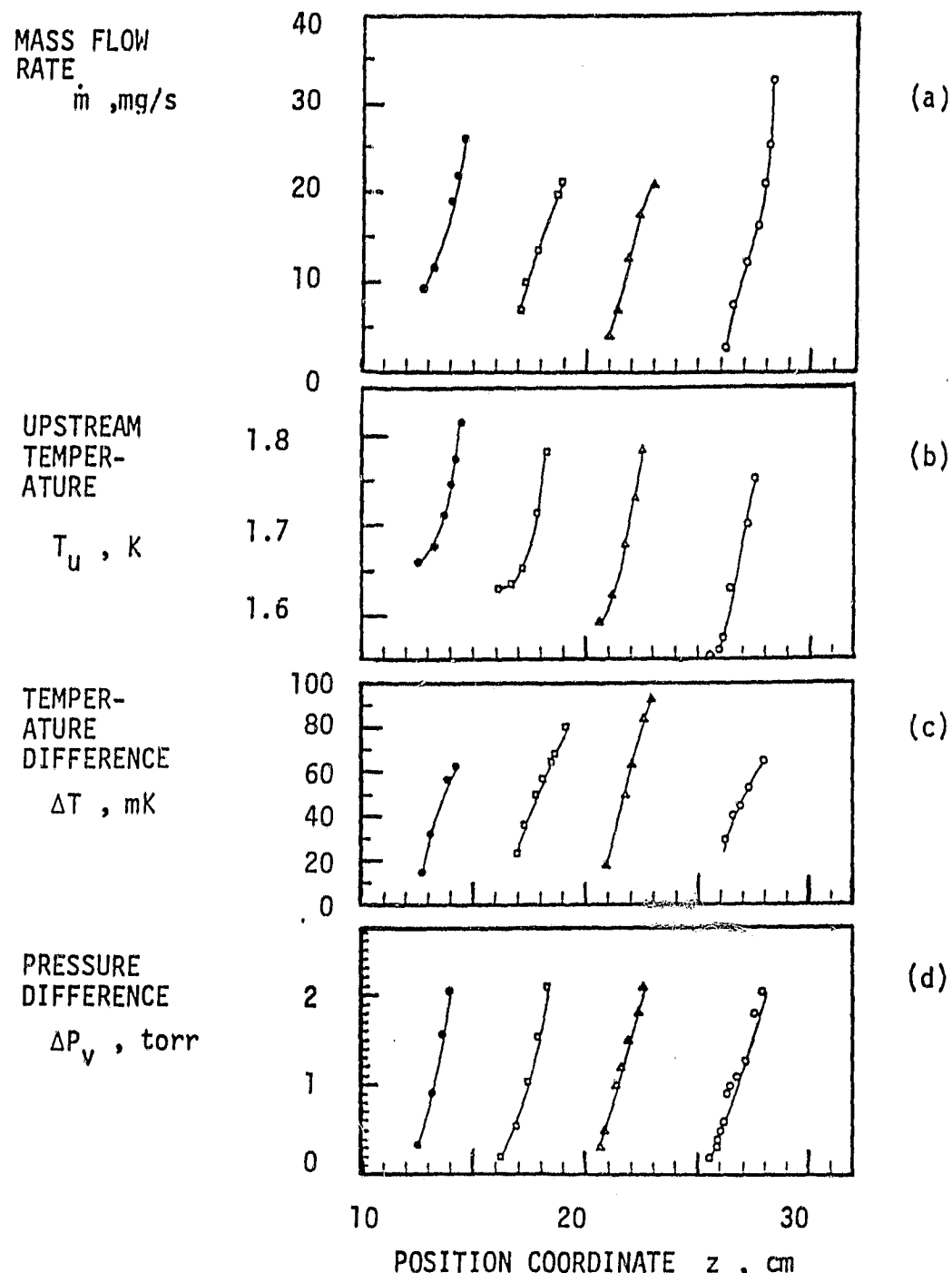


Figure 4. Phase separation parameters during runs with the stationary flow modulation system¹⁴ at various heater powers: ● 150 mW ; □ 100 mW ; △ 50 mW ; ○ 0 mW.

a sintered stainless steel plug of $2 \mu\text{m}$ size (nominal particle retention rate of filtration) is switched on. This results in a temperature gradient across the plug. Data obtained as thermal energy throughput versus the temperature difference are shown in Figure 6. The transport rate \bar{q}_0 is the superficial heat flux density = power dissipated per total (empty) cross section of the plug.

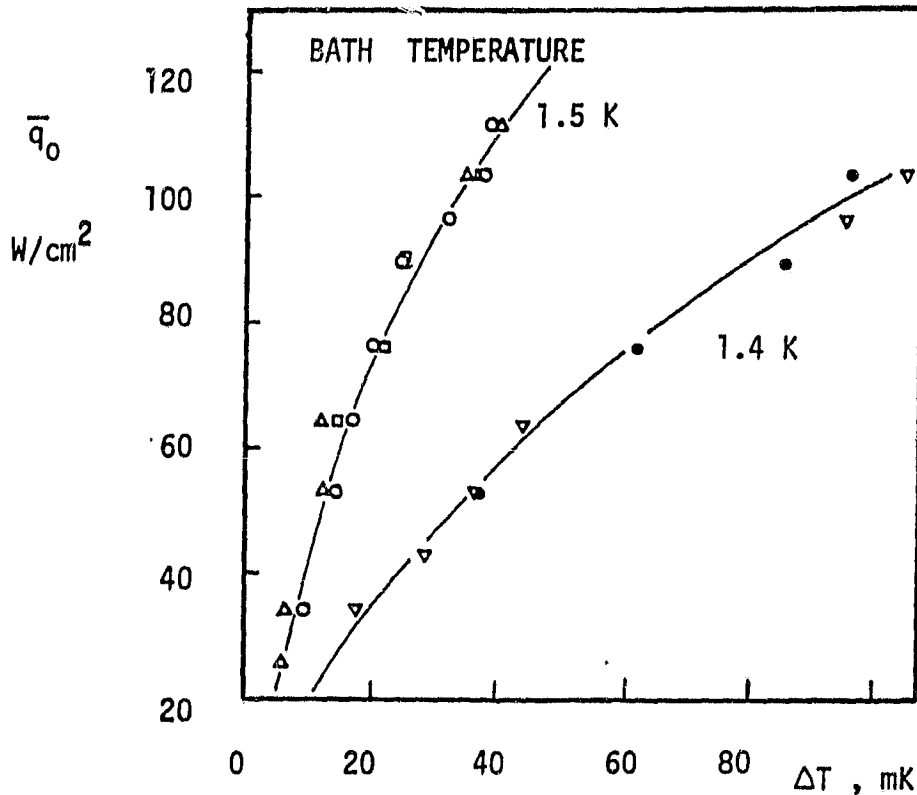


Figure 6. Heat flux density versus temperature difference at zero net mass flow ;($2 \mu\text{m}$ stainless steel plug).

DATA DISCUSSION

Zero net mass flow . The data for the $2 \mu\text{m}$ stainless steel plug (Figure 6) are presented in dimensionless form in Figure 7. It shows the dimensionless transport rate N_q of Equation (7) versus the dimensionless driving force N_{VT} of Equation (8). The permeability $K_{pn} = 3.0 \times 10^{-9} \text{ cm}^2$ is deduced from the linear regime characterized by $d \log N_q / d \log N_{VT} = 1$, i.e. the modified Darcy law , Equation (5) and (6) respectively.

. In the non - linear regime the normal fluid viscosity effects are no longer the dominant flow phenomena . Instead, liquid He II turbulence is established with a higher resistance to transport of entropy and heat . This is in agreement with the postulate of

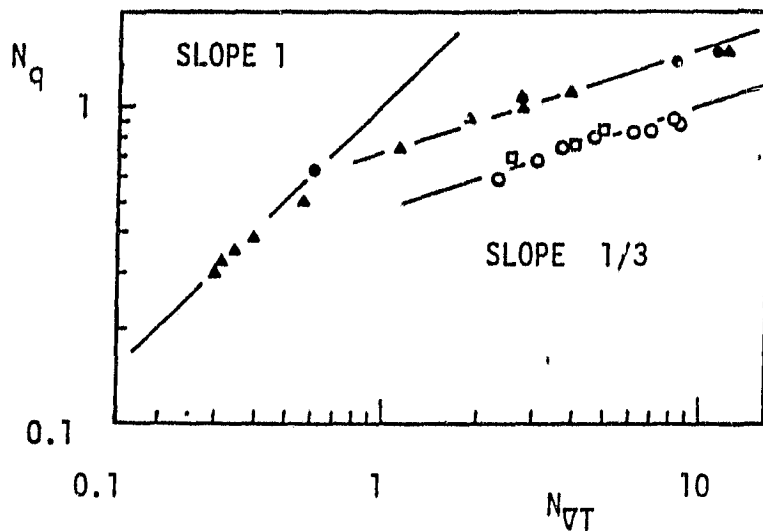


Figure 7 . Dimensionless normal fluid transport rate versus dimensionless driving force ; Full symbols: Bath temperature 1.4 K ; Open symbols ; 1.5 K .

Newtonian fluid behavior of the normal fluid of He II which interacts with the vortex system of the Gorter-Mellink transport regime. The data are described approximately by $d \log N_q / d \log N_{VT} = 1/3$. The related value of the Gorter - Mellink constant is $K_{GM} = 0.3$; (arithmetic mean of the data sets for 1.4 K and 1.5 K). The K_{GM} value is significantly below the value of $K_{GM} = 11.3$ for wide open ducts of high aspect ratio (length / diameter). Thus, the wide duct conditions constitute an upper bound to the porous media data at a specified temperature gradient.

The present zero net mass flow data for the 2 μm plug have been compared with literature data pertaining to a "single-pore" - grain system . A geometry representative of the size range under consideration appears to be the slit system studied by Keesom and Duyckaerts 16 . The dimensionless transport data are shown in Figure 8 as N_q versus N_{VT} . Within data scatter, there is again a well-defined linear regime of Darcy convection , a relatively sharp transition , and a non-linear regime of Gorter - Mellink turbulence involving mutual friction between the superfluid 's system of vortices and the normal fluid.

Vapor - liquid phase separation mode. The data have been taken with the stationary flow modulation device 14 . It is noted that the additional flow impedances of this system do not permit an exact quantitative comparison with the zero net mass flow results. The data comparison is based on the fully "open" position of the flow modulator. Figure 9 presents the data for this "open" case in the dimensionless variables of Equation (12) , i.e. $d \log (q/q_{ref})/$

ORIGINAL PAPER
OF POOR QUALITY

$d \log N_x = 4/3$; ($N_x = N_{VT} \rho_s / \rho_n$). It is seen that this power law appears to be a tangent to the data. The tangent is characterized by the value $K_{GM} = 0.2$. Thus, the order of magnitude is quite comparable to the zero net mass flow result for the same (nominal) size plug of $2 \mu\text{m}$.

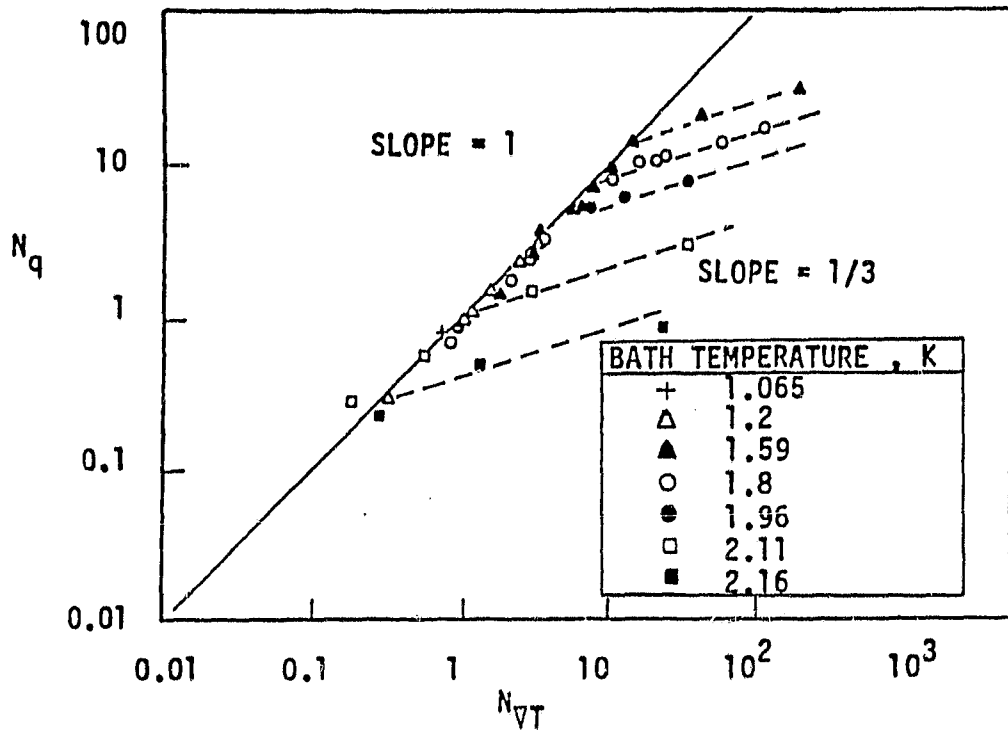


Figure 8 . Data of Keesom et al.¹⁶ plotted in dimensionless coordinates of the Darcy equation for normal fluid convection through porous media ; (dashed lines in the non-linear range have been drawn to guide the eye).

CONCLUSIONS

It is concluded that the permeability of Darcy transport of Newtonian fluids at room temperature is an upper bound to the normal fluid permeability of the modified Darcy law for the present stainless steel plugs with a nominal size of $2 \mu\text{m}$ (particle retention of filtration).

Further, any characteristic length of porous media may be a complicated function of another length which represents a different property of the medium. For instance, the equivalent particle diameter of the sintered plug is significantly larger than the nominal particle retention size. Therefore, it is proposed to make use of the Darcy permeability in order to characterize the flow through the entire plug in a meaningful way. This length $K_p^{1/2}$, and $K_{pn}^{1/2}$ may be more useful as

ORIGINAL PAGE IS
OF POOR QUALITY

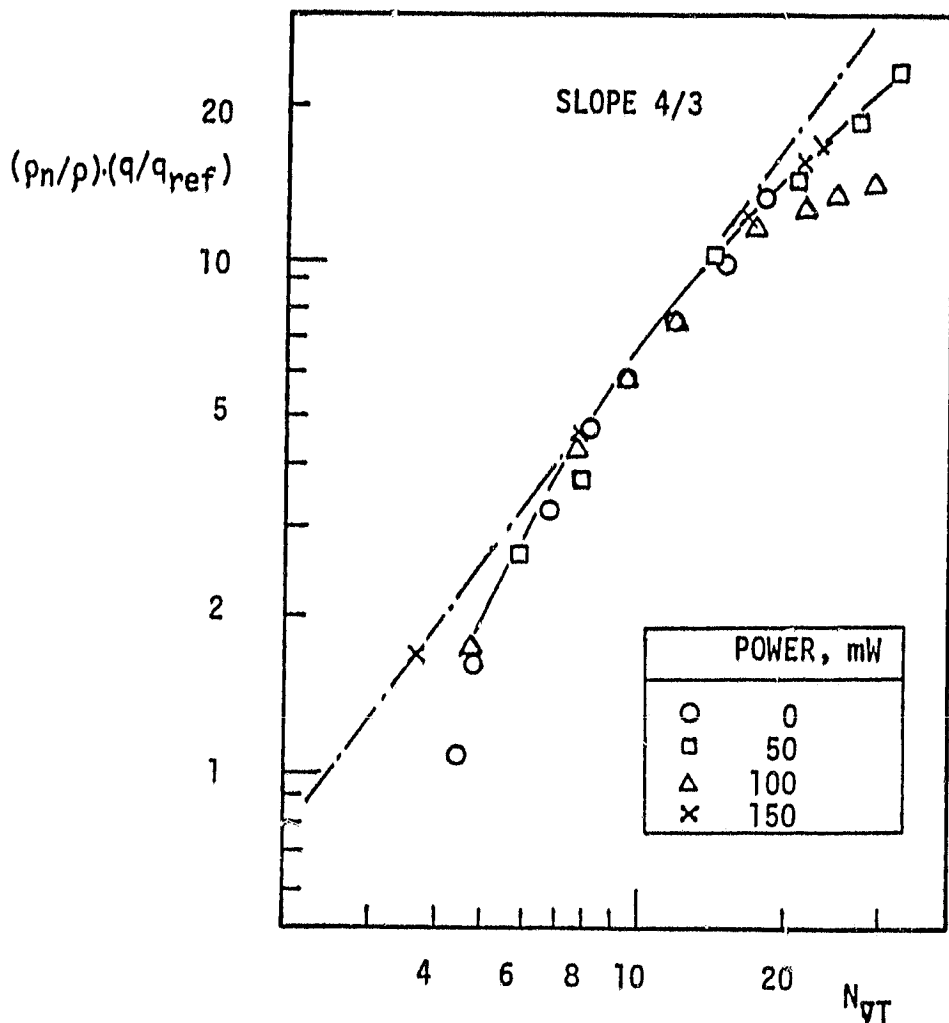


Figure 9 . Heat flux density ratio (Equation 12) versus the dimensionless driving force N_{VT} .

long as other more sophisticated parameters are not yet available for the porous media range of interest for liquid Helium storage and vent control.

Acknowledgment. The initial research effort has received partial support from NASA, Ames Research Center, and the separator transport research has been supported in part by the National Science Foundation. We acknowledge gratefully Mrs. Phyllis Gilbert's diligent typing and processing of this manuscript and related papers. We are indebted to Dr. Y. I. Kim and W. A. Hepler for input and contributions. Further, we acknowledge data reduction efforts by M. Johansson and S. Schmiederer.

REFERENCES

1. J. B. Hendricks and G. R. Karr, Proc. ICEC-9, Butterworths, Guildford, England, 1982, p. 190.
2. S. J. Puttermann, Superfluid Hydrodynamics, North Holland, Amsterdam, 1974; L. D. Landau, J. Phys. (USSR) 5, 1941, p. 71.
3. L. Tisza, Phys. Rev., 72, 1947, p. 838.
4. J. Wilks, The properties of liquid helium in "Liquid Helium Technology", IIR, Paris, Annexe 1966-5 to Bull. IIR 1966, p. 31.
5. O. Reynolds, Papers on mechanical and physical subjects, Cambridge University Press, 1900-1903.
6. J. Kozeny, Sitzgs. Ber. Wien, Acad. Sci. IIa 136, 1927, 271.
7. P. C. Carman, Trans. Inst. Chem. Engrs. 15, 1937, 150; Flow of gases through porous media, New York, Acad. Press, 1956.
8. S. Ergun, Chem. Engr. Progr. 48, No. 2, 1952, 89.
9. I. F. Macdonald, M. S. El-Sayed, K. Mow, and F. A. L. Duilin, Ind. Eng. Chem. Fundam. 18, 1979, p. 199.
10. A. E. Scheidegger, "Hydrodynamics in porous media, Encyclop. Phys. Vol. VII/2, Springer, Berlin, 1963; H. D'Arcy, Les fontaines publiques de la ville de Dijon, Paris, Dalmont, 1856.
11. S. W. K. Yuan, M.Sc. thesis, Univ. of Calif., Los Angeles, CA, 1981.
12. J. M. Lee, M.Sc. thesis, Univ. Calif., Los Angeles, CA, 1983.
13. S. W. K. Yuan and T. H. K. Frederking, Thermal Engng. Joint Conf., ASME-JSME (Eds. Y. Mori and W. J. Yang), March 1983, Vol. 2, p. 191.
14. T. H. K. Frederking, C. Chuang, Y. Kamioka, J. M. Lee and S. W. K. Yuan, Cryog. Eng. Conf., 1983, Colorado Springs, Paper CB-3.
15. S. C. Soleski and T. H. K. Frederking, Int. J. Heat Mass Transfer 23, 1980, p. 437.
16. W. H. Keesom and G. Duyckaerts, Physica 13, 1947, p. 153.

Comment on Reference 10 Concerning the Original Studies of Darcy

An initial search of the literature in the West Coast area did not have success in locating the original reference of the year 1856. It is noted that investigations of H. Holze (Investigations of the flow resistance of agricultural blade products, VDI-Forschungsheft 545, Vol. 37, 1971) showed in the reference list the version "D'Arcy". However, finally a look at the original work revealed the commonly known author Henry "Darcy". We are indebted to Mr. J. Verdier, CEA Grenoble, for helping to locate the reference and for making available this old publication.

A P P E N D I X C

APPENDIX C

CHARACTERIZATION OF SINTERED STAINLESS STEEL POROUS PLUGS FOR VAPOR - LIQUID PHASE SEPARATION OF HELIUM II *

1. Introduction

Phase separation by means of porous plugs has been considered primarily in conjunction with IR telescope system developments, in particular in conjunction with cryo-vessel support technology [1] [2].

The plug uses the thermo-osmotic (thermomechanical) pressure to oppose gravity and microgravity of flight conditions respectively.

Liquid fills the plug to its downstream side (seen from the thermal energy rejection point of view). Liquid evaporates on the downstream side to form vent gas used for the cooling of radiation shields.

One particular feature of the He II oxygen is its excellent thermo-static stability up to the maximum ("peak") transport rate [2]. For a detailed understanding and sizing of plugs, their properties ought to be known. The present work focusses primarily upon a stainless steel plug of nominal size of 2 μm .

CONTENTS

1. Introduction
2. Selected plug properties
3. Apparatus and experiments
4. Results and Discussion
5. Conclusions

Concerning basic properties of liquid Helium-4 below the lambda point, i.e. superfluid He II, the two-fluid model is used. The two-fluid model, introduced by Tisza [3] and Landau [4][5], has been supported by various experiments reported in the literature. Examples are the liquid gyroscope [6], the oscillating pendulum [7], and the zero entropy experiment of Kapitza [8] demonstrating that the superfluid component has zero entropy, while the normal fluid carries a finite entropy. Further, the work of Landau and others has led to a set of macroscopic equations for the two fluids of He II [9] used in conjunction with chemical potential constraints [10]. Thus, macroscopic equations have been available for the assessment of porous plug flow [11].

*) Condensed outline based on M.Sc. thesis of S.W. Yuan.

porous plug flow [11]. The normal fluid appears to be Newtonian, there have been simple solutions for steady flow and parallel motion [12]. In the related truncated form of the Navier-Stokes equations, subject to the special He II driving force due to temperature gradients, simple Stokes flow solutions have become known. Thus, it is interesting to check the validity of the solutions by comparison with experiments.

2 . Selected Plug Properties

2.1 Properties of stainless steel plugs (Intro.)

Porous media are solid bodies that contain small void spaces known as pores. The pores of a porous media may be interconnected or non-connected. The interconnected pores are known as the effective pores. Flow of fluid across the media is possible only if effective pores are present.

Porous media can be made from a large variety of materials such as ceramics, metal and fiberglass packings.

In this work we will direct our attention to sintered stainless steel porous plugs (from Mott Metalurgical Corporation Farmington, CO 80632).

2.2. Manufacture of sintered plugs

The consolidation of stainless steel powder into porous media can be accomplished by heating alone, known as the "no pressure sintering process"; or the powder can be precompressed into a plug by controlled pressure, and then heated to the sintering temperature. The latter method ~ used for the present plugs.

The sintering process is carried out in a reducing atmosphere with temperature below the melting point of the stainless steel. The reduced atmosphere aids in removing the surface oxide films from the powder particles and protects the surface throughout the sintering cycle. During the sintering process, the individual particles

bond to their adjacent neighbors by the process of solid state diffusion, thus transforming the packed system into a coherent matrix with interconnected pores.

Porous media can be characterized by a number of useful properties, however we will only consider a few of them here.

2.3 . Pore size and various characteristic lengths

One of the most common methods to measure the pore size is by the bubble point method^[3]. The entire plug to be measured is immersed in a fluid. Pressure is applied to one side of the surface. The pressure at which a first stream of bubbles is noticed is recorded. The pore size can thus be calculated by the following equation

$$R_s = 2\sigma/\Delta P \quad (2.1)$$

Where R_s is the radius of an equivalent capillary tube. σ is the surface tension between the fluid and the metal. ΔP is the recorded differential pressure.

However, this method has several disadvantages. First of all, since the bubbles are observed on the surface of the plug, what we have measured is only the maximum pore size at the surface. Secondly, for the application of porous media in vapor-liquid phase separation, the plugs have to be kept very clean. Because at such low temperature, any impurities in the plug will be frozen and thus reduce the permeability of the mass

ORIGINAL PAGE IS
OF POOR QUALITY

throughput across the plug. It is always recommended to put the porous media in a helium gas atmosphere before installing in the apparatus. Therefore in applying bubble point method, fluid will get into the pores which will contaminate the plug and is hard to clean afterwards.

Because of small surface tension in Liquid He⁴ no tests appear to have been conducted in Liquid He⁴ so far.

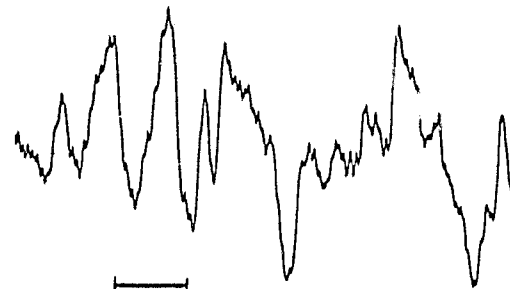
It is noted that manufacturer data may refer to particle retention rates in a filter application for solid-liquid separation processes, for instance Urbach et. al. (4) report that "five micron pore size filter material was intact between 25 to 30 microns in diameter."

Plug characterization tests were performed prior to the flow experiments trying to identify the plugs without contaminating them.

A profilometer (Micrometrical Manufacturing Co., serial #1895, 115 volts, 60 cycles) was used to check the details of the plug surface. The stylus tip of the profilometer had a tip radius of 0.05 cm. Surface variations resolved at the resolution limit are of the order of 0.3 μm . Experiments were performed on the 2 μm , 5 μm and the 10 μm plugs. Records for the three different stainless steel plugs are shown in Figures 2.1 to 2.3. During the runs the stylus was moved slowly across the plug, and the signal was displayed as a function of time on an X-Y-

ARB.
UNITS

ORIGINAL PAGE IS
OF POOR QUALITY

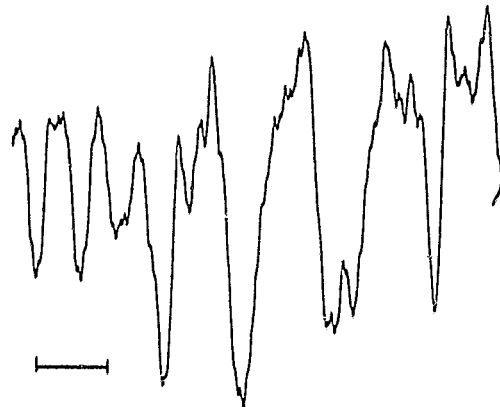


TIME

Figure 2.1. Trace of 2 μm -plug (X-axis, Time scale : 1 unit = 1 sec; Unit length in vertical direction = 50 mV).

ORIGINAL PAGE IS
OF POOR QUALITY

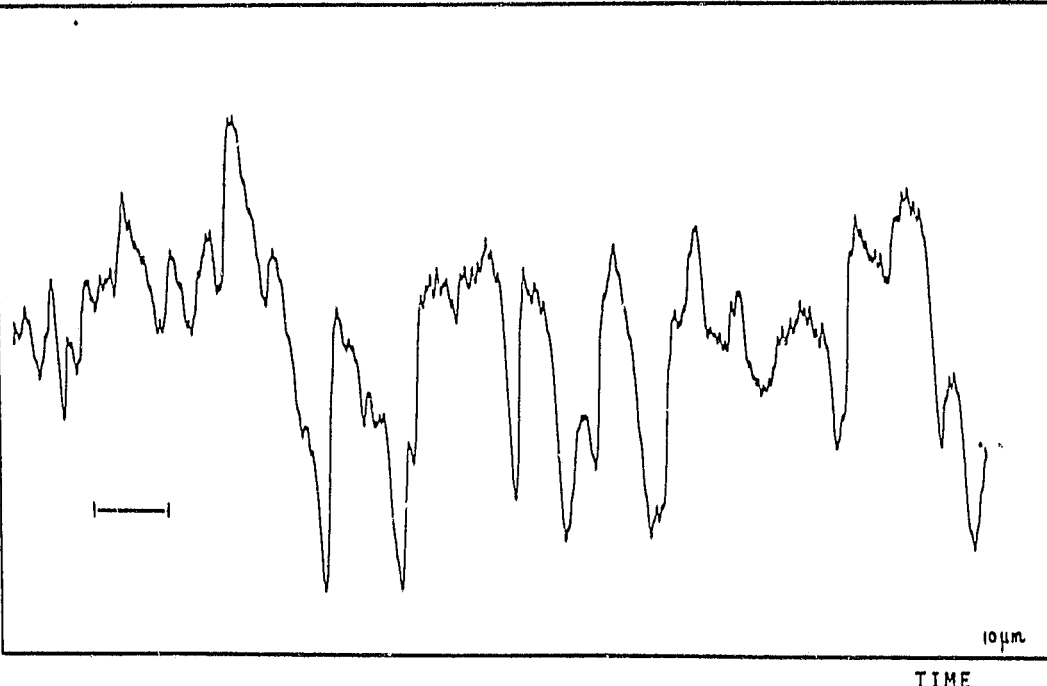
ARB.
UNITS



1 sec
TIME

Figure 2.2. Trace of 5 μm -plug (X-axis, Time scale : 1 unit = 1 sec; Unit length in vertical direction = 50 mV).

ARB.
UNITS



10 μm

Figure 2.3. Trace of 10 μm - plug; (X-axis, Time scale : 1 unit = 1 sec ; Unit length in vertical direction = 50 mV).

plotter (Houston Omigraphic 2000). The signals of plugs of one manufacturer are seen to be of sufficient difference. Thus, this simple method is quite useful for the identification of plugs.*

Porosity is the ratio of void space over the total volume of the plug. There are a number of methods that one can use to measure the porosity, namely the direct method, the optical method, the density method and the gas expansion method, etc. (For the details of these methods please refer to Reference 15.) However, not all of the above methods are suitable for sintered stainless steel porous plugs.

In a direct method, the bulk volume of the porous material is measured. The material is then compacted to destroy all its voids and the volume of the material is measured again. The ratio of the difference in volume over the bulk volume will give the porosity. In an optical method, a section of the porous media is studied under a microscope and the porosity is estimated by measuring the area ratio of the pores and the bulk area. The disadvantage of these two methods is that one has to destroy the plug being measured, and the porosity of the plug once destroys might not be the same as the one used in the experiment.

Surface roughness determination by means of profilometers with tracer points :
Extreme cases



Figure 2.4. Tip radius smaller than asperity size

ORIGINAL PAGE IS
OF POOR QUALITY



Figure 2.5. Tip radius comparable to grain size ;
The tip radius of the tracer point of
Micrometrical Manufacturing Comp. is
0.5 mil = 12.7 μm .

*) Figures 2.4 and 2.5 show extreme cases of profilometer conditions.

Among all the methods, the gas expansion method is very suitable for flow property determination, because it actually measures the effective porosity. Due to the presence of "blind porosity" only the effective pores will contribute to fluid flow. This method is done by enclosing the plug of known bulk volume and a certain amount of gas in a container of known volume under pressure. The container is then connected to an evacuated container of known volume. The new pressure is recorded, permitting one to calculate the volume of gas that was originally in the plug through Boyle's Law.

However, for the sake of simplicity, a density method was used in the present experiment

$$\epsilon = 1 - \rho_B / \rho_S \quad (2.2)$$

where ρ_S is the density of the stainless steel (grade 316), ρ_B is the bulk density.

For the porous plugs it has been pointed out "that approximately 50% of their apparent volume is void space" (21). However a porosity of about 30% was measured for 2 μm plugs using the density method.

If the particles are of nearly spherical shape, and if only a few contact points are connected by local fusion due to heating to the vicinity of the melting point, the particles may remain near spherical. An example is sintered tungsten (16) (17). However in general, particles do not have a spherical geometry. Also, they may change shape during sintering. Stainless steel particles are not spherical prior to sintering. Therefore permeability tests may be used to relate the effective pore size to other parameter known, for instance for near-spherical packed particle beds.

A well-defined semi-empirical equation was introduced by Ergun (8), by modifying the Carman-Kozeny permeability equation to describe the packed beds of nearly spherical particles as a function of D_p and porosity ϵ . In the limit of creeping motion, the permeability is

$$K_p = \frac{D_p^2}{180} \frac{\epsilon^3}{(1-\epsilon)^2} \quad (2.3)$$

For details of modification of Ergun's equation refer to Reference 19.

It should be noted that Equation (2.3) is only applicable for packed beds of spherical particles. For sintered porous plugs where the particles are not close to spherical geometry, the permeability values would be expected to deviate from the theoretical permeability calculated from the modified equation.

culated from Equation (2.3).

We can define a permeability ratio

$$\phi_{\pi} = \frac{K_p}{(K_p)_{\text{theor.}}} \quad (2.4)$$

Therefore for sintered porous plugs

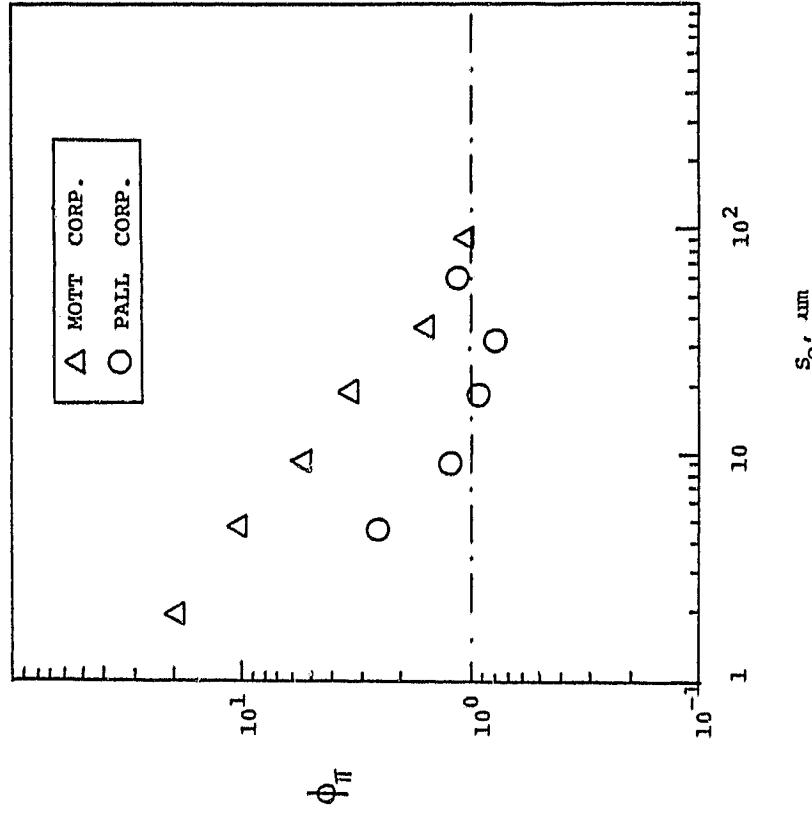
$$K_p = \phi_{\pi} \frac{D_p^2}{180} \frac{\epsilon^3}{(1-\epsilon)^2} \quad (2.5)$$

If the particles of the plug are spheres even after sintering, $\phi_{\pi} = 1$. As the geometric similarity of the porous media deviates from that of ideal packed bed, $\phi_{\pi} \neq 1$.

If particles are compressed during the sintering process so that there are more contact area between particles, $\phi_{\pi} > 1$. For plugs where cavities are created during sintering $\phi_{\pi} < 1$.

For some sintered media, in particular, it is worth noting that the validity of Equation (2.3) is quite well established for large D_p (of the order of 100 μm). An example is a study of W-particles²⁰. At low values of D_p , however, departures toward high permeabilities are found in commercial plugs of sintered materials.

The exact correlation between pore size and particle diameter is not known, however one would expect that the pore size is directly proportional to the particle diameter. Figure 2.6 is a plot of ϕ_{π} vs. S_o . The data are for the permeability of water, at room temperature from the



ORIGINAL PAGE IS
OF POOR QUALITY

Figure 2.6 Data of two different manufacturers:
Calculated permeability ratio based
on quoted "pore size" S_o .

manufacturers²¹⁾²²⁾. It is seen that indeed the data approach an asymptotic value considered to be representative of the geometric similarity accounted for by $\phi_{\text{II}} = 1$ at the limit of large S_0 or D_p .

2. 4. Permeability of Porous Plugs

One of the most useful properties characterizing porous media for vapor-liquid phase separation is the permeability. In classical Newtonian flow, the permeability governs the mass throughput, given a differential pressure across the plug. Measurement of permeability can be performed using Darcy's law¹⁵⁾⁽²³⁾

$$\dot{V}_o = \frac{\bar{A} p}{\eta} \frac{(K_p)_m |\nabla P|}{\bar{V}} \quad (2.6)$$

where A_p is the total area of the plug
 K_p is the mass permeability
 \dot{V} is the volumetric flow rate
 ∇P is the pressure gradient
and η is the viscosity

The permeability of the stainless steel plugs given by the manufacturer has different values for air and water (Appendix A). For example at high ΔP : $(K_p)_{\text{air}} = 8.7 \times 10^{-9} \text{ cm}^2$, at low ΔP : $(K_p)_{\text{air}} = 7.4 \times 10^{-9} \text{ cm}^2$ and for water $K_p = 4.0 \times 10^{-9}$. Compressibility effects may occur in gases (large ΔP), however differences resulting from fluid changes are not known.

In this work, we study the effect of temperature on

permeability with He gas as the fluid. In order to predict the mass throughput of He II across a porous plug in a phase separator, it is desirable to know the classical permeability of the plug at low temperatures (e.g. in He I at 2.2 K). However, unfortunately there is no known literature value of the permeability at this temperature. Therefore the first part of the experiment is devoted to studies of the effect of temperature on permeability values. Permeability values of He gas at room temperature, liquid nitrogen temperature and liquid He temperature are measured.

$$\bar{V}_0 = \zeta_0 |\nabla P| R_{id}^2 / \eta \quad (2.7)$$

If one substitutes the above expression into Darcy's law one gets

$$R_{id} = \sqrt{K_p / \zeta_0} \quad (2.8)$$

The related parameters of Equation (2.7) are contained in Table 2.1.

However in the sintered medium, in particular stainless steel filters (alloy 316) it is not possible to obtain well-defined ducts. Therefore only the order of magnitude may be obtained either for the capillary or the slit case, and the factor $\zeta_0 = 0.1$ is used.

A third reference length may be defined by including the porosity of the porous plug. In this case, the flow cross section A_{flow} equals the product of the porosity and the total cross section ($\epsilon \cdot A_{tot}$). Thus the mean speed of the fluid is \bar{V}_0 / ϵ . Accordingly, we obtain an effective hydraulic radius of the mass flow and normal fluid flow respectively of

$$R_m = \sqrt{(K_p)_m \epsilon / \zeta_0} \quad (2.9)$$

$$R_n = \sqrt{(K_p)_n \epsilon / \zeta_0} \quad (2.10)$$

With a throughput factor $\zeta_0 \sim 0.1$.

ORIGINAL PAGE IS
OF POOR QUALITY

TABLE 2.1. LAMINAR FLOW PARAMETERS FOR IDEAL GEOMETRIES

IDEAL CASE	HYDRAULIC RADIUS $R_{id} = \frac{2 \cdot \text{CROSS SECTION}}{\text{PERIMETER}}$	PARAMETER
A) CAPILLARY WITH CIRCULAR CROSS SECTION	$R_{id} = \text{RADIUS } R \text{ OF CAPILLARY}$	$\zeta_0 R_{id}^2 = R^2 / 8$ $\zeta_0 = 1 / 8$
B) SLIT OF CONSTANT VERY SMALL WIDTH (W)	$R_{id} = \text{SLIT WIDTH } (W) \text{ FOR VERY NARROW SLIT}$	$\zeta_0 R_{id}^2 = W^2 / 8$ $\zeta_0 = 1 / 12$

2.5. Transport of He II Across Porous Plugs

For He II, the classical equations are no longer valid. However, for zero net mass flow, normal fluid flow and heat flow may be possible in such a way that superfluid flow, in counterflow to the heat transport, compensates for the normal fluid flow. The resulting heat flow rate is described in terms of the normal fluid density ratio (ρ_n/ρ). This ratio is found to be a unique function of temperature

$$\frac{\rho_n}{\rho} = 1 - \frac{\rho_s}{\rho} \quad (2.11)$$

Experimental data show that laminar flow rate of normal fluid is proportional to the first power of the pressure gradient. This supports the postulate of classical Newtonian flow. Then the flow of normal fluid across the porous plug is governed by Darcy's law²⁴⁾

$$\bar{V}_{n_0} = K_p |\nabla P| / \eta_n \quad (2.12)$$

where ∇P is the pressure gradient across the plug and K_p is the permeability value.

In static thermo-osmosis, the magnitude of pressure gradient ∇P will be equal to the magnitude of thermomechanical pressure ∇P_T

$$-\nabla P = \nabla P_T = \rho S V T \quad (2.13)$$

Therefore for static thermo-osmosis

$$\bar{V}_{n_0} = K_{p_n} |\nabla P_T| / \eta_n \quad (2.14)$$

The heat flux density of normal fluid is described by the two-fluid model equation

$$\bar{q} = \rho_{ST} \bar{V}_n \quad (2.15)$$

In static thermo-osmosis the convection equation of the normal fluid can be written as

$$\bar{q}_o = \rho_{ST} \bar{V}_{n_0} \quad (2.16)$$

Combining Equation (2.14) and (2.16) we can get the permeability for normal fluid

$$(K_p)_n = \frac{\bar{q}_o \eta_n}{\rho^2 S_{TVT}^2} \quad (2.17)$$

From Equation (2.17) we can arrive at an "apparent thermal conductivity" of He II in the plug.

$$K_{app} = \frac{\bar{q}_o}{|\nabla T|} = (K_p)_n (\rho_S)^2 T / \eta_n \quad (2.18)$$

Thus, if K_{app} of the plug is measured the permeability of the normal fluid $(K_p)_n$ can be determined

$$(K_p)_n = K_{app} \eta_n / (\rho_S)^2 T \quad (2.19)$$

Equation (2.14) may be expressed in a dimensionless form by defining a normalized heat flow Reynolds number

$$N_q = \frac{\rho V_n L_c}{\eta_n} \quad (2.20)$$

and a normalized driving potential

$$N_{\nabla T} = \frac{\nabla T \rho L_c^2}{\eta_n^2} \quad (2.21)$$

If we set $L_c = \sqrt{K_p}$, then equating N_q to $N_{\nabla T}$

Equation (2.14) is recovered

$$N_q = N_{\nabla T} \quad (2.22)$$

Therefore if Darcy's law is valid, then a plot of N_q vs. $N_{\nabla T}$ will give a straight line passing through the origin with a slope of unity.

Using Equations (2.13) and (2.15), Equations (2.20) and (2.21) can be written as

$$N_q = \frac{q L_c}{\eta_n S_T} \quad (2.23)$$

$$N_{\nabla T} = \frac{\rho^2 S_T L_c^2}{\eta_n^2} \quad (2.24)$$

If we use the ideal hydraulic radius as the characteristic length, $L_c = 2R_{id} = 2\sqrt{K_p/\zeta_0}$ we get

$$\frac{\zeta_0}{4} N_q = N_{\nabla T} \quad (2.25)$$

Similarly with $L_c = 2R_m = 2\sqrt{K_p \epsilon / \zeta_0}$ we get

$$\frac{\zeta_0}{4\epsilon} N_q = N_{\nabla T} \quad (2.26)$$

2.6 Comparison With Experimental Data

Geometric Parameters

Figure 2.7 presents the classical ideal hydraulic radius $(R_m)_{id}$ as a function of pore size (ζ_0). The Mott data for sintered stainless steel appear to come close to other experimental results in the limit of large ζ_0 . The experimental data show approximately a linear dependence of R_{id} versus ζ_0 .

The hydraulic radius R_m versus pore size ζ_0 was plotted in Figure 2.8 for a throughput factor of $\zeta_0 = 0.1$. If we compare Figures 2.7 and 2.8 we see that R_m is slightly lower than R_{id} by the factor $\sqrt{\epsilon}$. The plug data of Figure 2.7 have been retained in Figure 2.8. The data seem to fit the linear function.

$$R_m = 0.1 \zeta_0 \quad (2.27)$$

Figure 2.9 is a plot of the three reference lengths, namely $K_p^{\frac{1}{2}}$, R_{id} and R_m versus the particle diameter. The data were deduced from the experimentally determined normal fluid permeabilities of Schmidt and Wiechert²⁶. All the reference lengths tend to vary non-linearly with the particle diameter. The radii R_{id} and $R_m = R_n$ come close to each other as ϵ is quite large. The lengths $\sqrt{K_p}$ are quite smaller than the other two reference lengths.

In some cases there is an interdependence between the particle diameter of the sintered plugs (prior to sintering) and the pore size.

ORIGINAL PAGE IS
OF POOR QUALITY

- ◆ MORF , technology information 21)
 - ◆ Denner - Klipping et al. 2)
 - ◇ Denner - Klipping et al. 2)
 - Urban-Katz-Karr 25)
 - Urban-Katz-Karr 25)
 - X Karr - Urban 11)
 - X Karr - Urban 11)
- $$R_m = \sqrt{\frac{E(K_p)_m}{\zeta_o}}$$

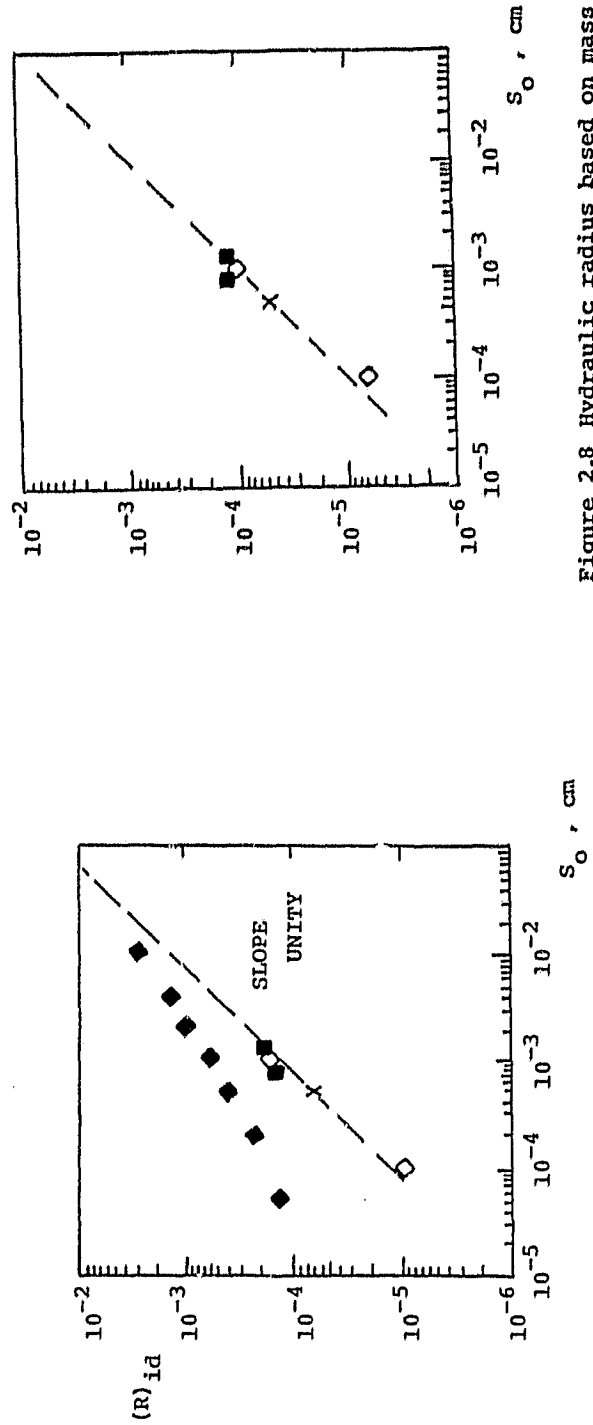


Figure 2.8 Hydraulic radius based on mass flow permeabilities ;
(throughput factor $\zeta_o = 0.1$).

Figure 2.7 "Ideal hydraulic radius" based on cylindrical parallel duct system versus pore size (s_o).

$$(R)_{id} = (K_p / \zeta_o)^{1/2} ; \zeta_o = 0.1$$

Figure 2.10 displays D_p as a function of S_o for sintered bronze plugs²⁴⁾ and sintered loose spherical powders²⁷⁾. As we can see that there is a linear relationship between D_p and S_o . S_o versus ratio D_p / S_o is shown in Figure 2.11. Besides the data sets of Figure 2.10, data for sintered tungsten plugs²⁷⁾ has been included. As expected, the ratio D_p / S_o is almost a constant.

$$\left. \begin{array}{l} \bullet \quad R_m = \sqrt{\frac{(K_p)_n \epsilon}{S_o}} \\ \circ \quad R_{id} = \sqrt{\frac{(K_p)_n}{S_o}} \\ \times \quad \sqrt{(K_p)_n} \end{array} \right\} \text{Schmidt-Wiechert} \quad 26)$$

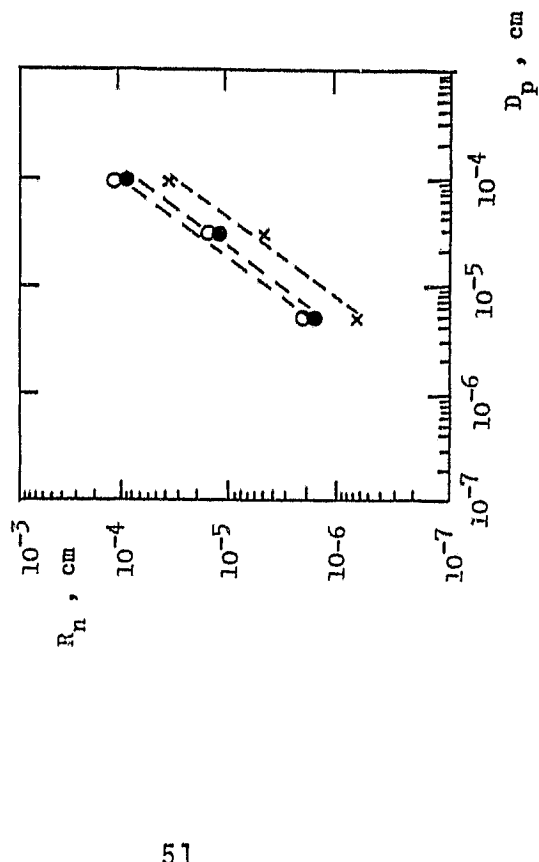


Figure 2.9 Hydraulic radii versus particle diameter.

Robinson¹⁶⁾ and Hall¹⁷⁾ have studied the flow of various fluids across sintered tungsten porous plugs. If we plot the permeability values of those plugs versus the modified particle diameters $D_p \epsilon^{3/2} / (1-\epsilon)$, the data lie on a straight line $K_p = \frac{1}{150} D_p^2 \frac{\epsilon^2}{(1-\epsilon)^2}$, which is the Ergun equation for packed beds (Figure 2.12). Thus we can see that the permeability of sintered plugs may be well described by Ergun equation if D_p is large ($> 10 \mu m$) and the particles are close to sphere shape.

ORIGINAL PAGE
OF POOR QUALITY

Before looking at the sintered plug data, we will study the packed particle system results first. Figure 2.13 is a plot of permeability versus temperature of He II at zero net mass flow ($\Delta T \ll T$) for various packed particle systems. From the data of Schmidt and Wiechert²⁶⁾ it is seen that for (nominal) particle diameters above and at

X SINTERED LOOSE SPHERICAL POWDERS 27)
 ◇ SINTERED BRONZE PLUGS 24)
 + POROUS TUNGSTEN (SPHERICAL POWDER) 27)

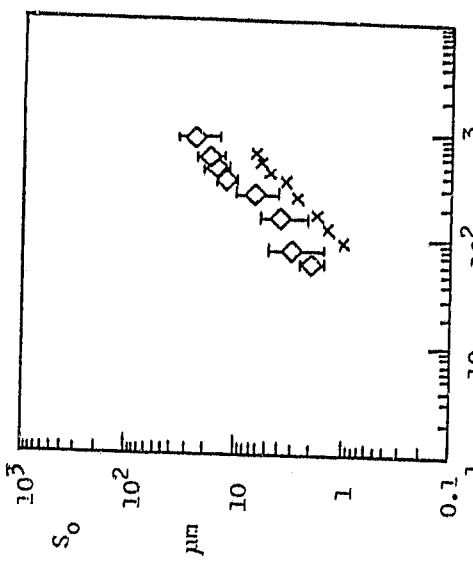


Figure 2.10 Pore size of sintered plugs as a function of particle diameter.

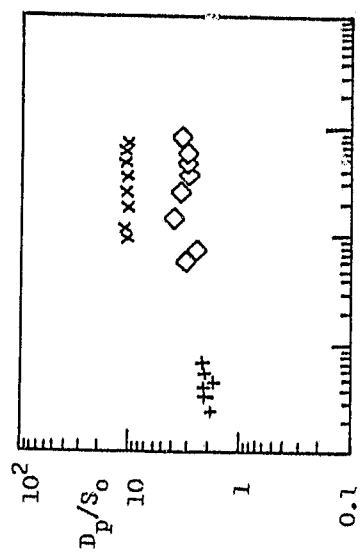


Figure 2.11 Ratio of particle diameter to pore size versus D_p .

EQUATION FOR PACKED BED SIMILARITY

$$K_p = (130)^{-1} D_p^2 \cdot \frac{\epsilon^3}{(1-\epsilon)^2}$$

ORIGINAL PAGE IS
OF POOR QUALITY

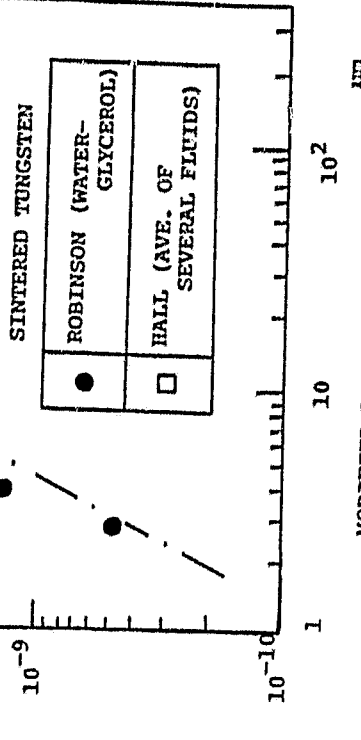


Figure 2.12 Permeability of sintered metal plug in the range of large particle diameters.

the order of magnitude $D_p = 0.1 \mu\text{m}$ (10^{-5} cm), there is no discernible influence of Knudsen flow, or mean free path effects between 1.2 and 2 K. However, below this particle diameter range the slip onset is seen as an increase in the permeability as the temperature is lowered (e.g. data for $D_p = 0.05 \mu\text{m}$ in Figure 2.13).

The zero net mass flow case appears to be understood better than the vapor-liquid phase separation mode, because much larger data sets are available in the literature (for recent works, see Reference 26 and 28).

Now, let us turn to the permeability of He II across porous plugs. Denner and Klipping et al.² have studied the transport of He II in 10 μm glass plug. The permeability of the plug at various temperature was deduced from the data and plotted in Figure 2.14. The mass permeability (K_p) and the normal fluid permeability were calculated by Equations (2.6) and (2.17) respectively. At rotton depletion (i.e. $\rho_s \gg \rho$ and $V_s \ll V_n$, $\beta_n < \beta_s$), one would expect the permeability of He II to approach the classical flow data. As the temperature is increased ($T \rightarrow T_\lambda$), the permeability will be lowered because of the influence of the superfluid velocity. From Figure 2.14 one can see that the permeability predicted by the London-Zijssel model (Equation 2.17) is supported by the 10 μm -plug data, whereas $(K_p)_m$ tends to decrease at the rotton depletion limit.

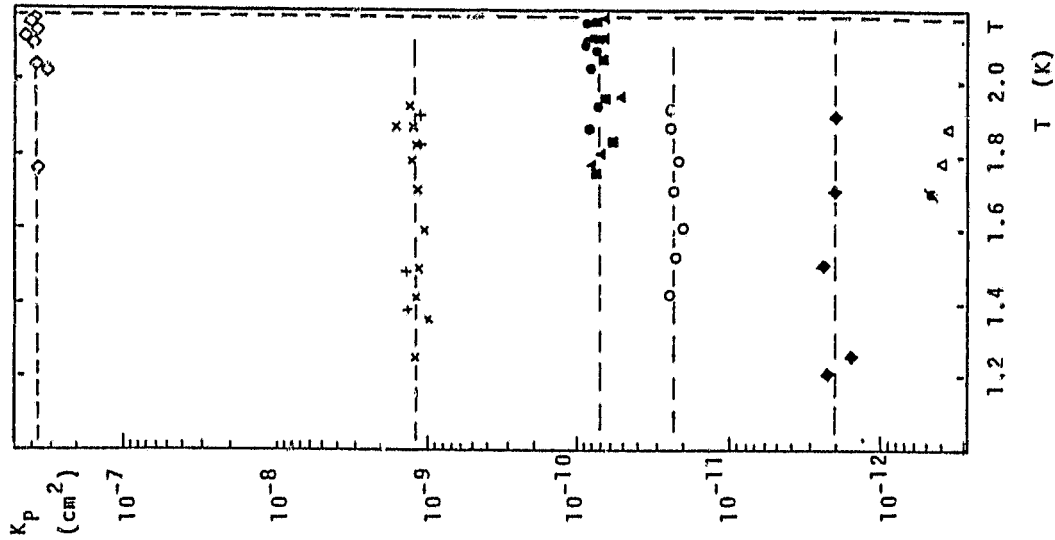


Figure 2.13 Permeability as a function of temperature for zero net mass flow systems.

ORIGINAL FROM
OF POOR QUALITY

Denner, Klipping et al.

10 μm glass plug 2)

The results of Figure 2.13 are plotted in dimensionless form in Figure 2.15 with $L_c = \sqrt{k_p}$. All the data lie on a straight line with a slope of unity, which agrees with Equation (2.22). This verifies that Darcy's law is valid for zero net mass flow of He II entropy transport in packed beds.

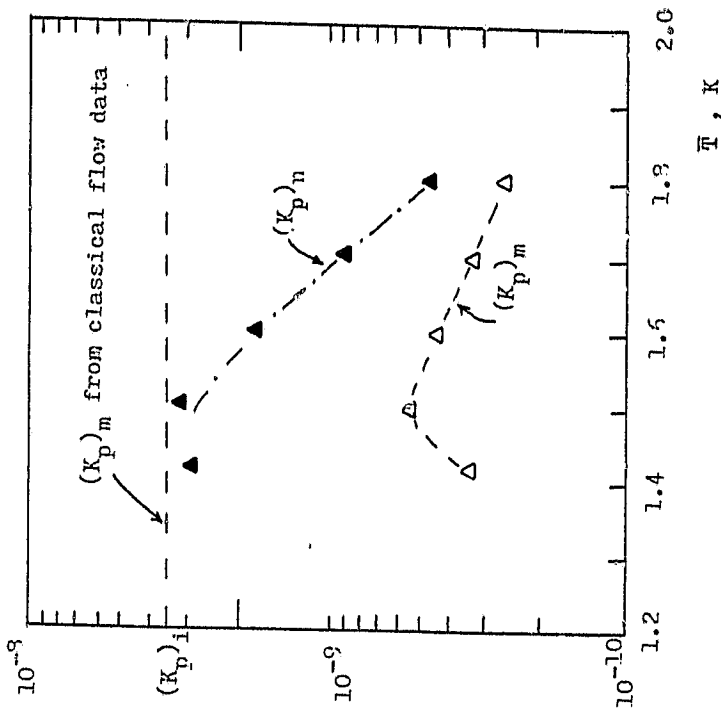


Figure 2.14 Permeabilities corresponding to various transport rates as a function of the plug mean temperature \bar{T} .

ORIGINAL PAGE IS
OF POOR QUALITY

♦ Data of packed material of Reference 28)

▼ $\eta=1.292\text{cp}$ Classical data of Glycerol-H₂O through tungsten matrices, Robinson 16)

□ $\eta=2.600\text{cp}$

▽ $\eta=5.041\text{cp}$

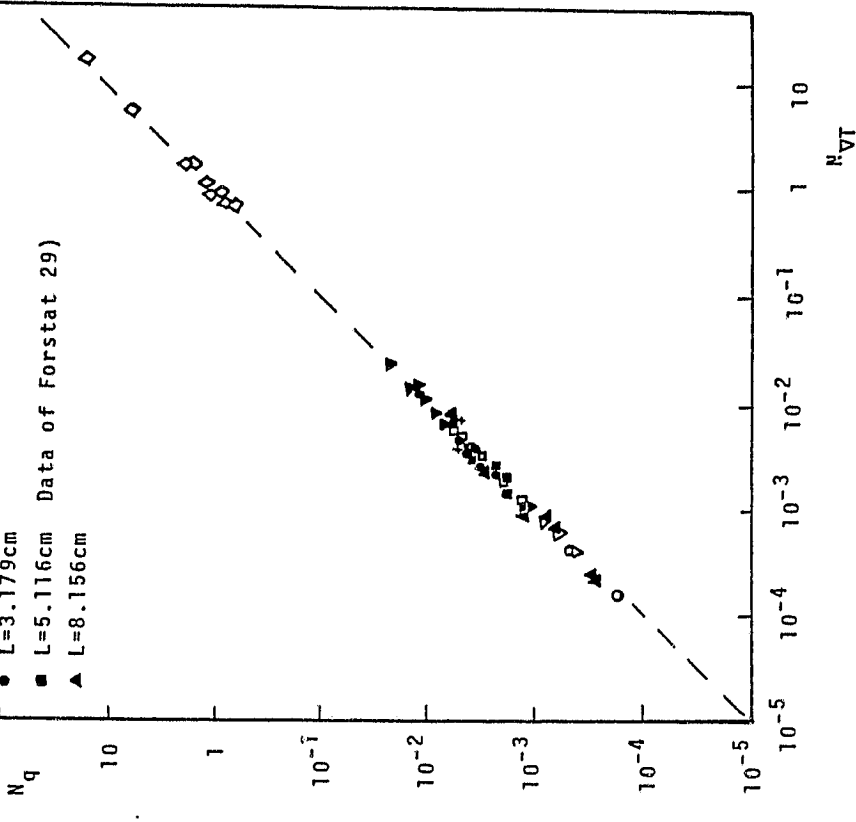
○ $d=0.17\mu\text{m}$ Data of Schmid et al. 26)

+ $d=1.25\mu\text{m}$

● $L=3.179\text{cm}$

■ $L=5.116\text{cm}$ Data of Forstater 29)

▲ $L=8.156\text{cm}$



2.7 The Vapor-Liquid Phase Separator

As mentioned in Chapter one, the vapor-liquid phase separator prevents the liquid He II from escaping out of the cryostat by means of the thermomechanical effect. The thermomechanical effect or the fountain effect was discovered by Allen and Jones in 1938. The apparatus of their experiment is depicted in Figure 2.16a. When heat is supplied to the inside of the vessel the temperature rises and the concentration of the normal molecules in the vessel increases (see Figure 2.2). Superfluid, with zero viscosity rushes through the capillary tube into the vessel to equalize the equilibrium concentration, while the normal molecules because of their friction cannot penetrate the tube rapidly. Thus, a pressure gradient is set up and the level inside the vessel rises. Figure 2.16b shows the fountain effect (in the fountain effect ΔP_T is converted in part into kinetic energy of "the fountain"), and Figure 2.16c shows the thermomechanical effect in a porous plug. With T_u and T_d as the upstream and downstream temperatures, the thermo-osmotic pressure is

$$\Delta P_T = \int_{T_d}^{T_u} \rho_s dT \quad (2.28)$$

If the temperature difference is small (i.e. $\Delta T \ll T$), systems and Robinson's classical data.

ORIGINAL PAGE IS
OF POOR QUALITY

Equation (2.28) can be written as equation

$$\Delta P_T = \overline{P}_{SAT} \quad (2.29)$$

In this case, the pressure difference can be related to the simplified Clausius-Clapeyron equation (if $\rho_v \ll \rho$)

$$\Delta T = \Delta P_v \frac{T}{Pv\lambda} \quad (2.30)$$

where ΔP_v is the vapor pressure difference between the upstream and downstream side of the phase separator, and λ is the latent heat of vaporization.

A plot of $\Delta P_T / \Delta P_v$ as a function of temperature is shown in Figure 2.17. We can see that the thermomechanical pressure is at least one order of magnitude larger than ΔP_v .

ORIGINAL PAGE IS
OF POOR QUALITY

However, in the case of a large ΔT , one has to integrate the thermomechanical equation. In substituting the entropy expression

$$S = S_\lambda \left(\frac{T}{T_\lambda} \right)^{5.6} \quad (2.31)$$

Equation (2.28) becomes

$$\Delta P_T = \int_{T_d}^{T_d + \Delta T} \rho_{S_\lambda} \left(\frac{T}{T_\lambda} \right)^{5.6} dT \quad (2.32)$$

Since the maximum temperature is T_λ we can integrate the above equation from T to T_λ , thus

$$\Delta P_T = \int_T^{T_\lambda} \rho_{S_\lambda} \left(\frac{T}{T_\lambda} \right)^{5.6} dT \quad (2.33)$$

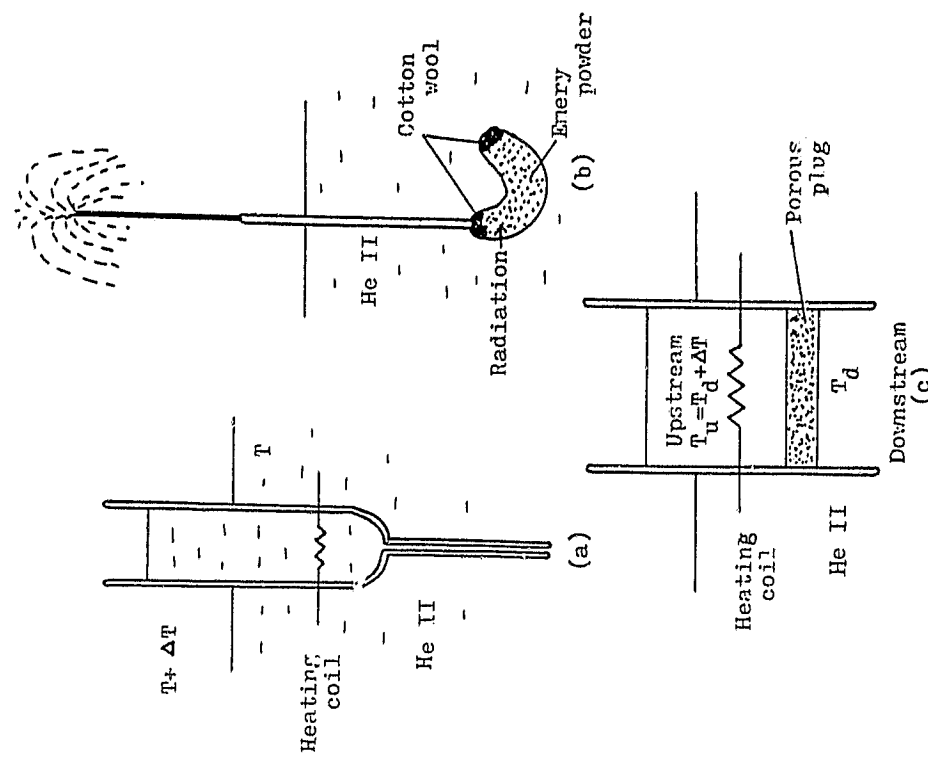


Figure 2.16 (a) The thermomechanical effect (Allen and Jones, 1938); (b) the liquid helium fountain; (c) the thermomechanical effect in a phase separator.

After integration one gets

$$\Delta P_T = \frac{\rho S_\lambda T_\lambda}{6.6} \left[1 - \left(\frac{T}{T_\lambda} \right)^{6.6} \right] \quad (2.34)$$

Figure 2.18 is a plot of ΔP_T vs. temperature. The thermomechanical pressure is almost constant at temperatures below 1 K. As the temperature increase, ΔP_T decreases and finally at T_λ there is no thermomechanical pressure.

Analogy of Thermo-Osmosis to Mass Osmosis

The thermo-osmotic pressure is analogous to the mass osmotic pressure as depicted in Figure 2.19.

In mass osmosis, if the concentration in the upstream is higher than the downstream, solvent will penetrate the membrane to the upstream to equalize the concentration, thus setting up the mass osmotic pressure (Π_{osm}). If the pressure due to the head $\Delta P = \rho g \Delta Z$ is less than Π_{osm} , the liquid level in the tube will rise until the two pressures are equalized. On the other hand if $\Delta P > \Pi_{osm}$, reverse osmosis will occur.

Similarly in thermo-osmosis, if the upstream temperature is higher than the downstream value, superfluid will penetrate the porous plug to the upstream thus setting up the thermo-osmotic pressure ΔP_T . If $\Delta P < \Delta P_T$ the liquid level in the tube will rise until $\Delta P = \Delta P_T$. On the other hand if $\Delta P > \Delta P_T$ the reverse will occur.

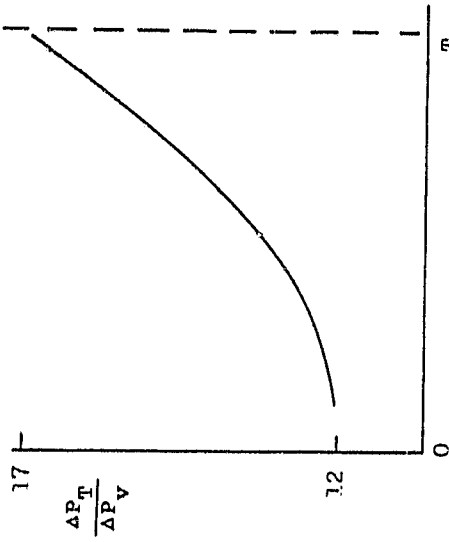


Figure 2.18 $\Delta P_T / \Delta P_V$ versus temperature (T_λ)

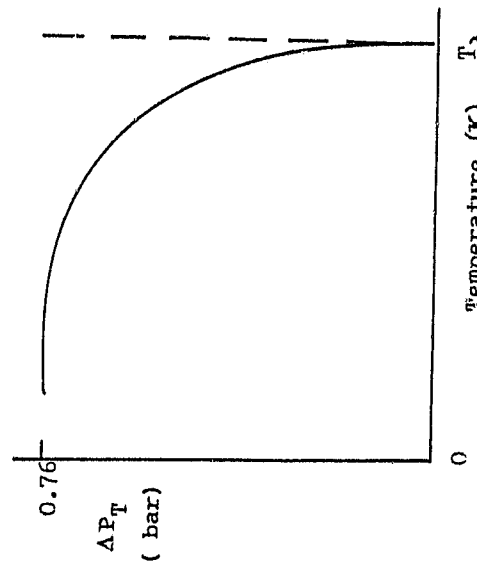


Figure 2.17 $\Delta P_T / \Delta P_V$ versus temperature (T_λ)

Figure 2.18 Thermo-Osmotic pressure as a function of temperature (for large ΔT).
Figure 2.17 $\Delta P_T / \Delta P_V$ versus temperature (T_λ)
OF POOR QUALITY

Equilibrium Conditions of Phase Separator

In order to understand the theory behind the vapor-liquid phase separator let us look at the different equilibrium conditions of a phase separator.

Figure 2.20 shows the temperature and pressure profile across a phase separator. For this case, we have

Liquid He II sitting on top of a porous plug. The downstream of the plug is opened to a pressure lower than the vapor pressure of liquid helium.

According to Bernoulli's equation for ordinary liquids.

$$\rho_L \frac{w_u^2}{2} + \rho_L g z + p_{vu} = \rho_d \frac{w_d^2}{2} + \rho_d g z + p_{vd} \quad (2.35)$$

Since the upstream density (density of liquid) is much larger than the downstream (density of gas), Equation (2.35) can be written as

$$\rho_L \frac{w_u^2}{2} + \rho_L g (H + L) + (p_{vu} - p_{vd}) = 0 \quad (2.36)$$

a) ideal case

If we assume an ideal static case where there is no velocity in the liquid, Equation (2.36) becomes

$$\rho_L g (H + L) + (p_{vu} - p_{vd}) = 0 \quad (2.37)$$

The equilibrium condition in Equation (2.37) implies that p_{vd} has to be larger than p_{vu} .

ORIGINAL PAGE IS
OF POOR QUALITY

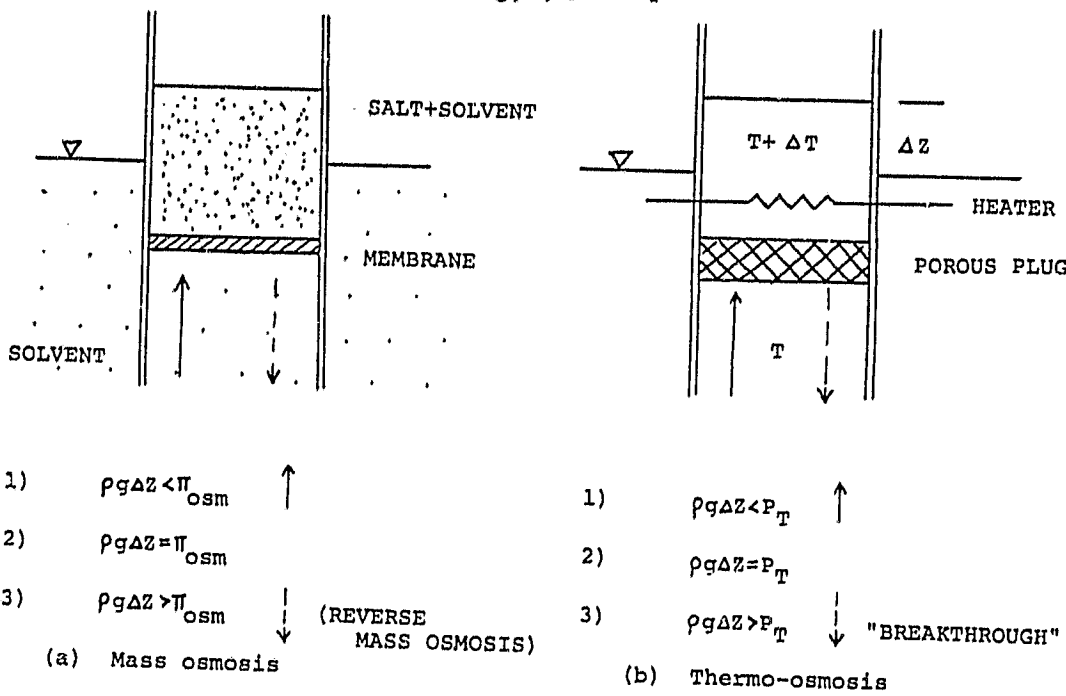


Figure 2.19 Analogy of mass osmosis and thermo-osmosis.

However in the vapor-liquid phase separator the downstream pressure is always kept below the vapor pressure of liquid helium. The equilibrium condition is possible, due to the presence of the thermomechanical pressure of liquid He II. In matching the pressure difference (see Figure 2.21) we get

$$\rho_{Lg} (H + L) + \Delta P_V = \Delta P_T \quad (2.38)$$

The above equation shows the equilibrium condition of the phase separator during normal operating condition, in the presence of gravity.

b) non-ideal case

In space operations, there is no gravitational force. Since ΔP_T is always larger than ΔP_V we can no longer assume that the velocity of the liquid is zero. Thus

$$\rho_{Lg} \frac{W^2}{2} + \Delta P_V = \Delta P_T \quad (2.39)$$

- i) In the rotation depletion limit ($\beta_s \sim \rho$, $W \sim v_n$, $\rho_h \ll \rho$) Equation (2.39) can be written as

$$\rho \frac{v_n^2}{2} + \Delta P_V = \Delta P_T \quad (2.40)$$

If the heat flux density q is known, the normal velocity in equation (2.40)

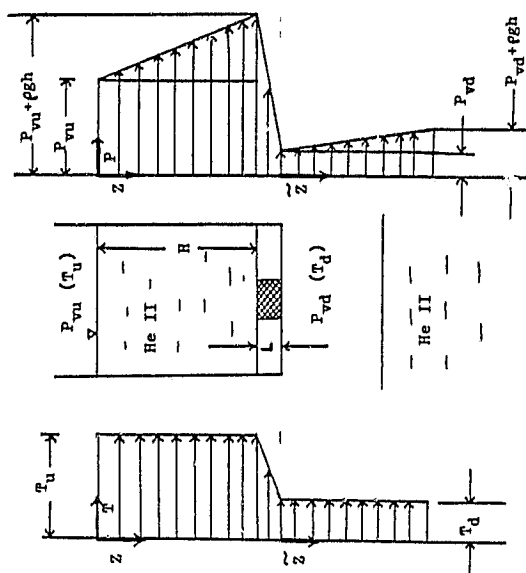


Figure 2.20 Temperature and pressure profile across a phase separator.

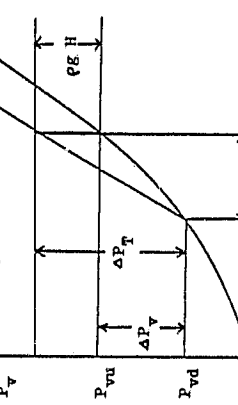


Figure 2.21 va, vr pressure versus temperature across a phase separator.

can be calculated by the two-fluid model

equation

$$q = \rho_{ST} V_n \quad (2.41)$$

- iii) If the temperature is close to T_λ , the superfluid velocity will be much larger than the normal velocity. Unfortunately little is known in this area. Therefore the second purpose of this work is to study the hydrodynamic flow of He II across the porous plug in this range.

3. APPARATUS AND EXPERIMENTS

There are two main parts of the experimental investigations, namely the permeability tests and the thermo-osmosis experiments.

3.1 Permeability Tests

3.1.1 Apparatus

The permeability tests were performed in an existing cryostat. The schematic diagram of the entire system is shown in Figure 3.1. He^4 gas passed through

a liquid nitrogen bath where He^4 gas was cooled to around 80 K. It then entered the He^4 cryostat (Figure 3.2) where the helium gas was further cooled by two stages of heat exchangers. The first stage of heat exchanger was made of copper tube O.D. 0.635 cm (1/4 in.) which consisted of eleven sets of spirals (Figure 3.3a). The second stage of heat exchanger was made of copper tube also O.D. 0.318 cm (1/8 in.) wound in a helix (Figure 3.3b). Passing through the test chamber He^4 gas would leave the cryostat and pass the flow meter (details of the test chamber will be discussed in the next section).

3.1.2 The Test Chamber

The plug holder or the test chamber was made of 3/8 tubes, one inside another as shown in Figure 3.4. The tubes were made of stainless steel (grade 304, the

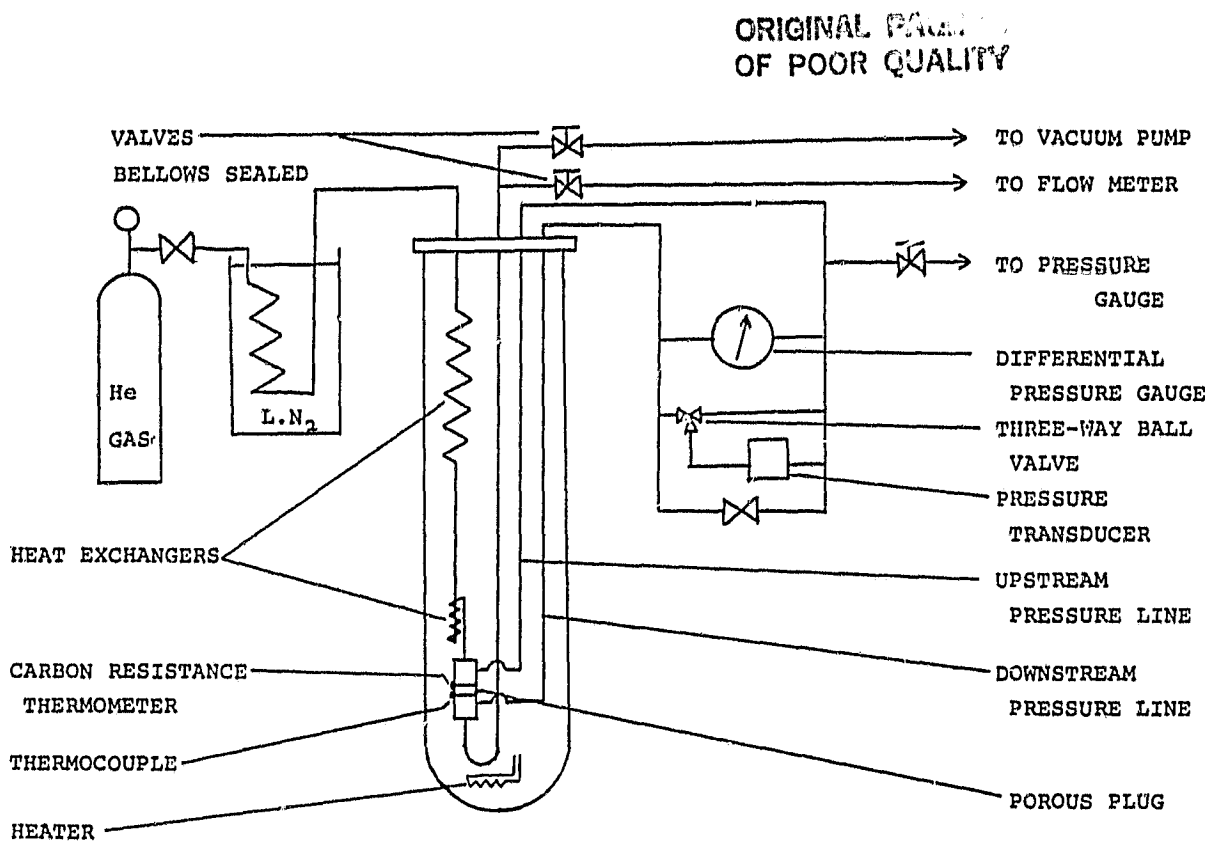


Figure 3.1 A schematic diagram of the permeability measurement system.

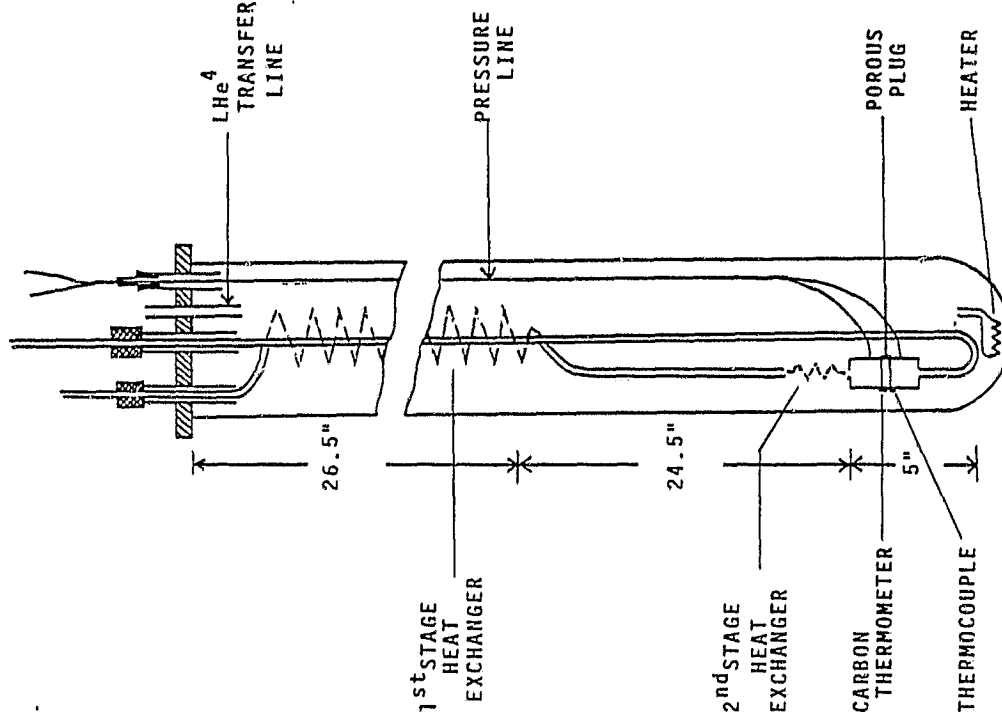


Figure 3.2 A schematic diagram of permeability measurement apparatus.

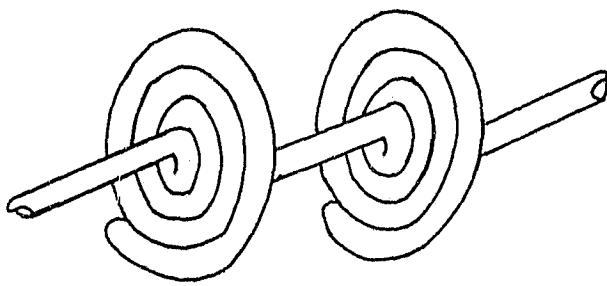


Figure 3.3a First stage heat exchanger.

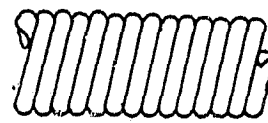
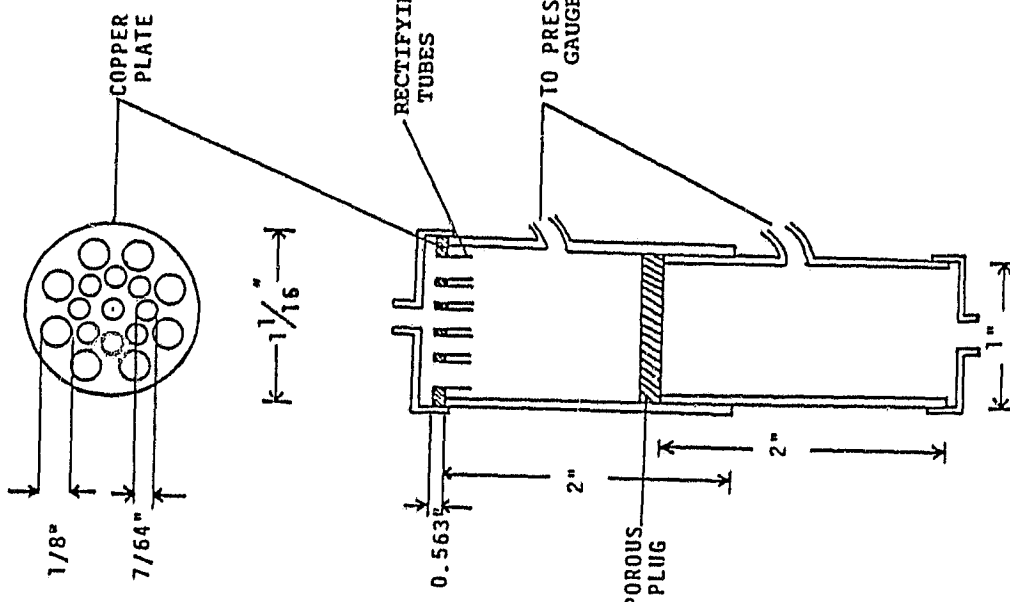


Figure 3.3b Second stage heat exchanger.



ORIGINAL PAGE IS
OF POOR QUALITY

Figure 3.4 Schematic diagram of the test chamber.

inside tube has an O.D. of 2.54 cm, both has a wall thickness of 0.065 cm). The porous plug was mounted between the tubes by Stycast (1266). On the top of the chamber (entrance) there was a rectifier made of copper plate and stainless steel tubes (Figure 3.4). At the side of the chamber a small hole was drilled on both the upstream and downstream of the plug and two stainless steel tubes (O.D. 0.318 cm) were brazed there. Those tubes were attached there for pressure sensing. A carbon resistance thermometer and a thermocouple were installed on the outside of the chamber close to the plug. Ten layers of 1" wide masking tape were wrapped around both thermometers for insulation.

A heater was attached below the test chamber (Figure 3.2) to boil off liquid He or nitrogen to get more efficient heat exchange.

3.1.3 Thermometry

The thermometers were made of 1/8 Watt Allen-Bradley carbon resistors with a nominal resistance of 39 ohms. Such resistors have been found to exhibit consistently high sensitivity and reproducibility. The carbon thermometer resistance was calibrated against the vapor pressure of He⁴ which in turn was related to the temperature through the T-58 scale for He⁴.

Prior to use, the plastic cover of the resistance

was removed by grinding. To further increase its thermal response time the resistor was sanded to a thin slab with a rectangular cross section. Two constantan wires (0.075 cm diameter) were soldered to each side of the thermometer. A thin layer of varnish was put on the resistor to insure electrical insulation and prevent thermal contact with metals. Teflon-coated copper wires (5 mil diameter) were then soldered onto the constantan wires to carry electrical signals out of the dewar.

In order to get the temperature from the resistance reading, a three parameter relation was used

$$\log \tilde{R} + \frac{\tilde{K}}{\log R} = \tilde{A} + \frac{\tilde{B}}{T} \quad (3.1)$$

\tilde{A} , \tilde{B} and \tilde{K} are experimentally determined constants. Calibrating the thermometer resistance against the He⁴ vapor pressure the three parameters A, B and K were calculated using the least mean squares method.

The three parameters will have different value for different thermometers due to the deviation in size. The error in temperature measurements are discussed in Appendix D (M . Sc.thesis of S.W. Yuan).

The thermocouple was made of nickel-chromium wire and copper-nickel wire (Omega Engineering, Inc.) The thermocouple had been calibrated against temperature at three fixed points.

ORIGINAL PAGE IS
OF POOR QUALITY

3.1.4 Instrumentation

Figure 3.5 is a block diagram of the electronic circuit for the carbon resistance thermometer and the heater. A current source (Keithley 255) supplied 1 mA of current to the thermometer. The voltage of the resistor was recorded by an X-Y plotter (Houston Instrument 2000). The heater was energized by a power supply (HP Harrison 6224B).

The voltage across the thermocouple was recorded by a digital voltmeter (Dana 4470).

The differential pressure across the plug was measured by a differential pressure gauge (Pennwalt, Model 62D-4C-004OD) and a pressure transducer (Validyne, Model DP 15-20, membrane 20) with a digital readout (Validyne, Model CD 25).

ORIGINAL PAGE IS
OF POOR QUALITY

The flow rate was measured by a Wet Test Meter (Precision Scientific Co., Model 63118). In addition, three floating-sphere meters (Books Instruments Co. Inc., Hatfield, PA. Model P-72-H-RO) were used. A calibration curve of the floating-sphere meters is shown in Figure E-2 of Appendix E.

3.1.5 Experimental Procedures

Prior to experimental runs the carbon resistance thermometer was calibrated. This was done by taking the resistance values at room temperature, liquid nitrogen temperature and liquid He temperature. A computer program

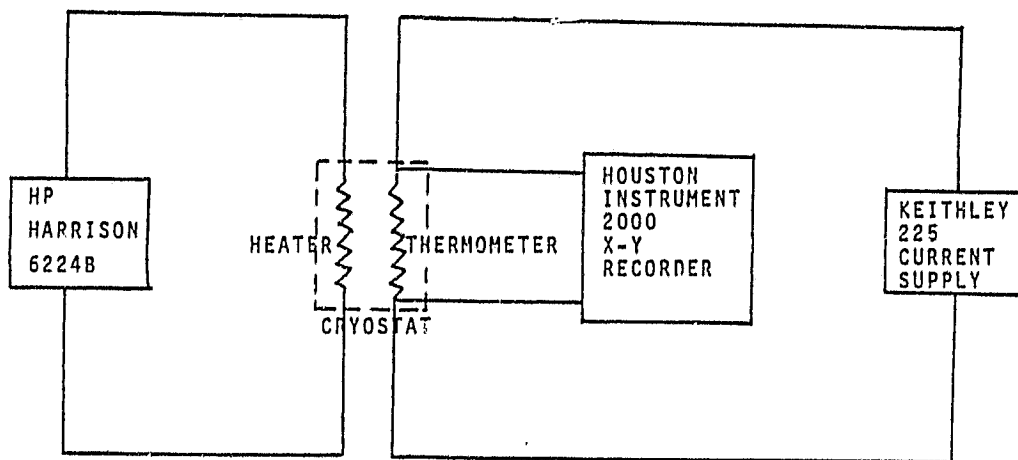


Figure 3.5 Circuitry for heater and thermometer.

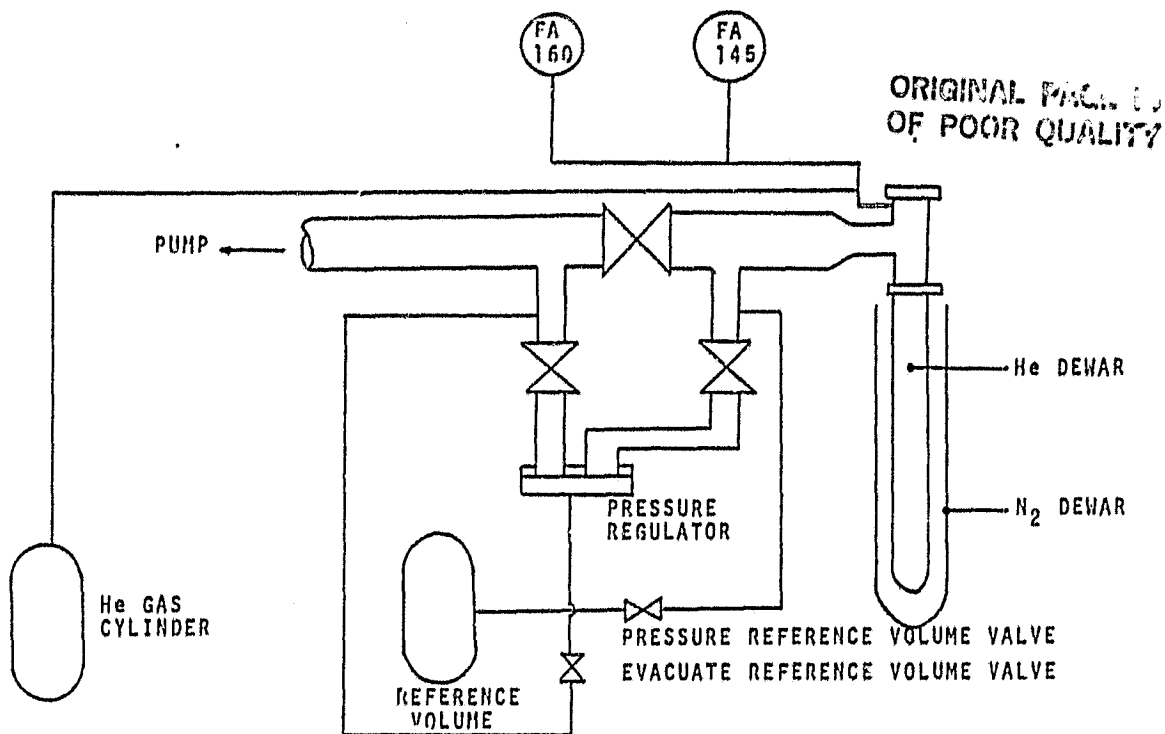


Figure 3.6 Schematic diagram of the cryostat system

was run to get the resistance temperature functions.

Before every run the apparatus was pumped by a diffusion pump for days to remove any impurities that might contaminate the plug. The procedures for recording data were the same for room temperature, liquid nitrogen and liquid He temperature runs, the only difference was the transfer of cryogens. For liquid N₂ runs liquid nitrogen was transferred to the inside jacket. For liquid He runs, liquid nitrogen was transferred to the outside jacket first and liquid He was transferred to the inside jacket.

During the runs, He⁴ gas was introduced into the system. After steady state was reached (i.e. temperature and ΔP not changing with time) the differential pressure, the thermometer resistance value and the flow rate were recorded.

Some data were taken above the boiling point of liquid nitrogen or liquid He. Temperatures above the boiling point could be reached during warm up or cool down period.

3.2 The Thermo-Osmosis Experiment

3.2.1 Apparatus

The thermo-osmosis experiment was performed in an existing cryostat. The schematic diagram of the cryostat system was depicted in Figure 3.6. Unlike the permeability apparatus the thermo-osmosis apparatus was an open

system (Figure 3.7) which could be modified to a close system. The upstream side of the porous plug was in contact with He II which penetrated the pores and vaporized at the downstream side. The vaporized He⁴ gas was then pumped out by a vacuum pump.

3.2.2 The Low Temperature Apparatus

The low temperature system is shown in Figure 3.8.

The stem of the apparatus was made of 304 stainless steel pipes (2.54 cm X 0.05 wall and 2.67 cm X 0.05 wall). A porous plug holder (Figure 3.9) was soldered to the end of the stem. The plug holder was made of 304 stainless steel also (O.D. 2.67 cm X 0.0127 wall) and the porous plug (2 μ m) was mounted in place by stycast (1266). A flow control plate was installed on top of the porous plug to restrict flow rate. The control plate was made of a perforated G-10 plate which had 40 holes with a hole diameter of 0.159 cm (= 1/16 in.).

For easy control and reading of the He II liquid level, a coaxial vessel of pyrex glass was attached to the stem of the apparatus by strings. The vessel has a lower kovar section (Figure 3.10).

Twenty layers of masking tape were wrapped around the kovar for insulation. A heater was mounted in the bottom of the container.

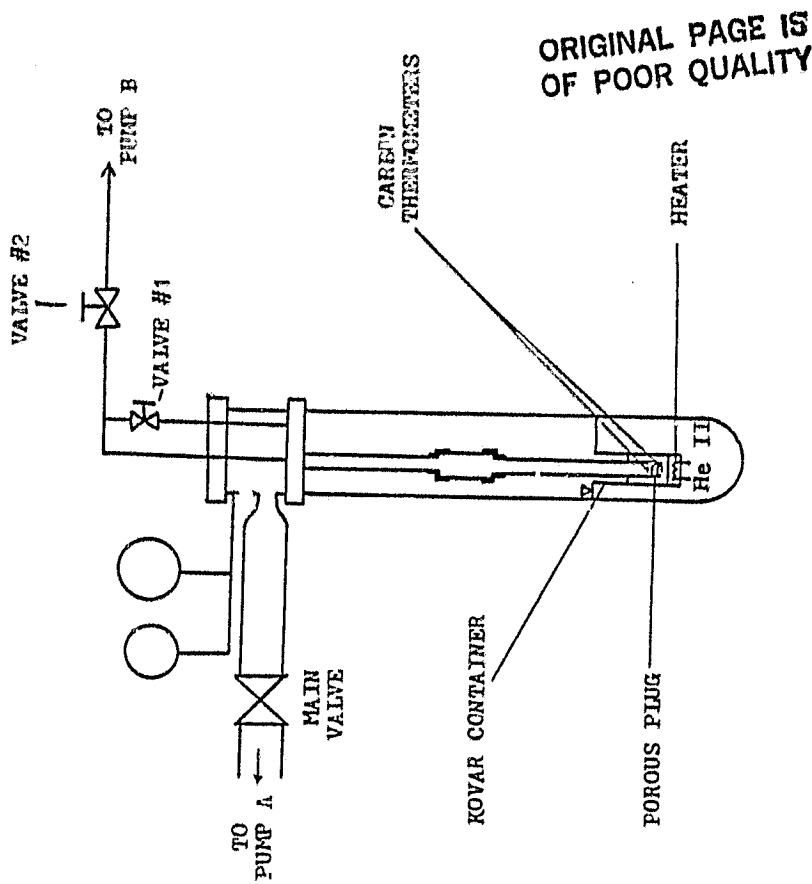


Figure 3.7 Schematic diagram of the low temperature system of the thermo-osmotic experiment.

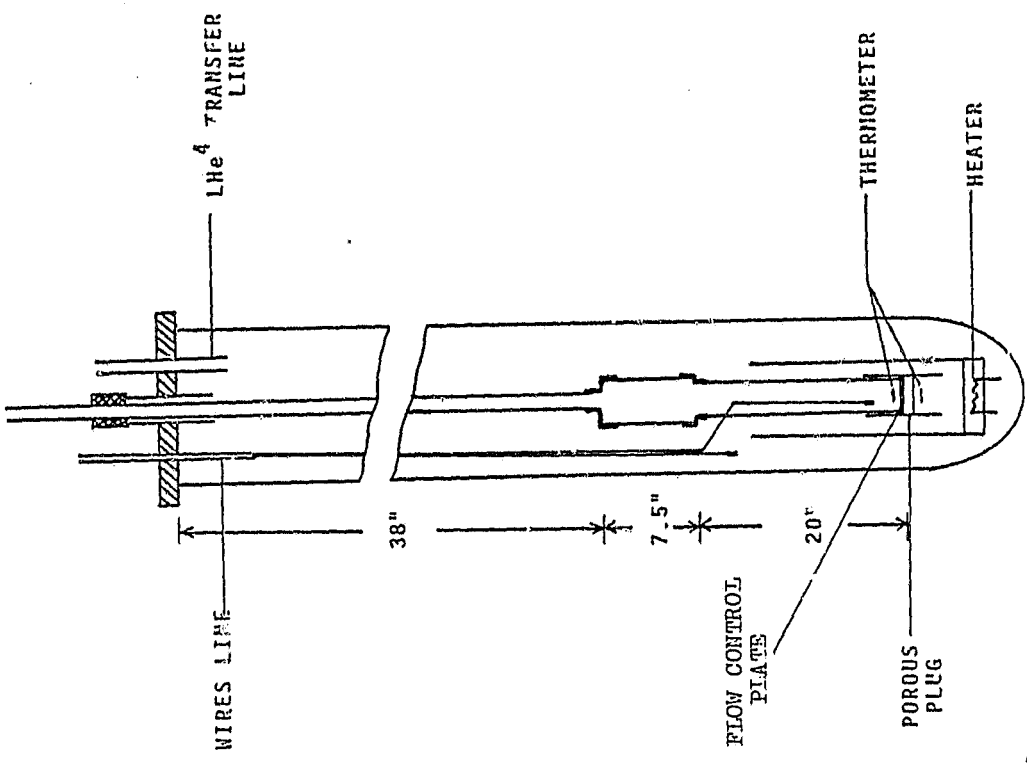


Figure 3.8 The schematic diagram of the low temperature of the thermo-osmotic experiment .

PLUG HOLDER

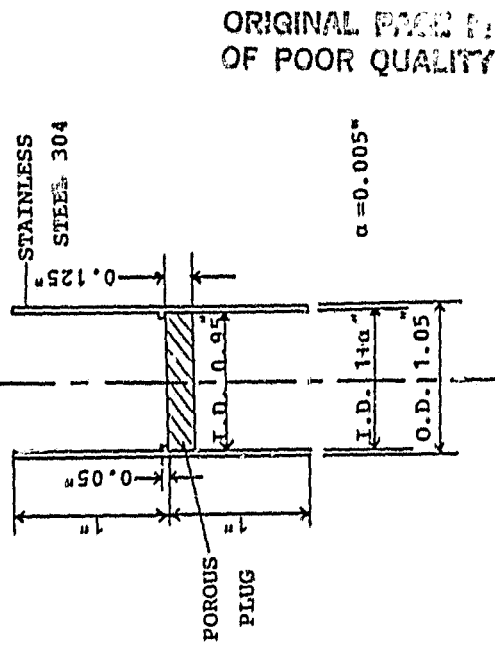


Figure 3.9 Schematic diagram of the porous plug holder .

3.2.3 Instrumentation

The circuitry for the upstream and downstream thermometers is shown in Figure 3.11. A Keithley 225 was used to supply current to the thermometers. The voltage across the resistors were measured by an x-Y recorded (Houston Instrument 2000).

Figure 3.12 is a block diagram of the electronic circuit for the heater. A DC power supply (HP "Garrison 6224B) was used to energize the heater. The current was measured by Simpson 1702 milliammeter and the voltage across the heater was recorded by an x-Y plotter (Woseley 7035A).

The vapor pressure difference of the upstream and downstream was sensed by pressure taps and measured by differential pressure gauge (Pennwalt, Model 623-4C-0040D).

3.2.4 Experimental Procedures

Before doing the experiment, the thermometers were calibrated as mentioned in section 3.1.5. The permeability value of the porous plug at room temperature was measured. This was done by a slight modification of the system. Ne_4 gas was introduced into the inner jacket of the crystal which passed the porous plug, through the stem of the apparatus and came out of the system after passing through the flow meter. The flow rate \dot{V} , differential pressure across the plug ΔP were recorded and the permeability can

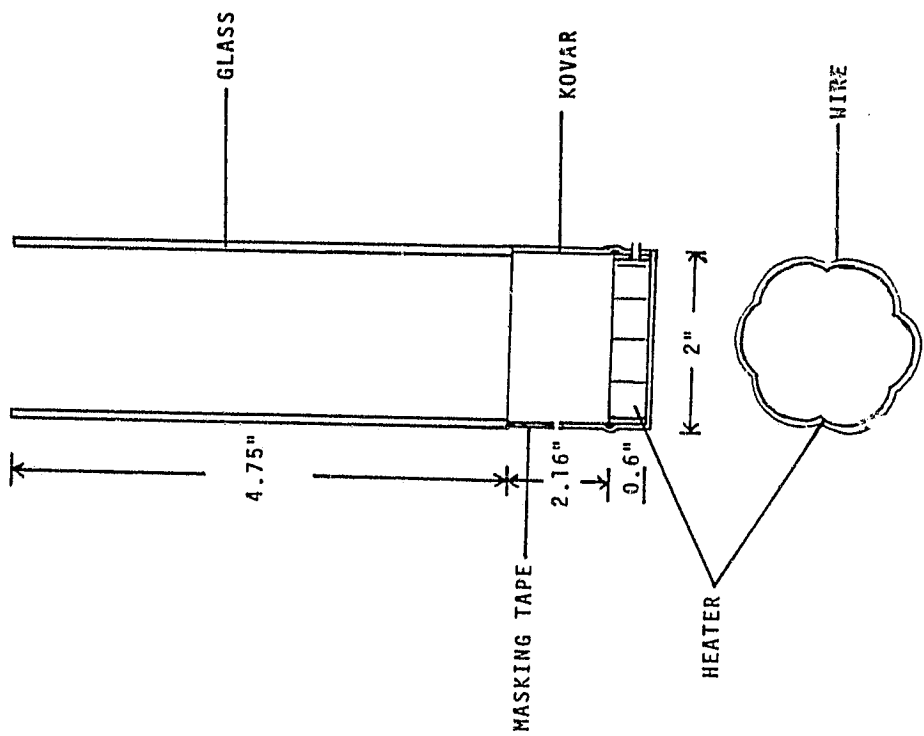


Figure 3.10 A schematic diagram of the kovar container with the heater.

ORIGINAL PAGE IS
OF POOR QUALITY

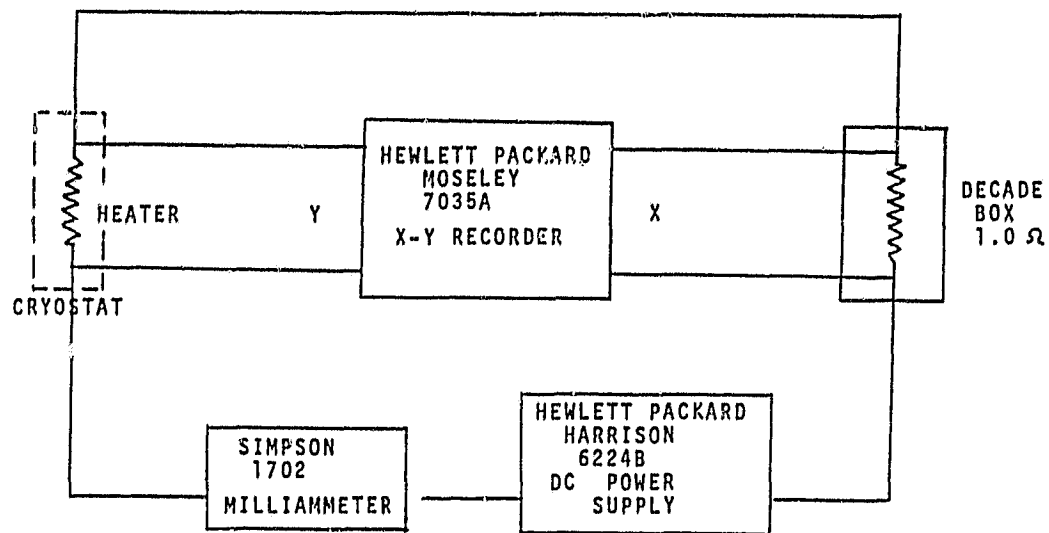


Figure 3.12 Circuitry for the heater.

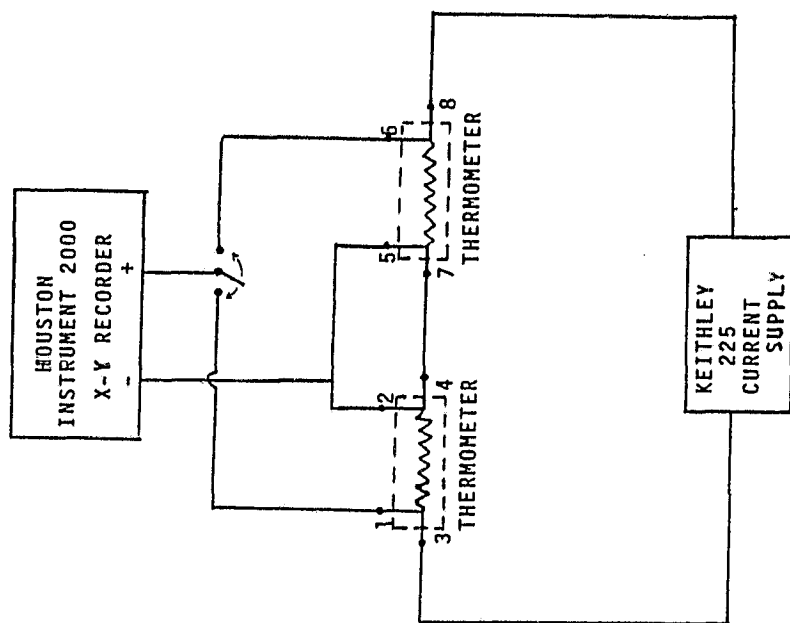


Figure 3.11 Circuitry for thermometers.

by calculated by Equation 2.26 as shown in the next section.

Prior to the experiment the whole system was evacuated. This was done by opening the "main valve" which connected the inner dewar to pump A (Figure 3.7). During the process, valve #2 was closed and valve #1 opened. After evacuation, the main valve was closed and He^4 gas was introduced into the system. Liquid nitrogen was transferred to the outer jacket of the cryostat.

Liquid He was then transferred into the inner jacket. The temperature of the inner jacket was pumped down to below the Lambda point (2.172 K) by manipulation of the main valve. The temperature range for the experiment was between 1.6 K - 2.1 K. When the desired bath temperature was reached the main valve was closed, pump B was turned on, valve #1 was closed and valve #2 was opened. The apparatus was then ready for the experiment.

The bath temperature (T_b), the differential vapor pressure (ΔP_v), and the liquid He II level inside the kovar container were recorded every one or two minutes. The upstream and downstream temperature were recorded by X-Y plotter. The procedures were repeated by applying heater current of 50 mW, 100 mW, 150 mW and 200 mW respectively.

3.3 Data Reduction

3.3.1 Calculation of the Classical Permeability at Various Temperatures

From the permeability test, the pressure difference across the porous plug and the volumetric flow rate at room temperature were recorded. The volumetric flow rate at low temperature (T_L) was calculated by

$$\dot{V}_L = \dot{V}_{\text{room}} \frac{\rho_{\text{room}}}{\rho_L} \quad (3.2)$$

If $\Delta P \ll P$, the pressure is essentially constant and from the ideal gas law , one obtains

$$\frac{\rho_{\text{room}}}{\rho_L} = \frac{T_L}{T_{\text{room}}} \quad (3.3)$$

The permeability value at low temperature can thus be calculated by Equation 2.26

$$(K_p)_m = \frac{\dot{V}_L \eta_L}{A_p |\nabla P|} \quad (3.4)$$

where η_L is the viscosity at the appropriate low temperature
 A_p is the total area of the porous plug

3.3.2 Calculation of the Normal Fluid Permeability (K_p)_n
The volumetric flow rate of He II across the porous plug is calculated from the change in liquid level of He II in the dewar. Since total mass is conserved, the liquid disappeared must have passed through the porous plug.

ORIGINAL PAGE IS
OF POOR QUALITY

$$\dot{V}_{\text{He II}} = \frac{\Delta Z}{t} A_0 \quad (3.5)$$

where ΔZ is the liquid level difference
 t is the time it took to change the level
 A_0 is the surface area of He II
 (cross section area of the dewar
 - cross section area of the apparatus)

The heat required to vaporize the He II on the downstream side is

$$\dot{Q} = \lambda \dot{m} = \lambda \rho \frac{\Delta Z}{t} A_0 \quad (3.6)$$

Then from Equation (2.15) we can calculate the normal fluid velocity.

$$\bar{V}_n = \frac{\dot{Q}}{\rho_{\text{STAE}}} = \frac{\lambda A_0 \Delta Z}{S \bar{T} A_E} \quad (3.7)$$

where S is the entropy of He II
 λ is the latent heat of vaporization of He II
 and A_E is the effective flow area of the porous plug

In the thermo-osmotic experiment, a flow control plate was installed on one side of the porous plug so that the flow area of the plug was reduced. From the previous measurements at 300 K the plug permeability at room temperature is known to be $K_p(300) = 5 \times 10^{-9} \text{ cm}^2$.

This value pertains to the 1 in. plug with a total area of 5.06 cm^2 . From the data in Table 3.1 the effective area $A_E = 3.2 \text{ cm}^2$ is calculated.

TABLE 3.1 ROOM TEMPERATURE DATA OF PERMEABILITY TEST FOR THERMO-OSMOTIC SYSTEM

RUN #	P, mbar	$\dot{V}, \text{cm}^3/\text{s}$
1	22.4	5.48
2	28.7	6.95
3	34.9	8.59
4	39.3	10.1

ORIGINAL PAGE IS
OF POOR QUALITY

Thus the normal fluid permeability can be calculated

$$(K_p)_n = V_n \eta_n / |\nabla P_T| \quad (3.8)$$

$$\text{or} \quad (K_p)_n = \frac{\lambda}{S_T} \frac{A_o}{A_E} \frac{\Delta Z}{t} \frac{\eta_n}{|\nabla P_T|} \quad (3.9)$$

If we substitute the thermomechanical pressure by Equation (1.16) we get

$$(K_p)_n = \frac{\lambda}{\rho_s^2 T} \frac{A_o}{A_E} \frac{\Delta Z}{t} \frac{\eta_n}{|\nabla T|} \quad (3.10)$$

4. RESULTS AND DISCUSSION

4.1 Classical Permeability Values of He⁴ Gas Across a 2 μm Stainless Steel Plug at Various Temperatures

Figures 4.1 and 4.2 are plots of the superficial flow velocity of He⁴ gas as a function of the pressure difference across the plug at room temperature. Figure 4.1 represents data at relatively small mass throughput, and Figure 4.2 shows data over an extended range in

throughput and ΔP. The data at liquid nitrogen temperature is shown in Figure 4.3. The data in each of the three figures lie in a straight line with a slope equals to $(K_p)_m / \eta_L$ (from Equation 2.6). This verifies that Darcy's law is valid and we have a well-defined permeability value at room temperature and liquid nitrogen temperature.

ORIGINAL PAGE IS OF POOR QUALITY

Figure 4.4 is an example of liquid nitrogen runs with a non-linear behavior of the superficial speed versus pressure difference. There are two possible reasons for the non-linear behavior. One explanation is that there was a transition from laminar to turbulent flow as the flow velocity \bar{V}_o is large. This possibility is ruled out by the fact that the Reynolds number is lower than the limit of laminar flow. The other possibility is that the heat exchanger system might function off the

ORIGINAL PAPER
OF POOR QUALITY

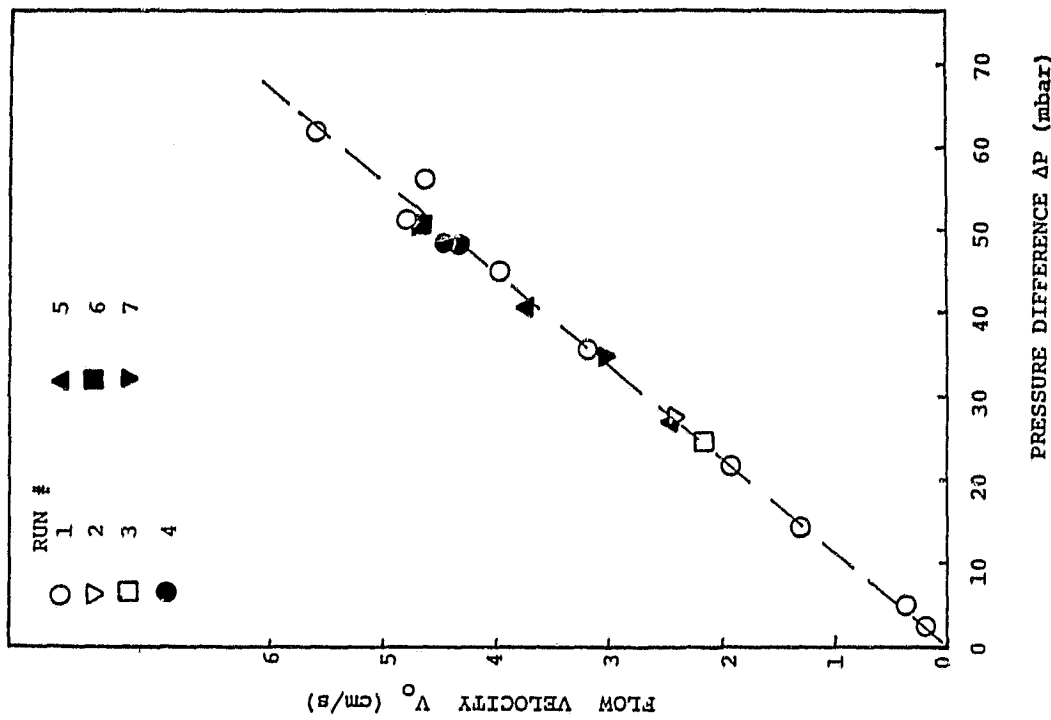


Figure 4.2 V_o versus ΔP at room temperature.

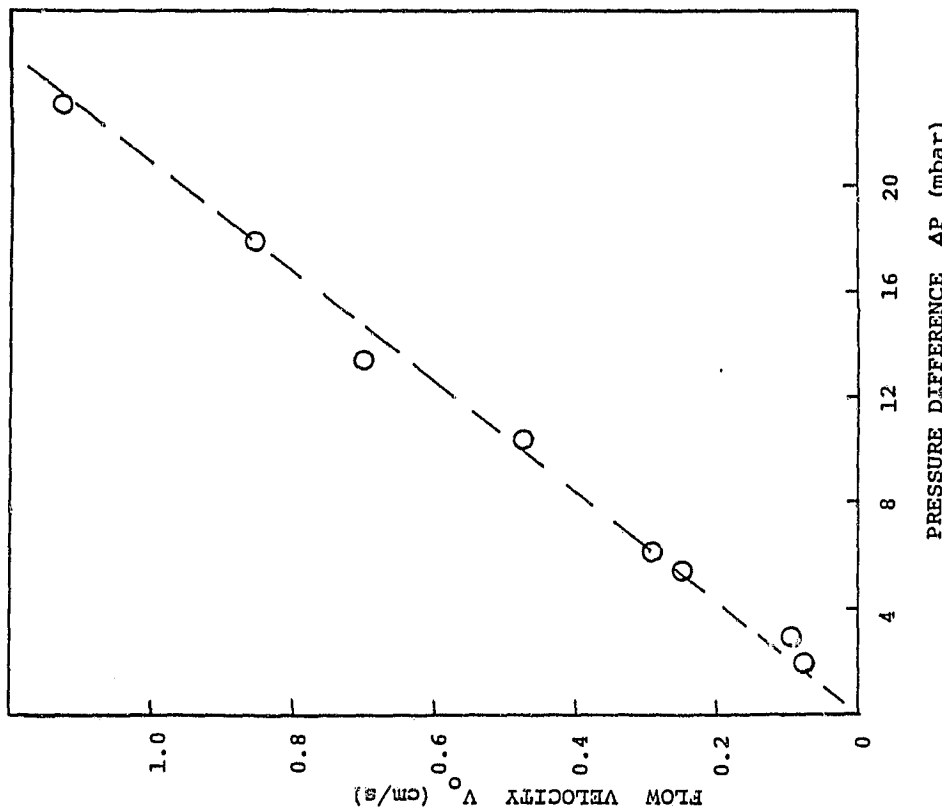


Figure 4.1 V_o versus ΔP at room temperature (small mass throughput).

ORIGINAL PAGE IS
OF POOR QUALITY

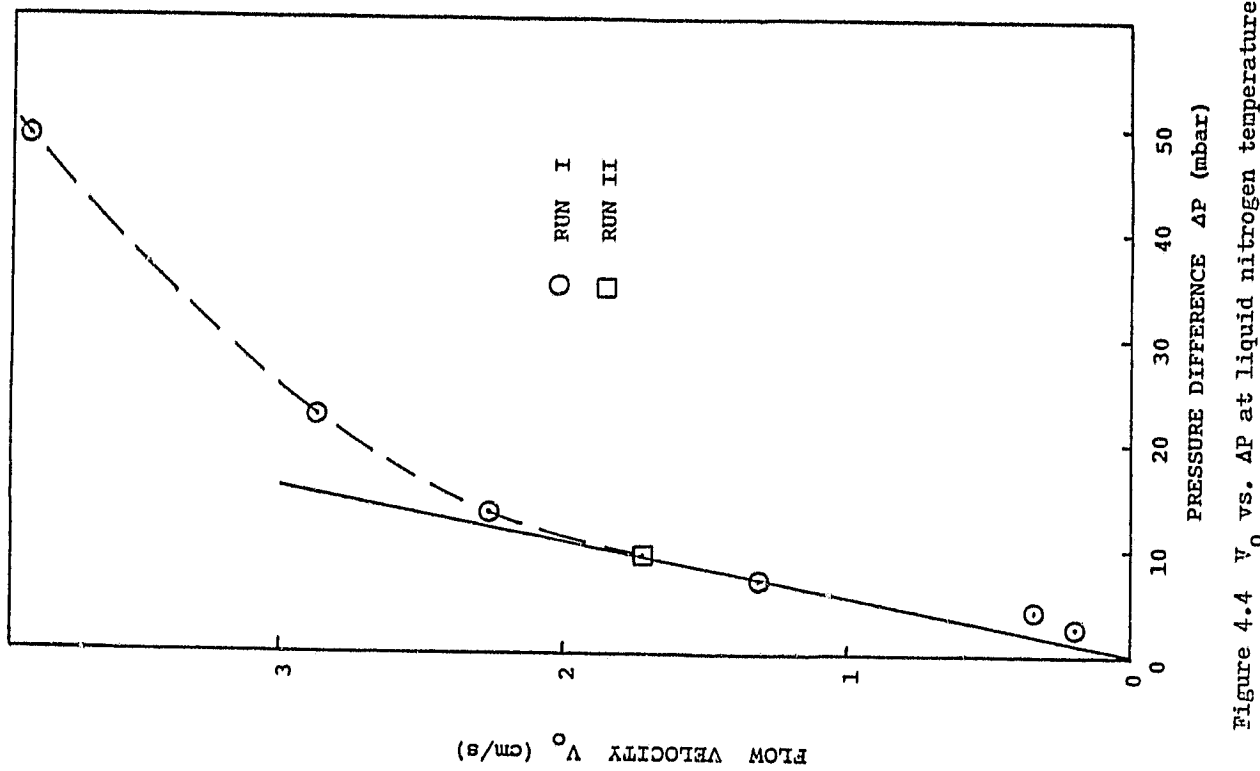


Figure 4.4 V_0 vs. ΔP at liquid nitrogen temperature.

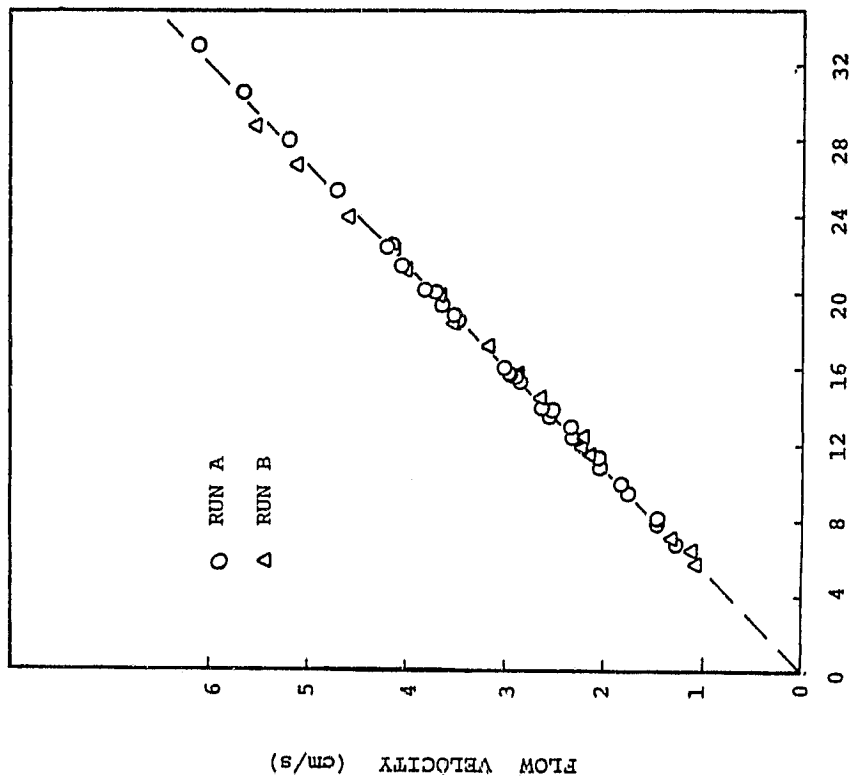


Figure 4.3 V_0 versus ΔP at liquid nitrogen temperature.

ORIGINAL PAGE IS
OF POOR QUALITY

TABLE 4.1 AVERAGE VALUE OF PERMEABILITY
AT VARIOUS TEMPERATURE

TEMPERATURE	$L He T^o$ (4.2 K)	$L N_2 T^o$ (77.4 K)	ROOM T^o (300 K)
PERMEABILITY (cm^2)	3.3×10^{-9}	4.90×10^{-9}	5.65×10^{-9}

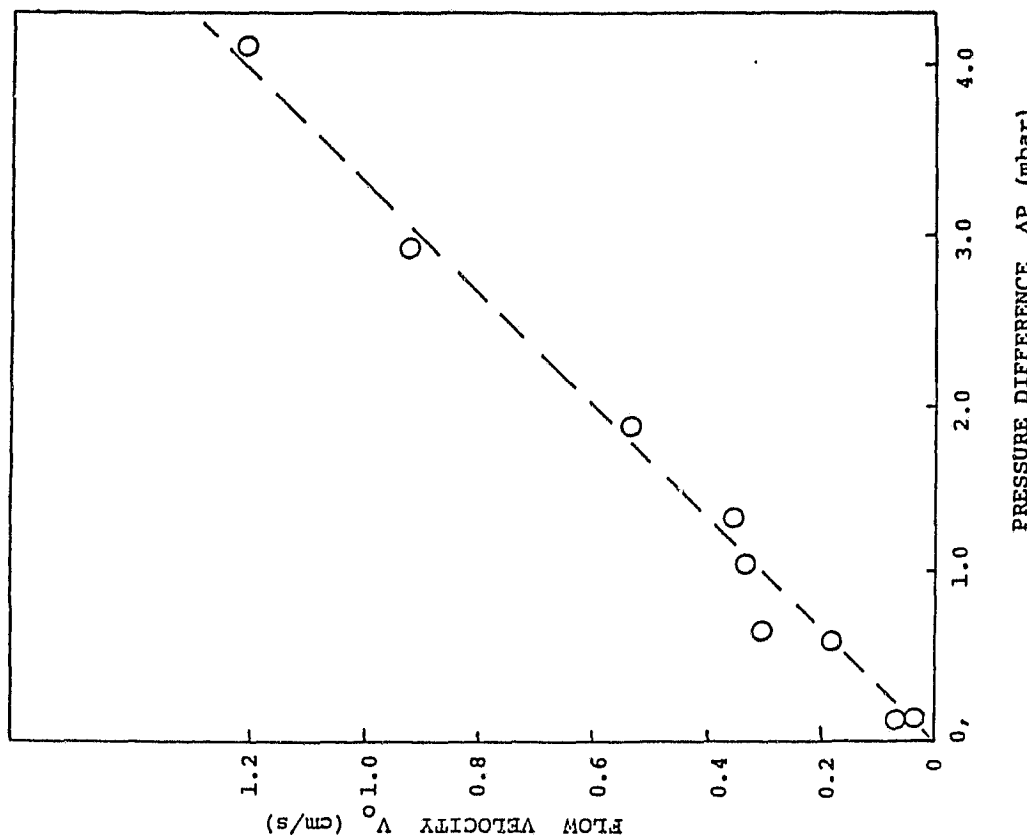


Figure 4.5 V_o vs. ΔP at liquid helium temperature.

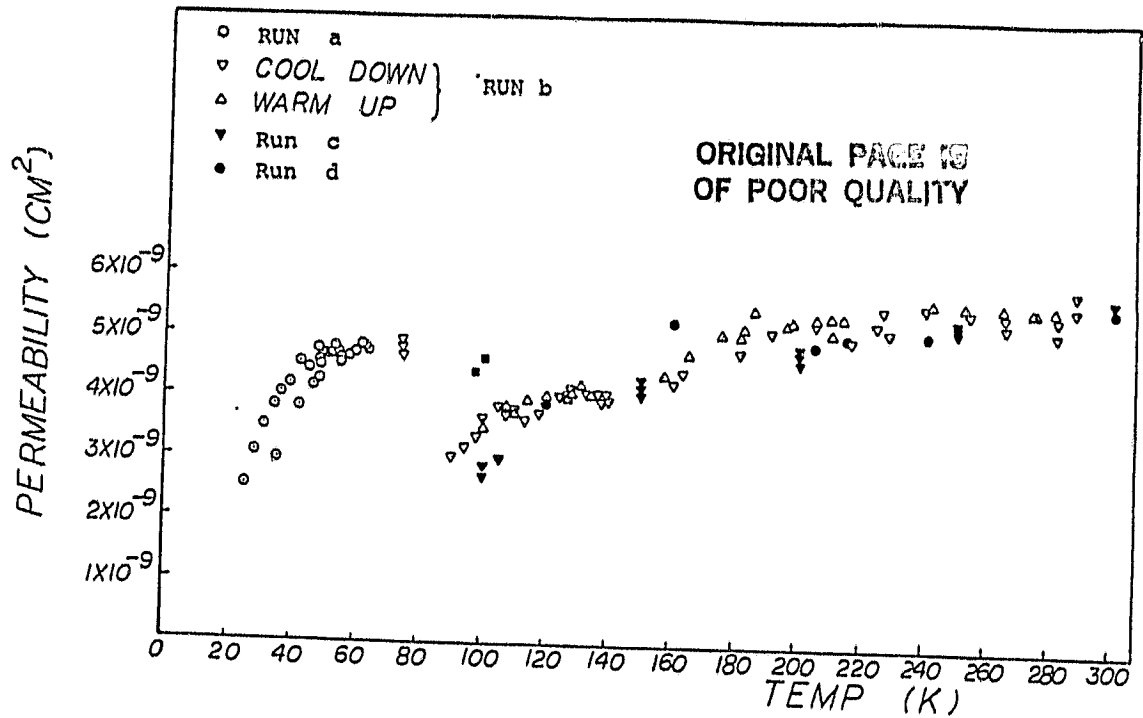


Figure 4.6 Permeability values at various temperatures .

design point at low effectiveness values. This means that the temperature of the gas passing through the porous plug was actually higher than the temperature measured (since the thermometers were installed on the outside of the test chamber). Insertion of property values at the liquid nitrogen temperature leads to a V_0 value which is too low. Thus the apparent permeability resulting from this procedure is smaller than the real permeability.

Figure 4.5 represents the permeability data taken at liquid He temperature. One can see that there is quite a bit of scattering among the data. Experiments performed at 4.2 K was difficult since He⁴ gas was condensed. The uncontrolled condensation of gas and vaporization of liquid He⁴ inside the system induced fluctuations in both the differential pressure gauge and flow meter. The reproducibility of data at this temperature is questionable.

The average values of permeability at room temperature, liquid nitrogen temperature and liquid helium temperature are tabulated in Table 4.1.

Figure 4.6 shows the permeability values as a function of temperature. These data were taken during the cool down or warm up of the experimental runs. It is seen that the permeability decreased as the temperature was lowered (from $5.65 \times 10^{-9} \text{ cm}^2$ at 300K to about $4.70 \times 10^{-9} \text{ cm}^2$ around 50 K).

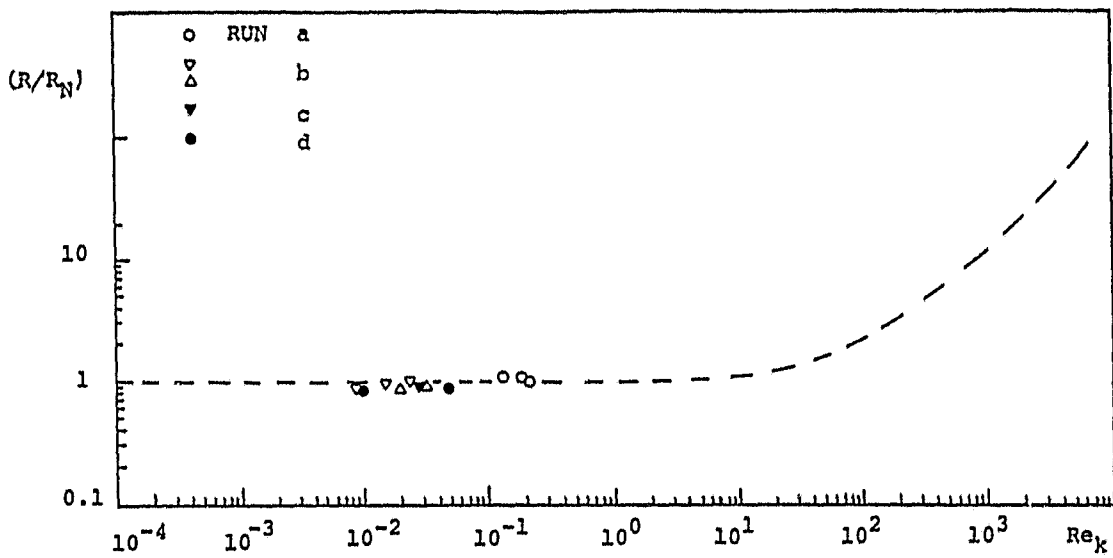


Figure 4.7 (R/R_N) versus Re_k .

There are two regions in Figure 4.6 where the permeability values drop drastically (from 80K-160K and below 50K). This is due to the inefficiency of the heat exchanger. With an improved heat exchanger system the permeabilities are seen to be raised considerably (solid squares on Figure 4.6).

The flow resistance ratio (R/R_N) is plotted as a function of the modified Reynolds number Re_k in Figure 4.7. The dotted line represents Ergun's equation for packed beds

$$\frac{R}{R_N} = 1 + 1.75 Re_k / 150 \quad (4.1)$$

$$where \quad Re_k = D_p \bar{V}_o \rho / \eta (1 - \epsilon)$$

$$R = \nabla P / \bar{V}_o$$

$$R_N = \frac{150 \eta (1 - \epsilon)^2}{D_p^2 \epsilon^3}$$

For laminar flow $Re_k < 1$, the flow resistance is unity. As the flow becomes turbulence R/R_N will deviate from unity. Using an effective particle diameter of 3.3×10^{-3} cm one can force the data to follow Ergun's equation. The data are seen to lie in the laminar regime which shows that Darcy's law is valid. At this range the Reynolds numbers are too small to show any geometric similarity between packed beds and porous plugs.

4.2 Results of the Thermo-Osmotic Experiment

The pressure drop across the porous plug is plotted as a function of temperature in Figure 4.8. We can see that the differential pressure decreased as the temperature was lowered. The result of this experiment can be compared to the data reported by Becker et al⁴¹ (Figure 4.9). A conical bronze plug was used in their system. The flow area of the plug is not known. There exists qualitative similarity between the two systems. Quantitatively there was a smaller pressure difference at low temperature for the system of Becker et al⁴¹. In general, the small pressure differences reflect low mass throughputs and small heat rejection rates.

Figure 4.10 is a plot of temperature difference across the plug versus the bath temperature. Like the differential pressure, the temperature across the plug was a strong function of temperature. As the bath temperature was decreased ΔT decreased sharply.

In Figure 4.11 the normal fluid permeability (K_p)_n calculated by Equation (3.10) is plotted as a function of bath temperature for different heat supply rates specified. The transport quantity (K_p)_n is seen to be a strong function of temperature. As mentioned in section 2.6.3, the permeability is expected to decrease from the classical value as the temperature is decreased from the

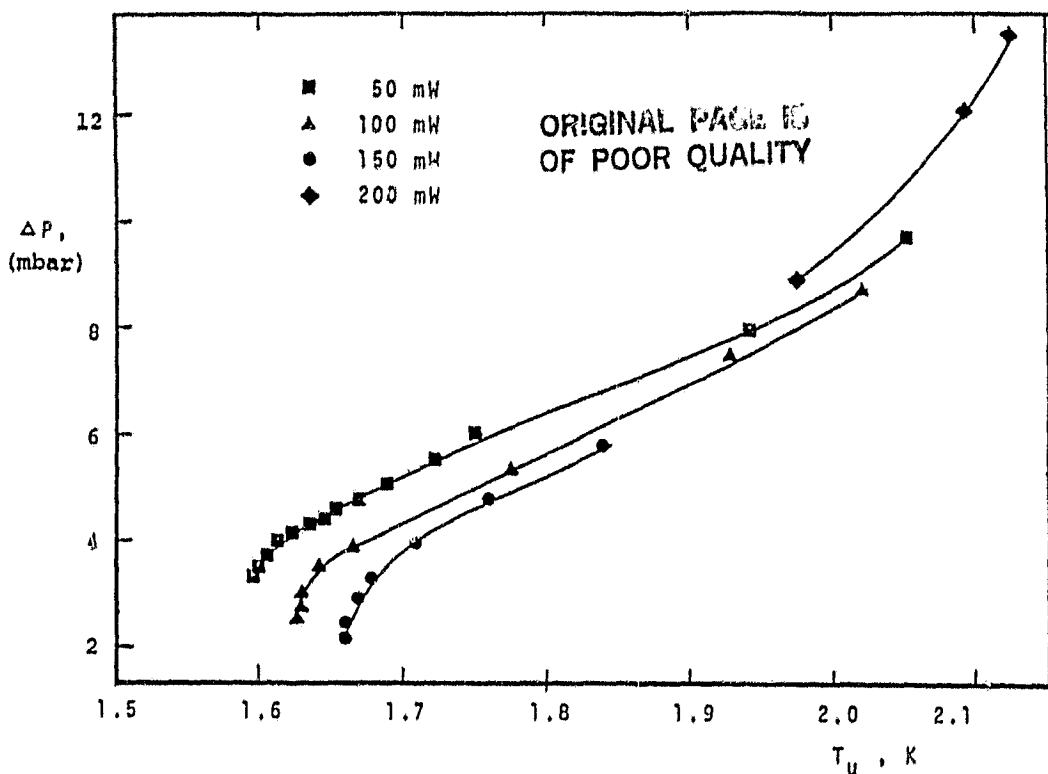


Figure 4.8 Pressure difference across plug for various externally supplied heating rates.

ORIGINAL PAGE IS
OF POOR QUALITY

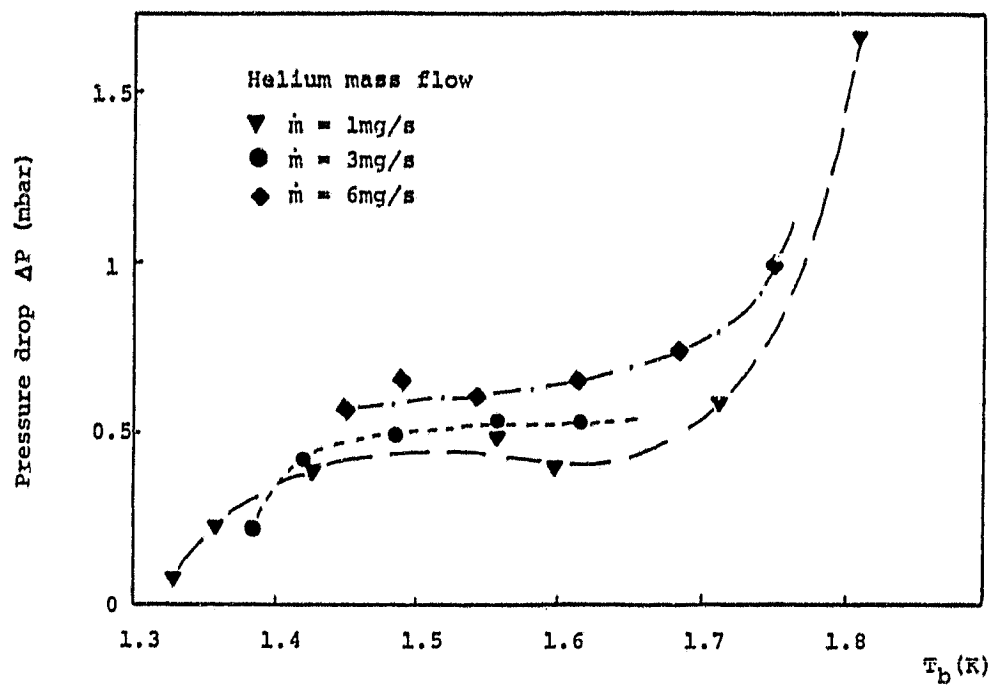


Figure 4.9 ΔP versus bath temperature for system of Becker et al.

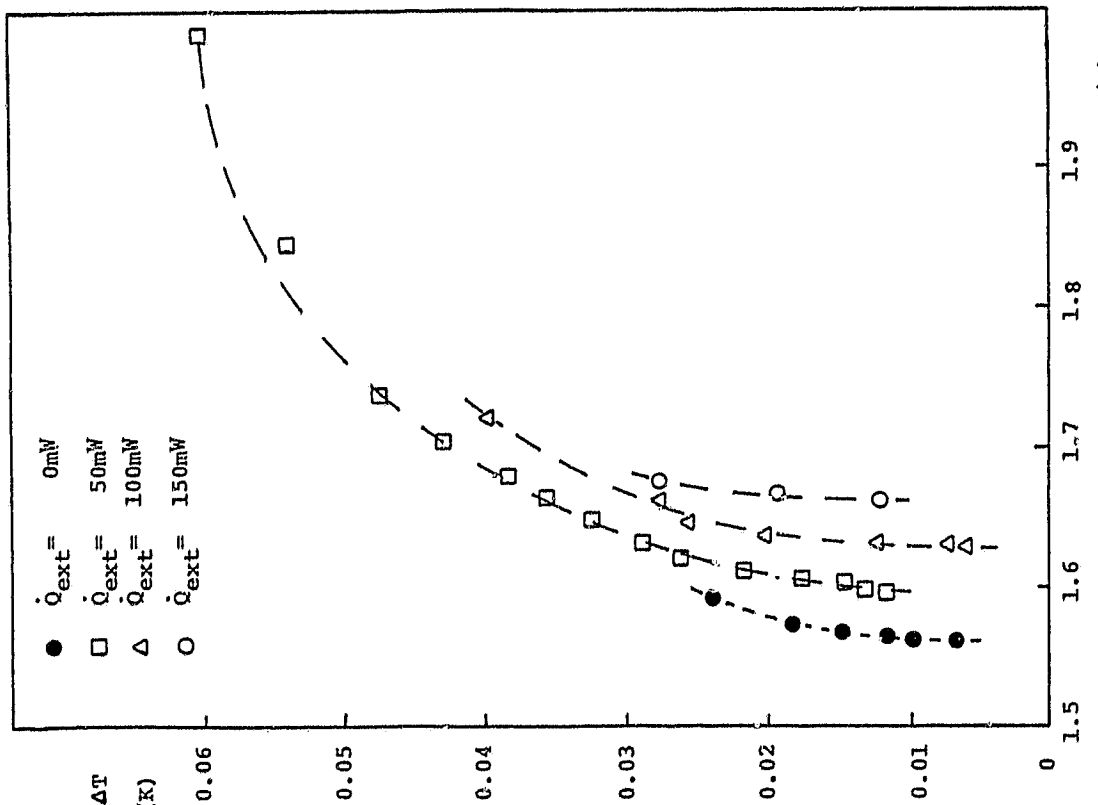


Figure 4.10 Temperature difference across the porous plug vs. bath temperature.

Lambda point into the He II range. This is interpreted as a result of the influence of the counterflow of the superfluid. If the temperature is further lowered ($\rho_s / \rho \sim 1$ and $W \sim V_n$) the normal fluid permeability will increase.

Finally it appears to return to the vicinity of the classical value. From Figure 4.11 one can see that at the low temperature accessible, permeability values of the order of magnitude of the classical permeability are reached in agreement with expectation for ($\rho_s / \rho \sim 1$). The dimensionless thermo-osmotic driving force values calculated by Equation 2.21 is tabulated in Table 4.2. The R_{at} values are seen to be in the same order of magnitude as the Rayleigh numbers calculated using different boundary conditions ($R_{at} \sim 10^3$). The fact that most of the R_{at} for the experiment were larger than the critical values implies that thermal circulation convection in the porous plug did occur.

Figure 4.12 is the dimensionless plot of N_q versus N_{VT} . The data is seen to deviate from the zero net mass flow data of the packed bed systems (Figure 2.15). This is expected because the experimental data were taken at temperatures close to the Lambda point. Due to the counterflow of superfluid ($V_n < W$), the heat flow Reynolds number (N_q) calculated from Equation 2.20 is smaller. Thus one would expect the data to lie below the line $N_q = N_{VT}$.

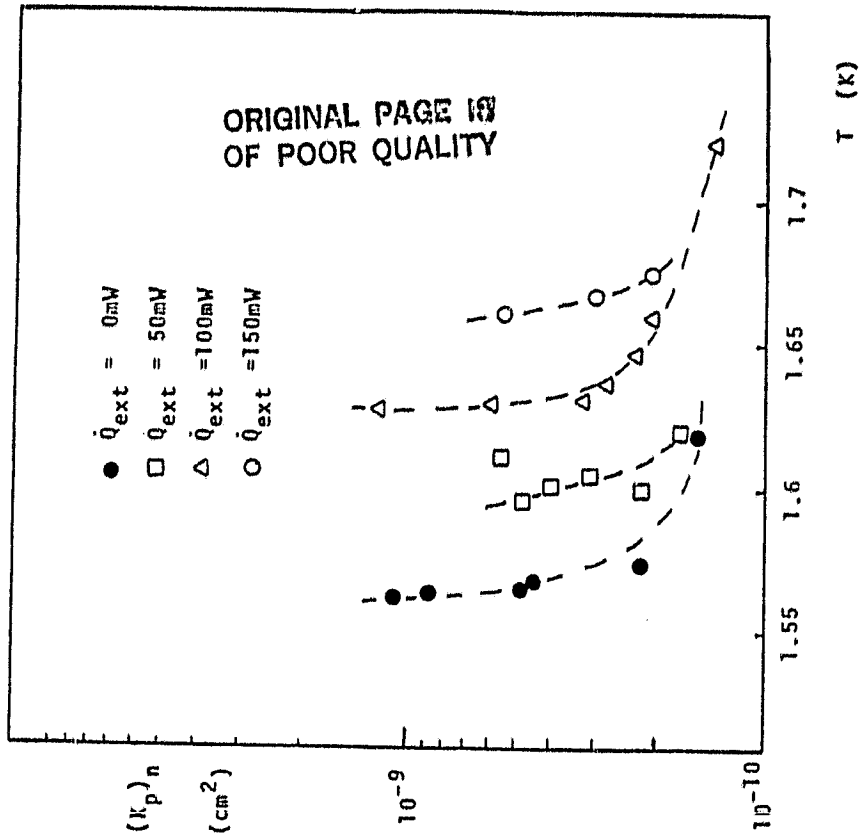


Figure 4.11 Normal fluid permeability (K_p)_n as a function of liquid bath temperature.

$N_q = N_{VT}$. At the limit of zero depletion ($V_n \sim w$) the data are expected to coincide with the data of the zero net mass flow packed bed systems.

ORIGINAL PAGE IS
OF POOR QUALITY

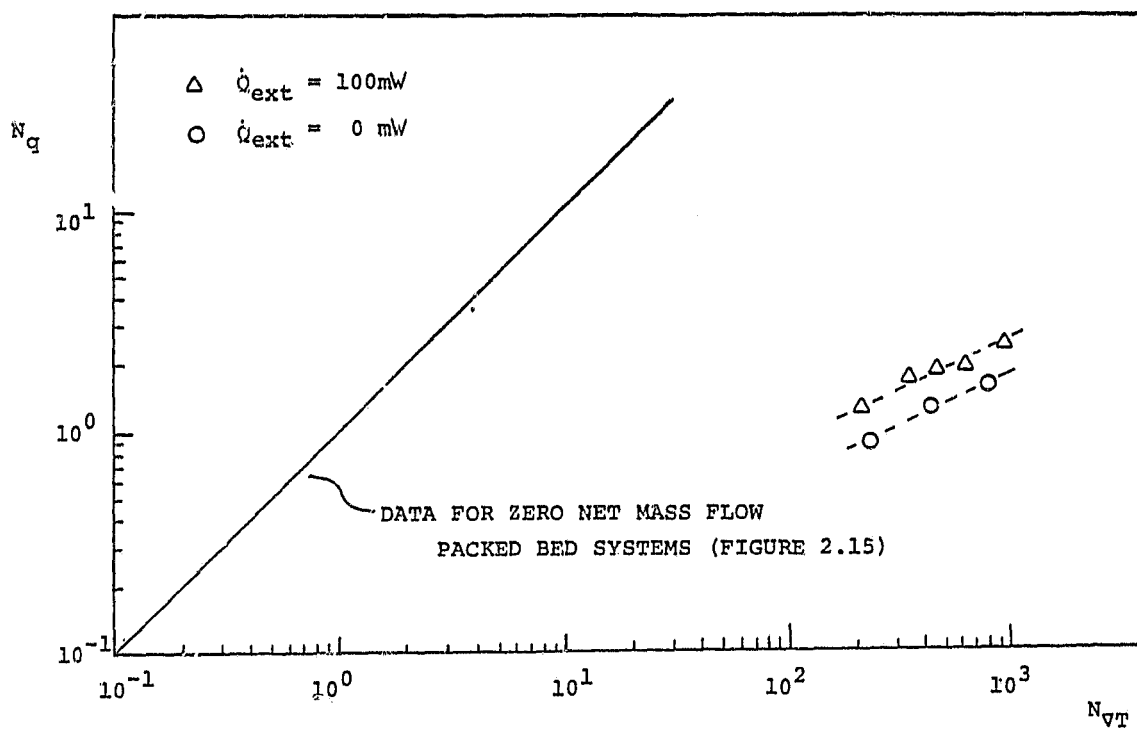


Figure 4.12 N_q vs. N_{VT} for the thermo-osmotic experiment.

Table 4.2 Table of the dimensionless thermo-osmotic driving force numbers

Table 4.2 (cont .)

Γ	$Ra_T = N_{VT} \frac{\rho_s}{\rho_n}$	$\dot{Q}_{ext} = 100mW$	$\dot{Q}_{ext} = 150mW$	$\dot{Q}_{ext} = 200mW$	$\dot{Q}_{ext} = 50mW$
—	—	—	—	—	—
$\dot{Q}_{ext} = 0mW$					
1.848	1861	1.6015	1.599	1.5965	1.6015
1.780	2364	1.599	1.599	1.599	1.599
1.733	2550	2758	2758	2758	2758
1.71	2414	2048	2048	2048	2048
1.678	2291	1892	1892	1892	1892
1.643	2184	1487	1487	1487	1487
1.619	2025	913	913	913	913
1.592	1726	564	564	564	564
1.575	1503	454	454	454	454
1.568	1066	3133	3133	3133	3133
1.565	834	3153	3153	3153	3153
1.565	708	2646	2646	2646	2646
1.5615	475	2033	2033	2033	2033
1.845	2827	1418	1418	1418	1418
1.736	3180	874	874	874	874
1.706	3026	—	—	—	—
1.68	2785	—	—	—	—
1.665	2601	—	—	—	—
1.647	2368	—	—	—	—
1.619	1895	—	—	—	—
1.611	1564	—	—	—	—
1.6055	1278	—	—	—	—

ORIGINAL PAGE IS
OF POOR QUALITY

5. Conclusion
From the results of chapter 4 one can draw the following conclusions.

For the flow of He^4 gas through stainless steel porous plugs at various temperatures, the velocity is found to be a linear function of the pressure drop. Within the experimental range Darcy's law is verified to be valid.

Using Darcy's law, the permeability of a 2- μm plug is found to be $5.65 \times 10^{-9} \text{ cm}^2$ at room temperature and $4.9 \times 10^{-9} \text{ cm}^2$ at liquid nitrogen temperature. The permeability of the plug tends to decrease as the temperature is lowered (decrease by 13% from 300 K - 77.4 K). The decrease in permeability is much larger than the con-

traction rate of bulk stainless steel which is about 0.3% (from 300 K - 0 K) thus other variables are involved.

The hydraulic radius (R_m) of the porous plug is found to be $1.33 \times 10^{-4} \text{ cm}$ (by Equation 2.9) at room temperature. The particle diameter of the plug is found to be $3.3 \times 10^{-3} \text{ cm}$ using Ergun's equation for packed beds. The data lie within the laminar range and the modified Reynolds numbers (Re_{kr}) are too small to show any geometric similarity between porous plugs and packed beds.

In the thermo-osmotic experiment, the pressure drop

and temperature difference across the porous plug are strong functions of the bath temperature. As the temperature is increased both ΔP and ΔT increase.

In the He II range, the normal fluid permeability increases as the temperature is lowered and tends to approach the order of magnitude of the classical permeability. This can be explained as a consequence of less interference with the superfluid counterflow as temperature is lowered.

Within the experimental range, the dimensionless heat transfer numbers N_q lie within the laminar regime due to the counterflow of superfluid whereas the dimensionless driving force N_T can be either in the laminar or turbulent regime.

The fact that most of the dimensionless thermo-osmotic driving force values of the experiment exceed the critical values suggests that thermal circulation convection occurs in the porous plug.

REFERENCES

1. J.W. Vorreiter, "Cryogenics for Spacecraft", Proc. 7th Intern. Cryog. Eng. Conf., IPC Sci. and Technol. Press, Guildford, Surrey, England, 1978, pp. 1-17.
2. H.D. Deamer, G. Klipping, I. Klipping, Menzel, Ruppert, "Flow of Helium II through Porous Plugs", Research and Technical Notes 1977.
3. L. Tisza, "Sur la Théorie des Liquides Quantiques: Application à l'Helium Liquide, I & II", J. Phys. Radium, 1: 164-172, May 1940, and 1: 350-358, October 1940.
4. J.D. Landau, "Theory of Superfluidity of He II", Phys. Review, 60: 356-358, August 1941.
5. J.D. Landau, Collected Papers of L.D. Landau New York, Gordon and Breach, 1965. pp. 301-330.
6. J.S. Langer and J.D. Reppy, "Intrinsic Critical Velocities in Superfluid Helium". Progress in Low Temperature Physics, VI: 1-35, 1970.
7. E. Andronikashvile, "A Direct Observation of Two Kinds of Motion in Helium II". J. Phys. USSR, 10: 201-206, 1946.
8. P.I. Kapitza, "Heat Transfer and Superfluidity of He II". J. Phys. USSR, 5: 59-69, 1941.
9. R.J. Donnelly, Experimental Superfluidity. The University of Chicago Press, 1967, pp. 30-34.
10. P. London, Superfluids. Vol. II, New York, Wiley, 1954.
11. G.R. Karr and E.W. Urban, "Superfluid Plug as a Control Device for Helium Coolant". Cryogenics May 1980, pp. 260-270.
12. H. Schlichting, Boundary Layer Theory 7th edit on. McGraw Hill 1979, pp. 81.
13. Annual Book of ASTM. "Maximum Pore Diameter and Permeability of Rigid Porous Filters for Lab. Use." Pt. 41 El28 pp. 146-149.
14. A.R. Urbach, P.V. Mason, and W.F. Brooks, "Progress Report on the Infrared Astronomical Satellite Cryogenic System", CEC and ICIC Conference, San Diego, BE-2, 1981.
15. A.E. Scheidegger, The Physics of Flow Through Porous Media 3rd edition. Toronto 1974.
16. A.T. Robinson, "Permeability of Tungsten Matrices as a Function of Density, Particle Size, and Shape". Trans. of the ASM, Vol. 57, 1964, pp. 650-657.
17. R.B. Hall, M. Sc. Thesis, Univ. California, Los Angeles 1967.
18. S. Ergun, "Fluid Flow Through Packed Columns", Chem. Eng. Vol. 48, (1952), pp. 89-94.
19. I.F. Macdonald, El - Sayed, M.S., Now, K., and Duilién, F.A.I., "Flow Through Porous Media - The Ergun Equation Revisited", Ind. Eng. Chem. Fundamentals, Vol. 18, 1979, pp. 199-208.
20. R.E. Collins, Flow of Fluids Through Porous Materials. Reinhold, New York, 1961.
21. Mott Metallurgical Corporation, "Introduction to Engineering Controlled Porosity Products", Catalog No. 1000.
22. Pall Trinity Micro Corporation, "The Pall Porous Metals Filter Guide", Bulletin No. PSS 700B.
23. M. Muskat, The Flow of Homogeneous Fluids, J.W. Edwards, Inc. (1946).
24. Frederking, Elsner, Klipping, Adv. in Cryo. Eng. 18 (1975), pp. 132-140.
25. E.W. Urban, L. Katz and G.R. Karr, JT-14, Vol. 4, North-Holland, Amsterdam (1975), pp. 37.
26. R. Schmidt and H. Wiechert, "Heat Transport of Helium II in Restricted Geometries", Z. Physik B 36, (1979), pp. 1.
27. H.H. Hausner, Handbook of Powder Metallurgy, Chem. Publishing Co. Inc., New York 1973.
28. T.H.K. Frederking, H. Van Kempen, M.A. Meen and P. Wyder, "Critical Counterflow in Narrow He II - Filled Channels". Physica 103B, (1981), 1129.
29. H. Forststat, "Length Effect in the Heat Transport in Helium II". Physical Review. 3: 1450-1452, 1958.
30. G.V. Heijden, W.J.P. De Voort and H.C. Kramers, "Forces in the Flow of Liquid Helium II" Physica 59, 1972, pp. 473-497.

ORIGINAL PAGE IS
OF POOR QUALITY